ADVANCED MASTERS IN STRUCTURAL ANALYSIS
OF MONUMENTS AND HISTORICAL CONSTRUCTIONS

Master's Thesis

Alberto Bonetto

Numerical Analysis of the Reinforced Arch Method.

UNIVERSITAT POLITÈCNICA
DE CATALUNYA

Education and Culture

Erasmus Mundus

DECLARATION

Name:	Alberto Bonetto
Email:	bonetto.al@gmail.com

Title of the Msc Dissertation:	Numerical Analysis of the Reinforced Arch Method
Supervisor(s):	Prof. Pere Roca, Prof. Lorenzo Jurina
Year:	2016/17

I hereby declare that all information in this document has been obtained and presented in accordance with academic rules and ethical conduct. I also declare that, as required by these rules and conduct, I have fully cited and referenced all material and results that are not original to this work.

I hereby declare that the MSc Consortium responsible for the Advanced Masters in Structural Analysis of Monuments and Historical Constructions is allowed to store and make available electronically the present MSc Dissertation.

University:	Universitat Politècnica de Catalunya
Date:	July 14, 2017
Signature:	

ACKNOWLEDGEMENTS

I would like to thank my supervisors, Professors Pere Roca and Lorenzo Jurina for their availability and all the help and suggestions they provided me during the entire dissertation period in Barcelona. Thanks also to the lecturers of the Master Programme in Padova, especially Professor Climent Molins and Enrico Garbin for their illuminating lessons. Thanks to the Consortium, for the scholarship supplied.

A special thanks to my parents for all the support they gave me during all the Master's period, and to all of my classmates, my friends and all the people that supported me during the whole dissertation time, especially Vera, Marco, Sara, Alicia and Armando.

ABSTRACT

Masonry arches, vaults and domes are architectural elements diffusely present in a great part of the human construction heritage. Brought to its maximum magnificence from the Roman genius, and then spread all over the World throughout History, especially in the Occidental and Mediterranean countries, the arch has become one of the most recognizable mark of our architectural legacy. The Reinforced Arch Method is a rather recent strengthening technique for masonry arches and vaults that entails the application of steel post-tensioned cables at their extrados or intrados, in order to enhance capacity and ductility. Many experimental tests have been performed on this technique, but numerical modelling has not been yet fully deepened. Indeed, by means of numerical Finite Element models, the present work mainly aims at confirming the effectiveness of this procedure. At the same time, it envisages calibrating and validating the numerical tools, by comparing their results with the ones derived from an experimental campaign on scale models, performed by Prof. Lorenzo Jurina at the Polytechnic University of Milan. Macro-models, based on smeared crack material, and micro-models, based on elastic blocks with hinge opening, have been produced and tested. A comparative study on the results obtained with both procedures has been performed, underlying their specific qualities and drawbacks, especially regarding their capability to capture the collapse phenomenon and the interaction between the original structure and the strengthening system.

RESUMEN

Los arcos, bóvedas y cúpulas de mampostería son elementos arquitectónicos ampliamente presentes en el patrimonio construido de la humanidad. Fueron llevados a su máximo esplendor por los genios Romanos, y su uso se propagó por todo el mundo a lo largo de la historia. Especialmente en occidente y en los países mediterráneos el arco se ha convertido en uno de los símbolos más reconocidos del legado de la arquitectura. El método del arco reforzado es una técnica de refuerzo estructural para arcos y bóvedas relativamente reciente que implica la utilización de cables postensados en el intradós o extradós, con el fin de aumentar la resistencia y la ductilidad. Se han realizado muchas campañas experimentales con esta técnica, sin embargo, no se ha desarrollado aún en profundidad el modelado numérico. Por lo tanto, el objetivo de este trabajo es confirmar la eficacia del método del arco reforzado mediante el uso de modelos numéricos de elementos finitos. Al mismo tiempo, contempla la calibración y validación de las herramientas numéricas, comparando los resultados con los obtenidos en la campaña experimental en modelos a escala, realizada por el Prof. Lorenzo Jurina de la Universidad Politécnica de Milán. Se han elaborado y probado macro-modelos, basados en 'smeared crack material', y micro-modelos, basados en bloques elásticos con apertura de rótulas. Además, se ha realizado un estudio comparativo de los resultados obtenidos con ambos procedimientos, destacando tanto sus cualidades específicas como sus desventajas, poniendo especial atención a su capacidad de capturar correctamente el fallo de la estructura y la interacción entre la estructura original y el sistema de refuerzo.

ABSTRACT

Archi, volte e cupole in muratura sono elementi architettonici diffusamente presenti in gran parte del patrimonio architettonico dell'Umanità. Portato al massimo splendore dal genio Romano, e poi diffuso in tutto il Mondo durante la Storia, specialmente nei paesi occidentali e del Mediterraneo, l'arco è divenuto uno dei simboli più riconoscibili della nostra tradizione architettonica. Il metodo dell'arco armato è una tecnica relativamente recente per il consolidamento degli archi e delle volte in muratura, che prevede l'applicazione di cavi in acciaio post-tesi all'estradosso o all'intradosso degli stessi, allo scopo di migliorarne la capacità resistente e la duttilità. Su questa tecnica molte prove sperimentali sono state svolte, ma la modellazione numerica non è stata ancora approfondita in maniera esaustiva. Proprio tramite l'utilizzo di modelli numerici a elementi finiti, il presente lavoro mira principalmente a confermarne l'efficacia. Allo stesso tempo prevede la calibratura e la validazione degli strumenti numerici, attraverso il confronto dei risultati ottenuti con quelli derivanti dalle prove della campagna sperimentale su modelli in scala ridotta, svolta dal Prof. Lorenzo Jurina presso il Politecnico di Milano. Macro-modelli, basati su materiale a frattura diffusa, e micro-modelli, composti di blocchi elastici con libera apertura di cerniere, sono stati prodotti e testati. Si è svolto quindi uno studio comparato sui risultati ottenuti con entrambe le procedure, sottolineandone nello specifico pregi e difetti, in particolare in merito alla loro capacità di cogliere il fenomeno del collasso e l'interazione tra la struttura originaria e il sistema di consolidamento.

TABLE OF CONTENTS

LIST OF FIGURES

LIST OF TABLES

1. INTRODUCTION

1.1 Generalities

Masonry arches and vaults have been largely used throughout the history of constructions, since the Roman age. Before the advent of reinforced concrete, in the late 19th century, they have always been the most valuable technique available to cover any span and create openings in the ancient buildings. The Reinforced Arch Method is a rather recent strengthening technique, for arches and vaulted structures, developed by Prof. Lorenzo Jurina at the Polytechnic University of Milan. It consists on the application of steel cables at the extrados or the intrados of the structure, to improve the capacity by providing extra tensile resistance. Moreover, the application of a post-tension force at the cables, activate a re-centring of the thrust line inside the element, and therefore increase its geometrical safety factor. So far, Prof. Jurina has been performing more than 500 tests on reduced and real scale arch models, proving the effectiveness of this innovative technique. One of the most recent campaign was carried out by inducing collapse at wooden semi-circular arches scale models, with punctual incremental loading, provided of different arrangements of cable reinforcement.

1.2 Objectives

The aim of the present document is to prove, once again, the RAM strengthening technique effectiveness. This time by means of numerical simulations. The semi-circular scale model experimental campaign, described above, has been taken into consideration. The results obtained from numerical finite element models, produced with Diana FEA and calibrated with limit analysis, have been compared with the experimental ones, to confirm their validity. Moreover, the aim of analysing the experimental cases with numerical tools, is also to provide the ability to deeper investigate the collapse phenomenon and the behaviour of the strengthening system in details, with the possibility to simulate many different conditions. Different types of models and ways to apply the reinforcement have been studied, with the goal of determining qualities and drawbacks of them, for further developments. In particular, two approaches have been followed and compared: micro-modelling, with the simulation of actual hinge opening at interfaces of the arch elements, and macro-modelling, with the application of a smeared-crack material model, suitable for masonry structures.

1.3 Content

First, a bibliographic review of the most recent techniques for numerical analysis of masonry arches has been carried out. Then the RAM technique has been presented and explained, with the description of the experimental campaign on scale models concerned. After that, the types of models used for the numerical simulations have been explained. Limit analysis has been performed, to calibrate the

geometry of the numerical models, to make them consistent with the experimental ones. Then, micro-models have been used to simulate the collapse behaviour of the arches, investigating the unreinforced cases and the reinforced ones, even studying the friction phenomenon between steel cables and arch influence on the arch capacity. Macro-models have also been used for the same purposes and eventually a comparison of the two modelling procedures has been performed, underlying qualities and drawbacks of both.

2. STATE OF THE ART: STRUCTURAL ANALYSIS OF MASONRY ARCHES

Structural analysis of arches and vaulted structures has been a concern since the ancient times, when firstly these kinds of elements revolutionized the history of architecture and engineering. The first approaches were merely geometric, especially for the Gothic constructions: the main issue was the design of the depth of the arch and the buttress, due to the span of the arch. The first rational approach was achieved with the Scientific revolution in the 17th century, introducing also the concept of *inverted catenary*. This principle, then used in the 18th century also by Poleni for the stability of St. Peter's dome in Rome (Figure 1), has been historically attributed to Robert Hooke. With an anagram, discovered after his death in 1705, he stated: "Ut pendet continuum flexile, sic stabit contiguum rigidum inversum" - as hangs a flexible cable, so inverted, stand the touching pieces of an arch (Heyman, 1966).

Then, during the following centuries, also graphic static was introduced, with the introduction of the concept of thrust line. Finally, the problem of the equilibrium of arches and vaults was analytically closed by Heyman in 1960's with the limit analysis formulation. This approach is still much convenient, because of its ease in the application, even with simple computing tools. Because of its hypothesis, no information is needed on the resistance or the deformability of the masonry, and it can be applied using simple geometrical considerations, imposing the equilibrium condition by the Principle of Virtual Works. This is the reason why this procedure is still widely used for determining the capacity of masonry arches.

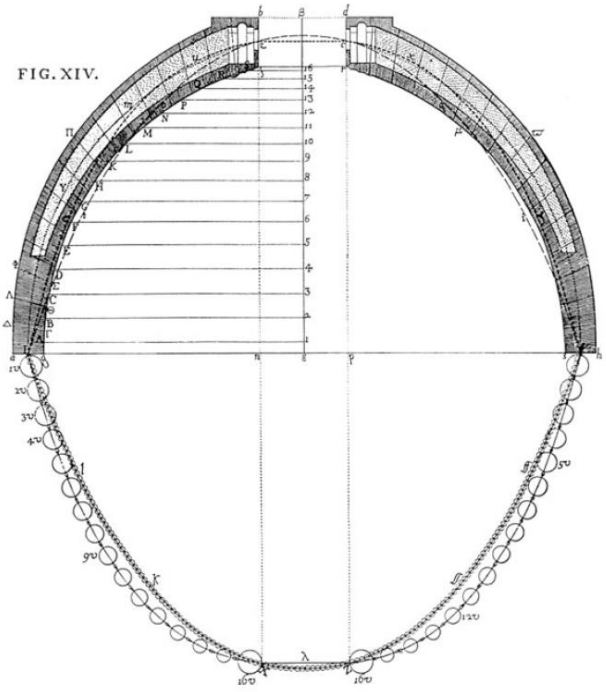

Figure 1 – Poleni's inverted catenary solution of San Peter's dome in Rome. (Poleni, 1748).

Nevertheless, with the great development of numerical models, during the last decades, more sophisticated approaches can be rather easily chosen. For instance, Finite Element models (FEM) can capture elastic deformability and take into account the resistance of the masonry, by the application of several constitutive laws to the material. Two different approaches can be followed in FE procedures: micro-modelling and macro-modelling. The first is more computationally demanding: each element of the structure, with the respective material properties, is modelled (e.g. bricks and mortar). This method is suitable for very complex problems, with relatively small dimensions and simple geometries. The second one, more widespread, implies an averaging of the material characteristics at a wider scale, compared with the micro-modelling, since usually the dimensions of the elements are significantly bigger than the elements dimensions (e.g. masonry as sum of brick and mortar). In any FE modelling, despite their accuracy and their possibility to provide also deformation and stress parameters as results, besides mere capacity, the calibration of the parameters involved is not always immediate, because of their variability. Less used, but much interesting for arches analysis, is the Discrete Element Method (DEM), based on the modelling of rigid blocks interacting along the boundaries. In fact, this approach can include shear/friction failure between the masonry units of the arch.

2.1 Analytic Approach: Limit Analysis

The limit analysis (Heyman, 1966) is still one of the most used procedure for evaluating the safety of arched structures. This analytical formulation consists on the application of the *lower bound theorem* and the *upper bound theorem*, that can be summed up in the *uniqueness theorem*.

The lower bound (or *safe*) theorem is based on the following hypothesis:

1- Infinite compressive strength;

2- No tensile strength;

3- No sliding between blocks.

Under these hypothesis, if a thrust line, due to a load configuration, can be fitted in the structure geometrical boundary, then the external load that corresponds to that thrust line is a lower bound of the actual collapse load. The maximum statically admissible external load is the actual collapse one. Evidently, an infinite number of thrust lines can be found in an arched structure, since the base reaction points and the horizontal thrust value must be chosen arbitrarily. This procedure is also called *static approach*, because it involves statically determined load configurations. Moreover, when only one thrust line can be fit in the arch geometry, it means that the correspondent external load is the limit one, under the aforementioned hypothesis (Figure 2). Based on the lower bound theorem, many commercial programs for graphic statics have been developed: varying the input parameters they are able to fit an enormous number of thrust lines, when statically possible.

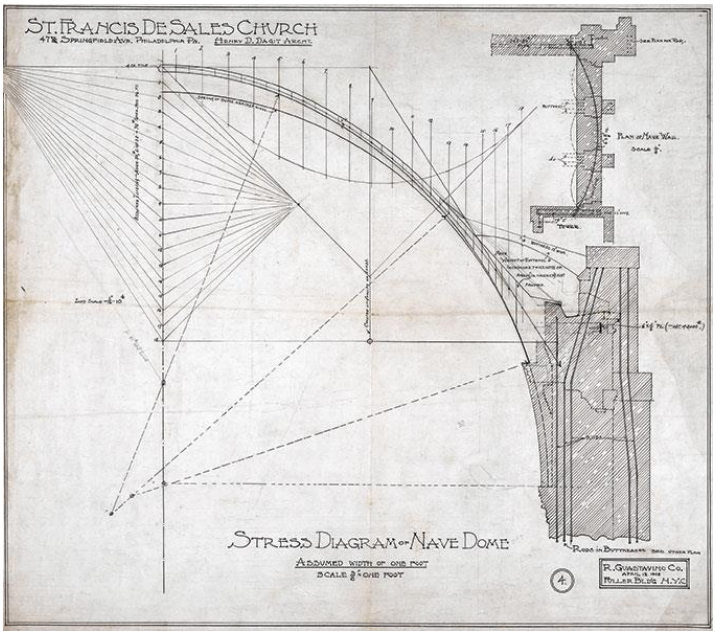

Figure 2 – Guastavino Jr's graphic statics of St. Francis de Sales Church in Philadelphia, 1909. (Ochsendorf, 2005).

The complementary approach to the static one is the *kinematic approach*. The upper bound theorem states that if the work done by the external forces, on a kinematically admissible mechanism, is positive or null, then the structure will collapse. In the case of arches, this approach is carried out by choosing a hinge distribution along the structure, and then computing the external corresponding collapse load through the Principles of Virtual Work (PVW): that load is an upper bound of the actual collapse one. Therefore, the minimum collapse load found among any hinges distribution is the actual collapse load. Based on the upper bound theorem, many programs for determining arches capacity have been developed, such as RING (LimitState 2007b), Gelfi ARCO and ArchieM (Obvis 2007). These programs are able to scan many possible collapse configurations and find the minimum collapse load among all the mechanisms analysed. An enhanced approach, based on the safe theorem, was proposed by O'Dwyer (1999) for solving 3D arched vaulted structures. It is based on the fitting of a system of bars inside the geometry of the vault. Similarly, Gilbert et al. (2005) proposed a truss optimization procedure for assessing the possible thrust line paths inside a 3D structure.

The upper bound and the lower bound theorems converge to the same value, correspondent to the actual collapse load (uniqueness theorem, Figure 3). In other words, a limit condition is found when both statically and kinematically admissible collapse mechanism can be found. These two theorems can be used mutually to check the values obtained, but also to determine an interval sufficiently small in which the collapse load is included.

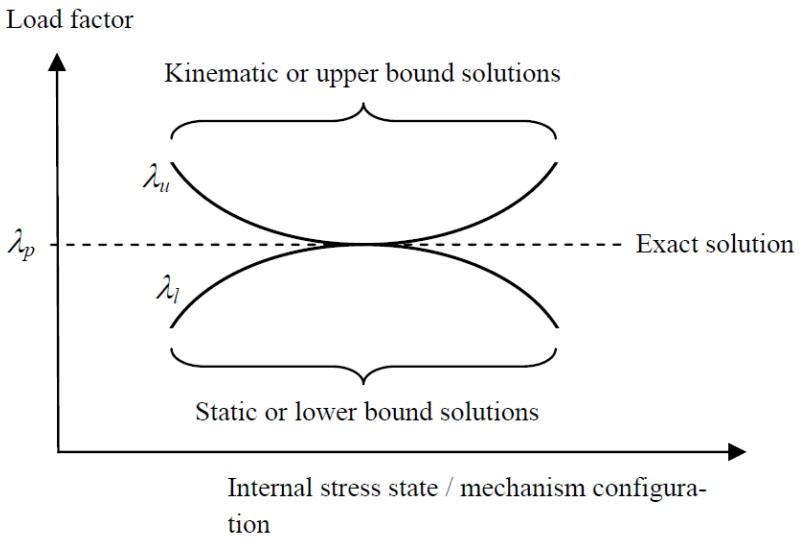

Figure 3 – Uniqueness theorem. (Gilbert, 2007).

2.2 Numerical Approach

Lourenço (1996) categorizes three types of numerical modelling approaches for masonry:

a) Detailed micro-modelling: units and mortar in the joints represented as continuum, whereas the unit/mortar interfaces are modelled by discontinuous elements;

b) Simplified micro-modelling: ‘‘geometrically expanded’’ continuum units, with discontinuous elements, covering the behaviour of both mortar joints and interfaces;

c) Macro-modelling – where the principal features of structural masonry are represented by an equivalent homogenized continuum.

In this framework, Finite Element Models and Discrete Element models can be identified. In the case of masonry arches all these approaches can be followed. Nevertheless, detailed micro-modelling, despite its deep fidelity in the reproduction of the behaviour of the elements composing masonry, can be computationally not convenient, and difficult to handle. At the same time macro-modelling, despite its greater ease in the modelling phase, is not able to capture some phenomena that can occur within the mortar joints, such as shear slipping. Moreover, assessing masonry parameters, in this latter homogeneous approach, is not always easy. In fact, that implies an averaging operation between blocks and joints characteristics, that often show a high variability on their complexion and state, especially in historical constructions

A rather recently developed approach is also available nowadays, the Finite/Discrete elements modelling. It consists on a mixed Finite/Discrete Elements formulation, that will be shortly presented and discussed below.

2.2.1 Finite Element Models

Finite Element analysis, in masonry structures, is much diffused nowadays. This approach is most of the time based on a continuum solid modelling. Depending on the detail of modelling, *micro-modelling* and *macro-modelling* can be distinguished, as explained above for the cases a) and c) by Lourenço, (1996). A typical drawback in masonry structures macro-modelling (Roca et al., 2010) is that the smeared crack constitutive law, normally used in commercial programs, very often do not allow to localize the damage pattern as in the reality. In fact, in unreinforced masonry usually cracks form in highly confined areas of panels, while this kind of models tend to show a diffused crack pattern. This problem has been overcome through a novel crack-tracking algorithm (Clemente et al., 2006), that allows to localize better the damage path (Figure 4).

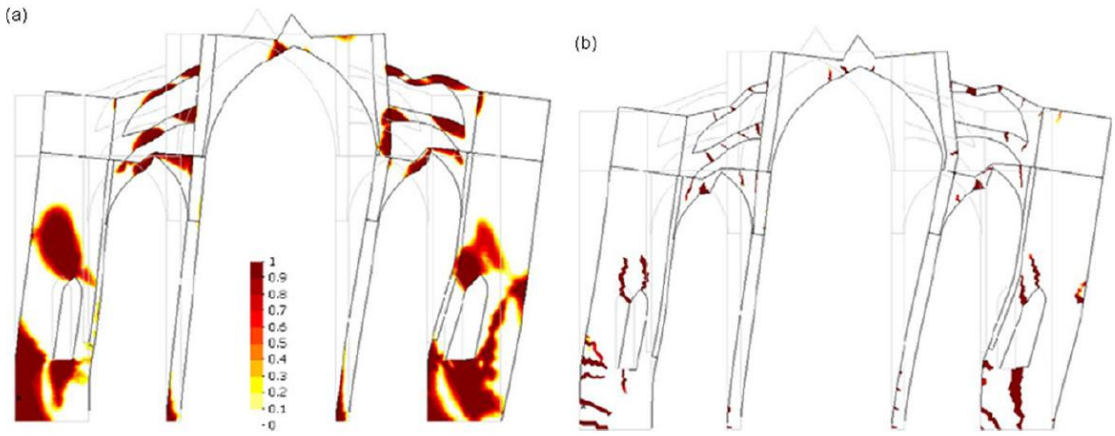

Figure 4 – Mallorca cathedral: comparison between smeared crack model analysis and crack-tracking one, in case of transversal response under seismic load (Clemente et al., 2006).

Micro-modelling is a less diffused approach, due to its difficulty to handle. It is more used for analysing special problems with localized phenomena that especially involve interaction between blocks and joints.

Concerning masonry arches and vaults, several examples of FE analysis are available. Lourenço (2002) analyses a masonry arch loaded at ¼ of the span, comparing macro-modelling FEA results with limit analysis one. Both physical and geometrical non-linear approaches are carried out, and even two different values of tensile strength are considered. From the comparison of the results obtained, it can be stated that by increasing the tensile resistance the safety factor raises, with a peak-like response curve, but the residual value is not affected by these parameters. Since limit analysis encompasses no tensile resistance, models with f_t =0 showed a better accordance with theoretical results, without the presence of peaks. Finally, adding the contribution of non-linear geometry does not affect much the final response (Figure 5).

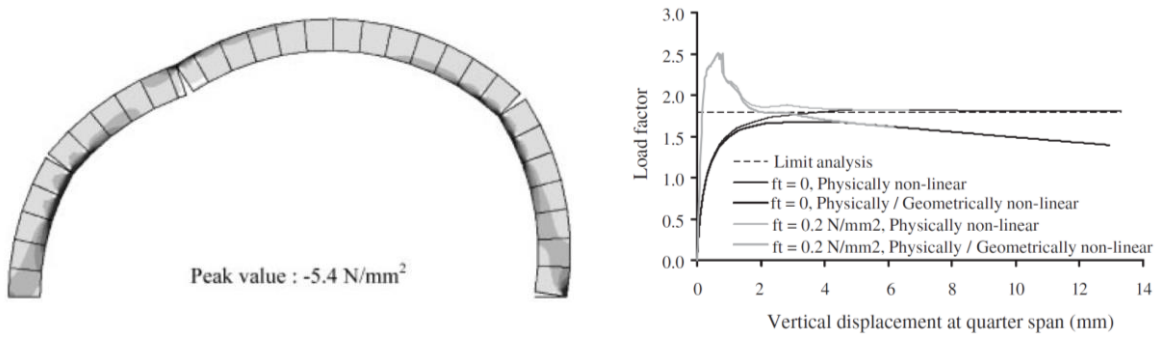

Figure 5 – Collapse mechanism obtained and comparison between results of a FE masonry arch model, loaded at span quarter (Lourenço, 2002)

Similar analyses have been carried out by Kumar and Bhandari (2005), through the comparison of experimental results on masonry arches loaded at the span quarter, and an 80 8-noded 2D elements FE model. The constitutive law included crushing and cracking, and its parameters were calibrated through the experimental values previously obtained. Even in this case, experimental 3D arches and 2D FE models show a good accordance in terms of capacity curve, as shown in Figure 6.

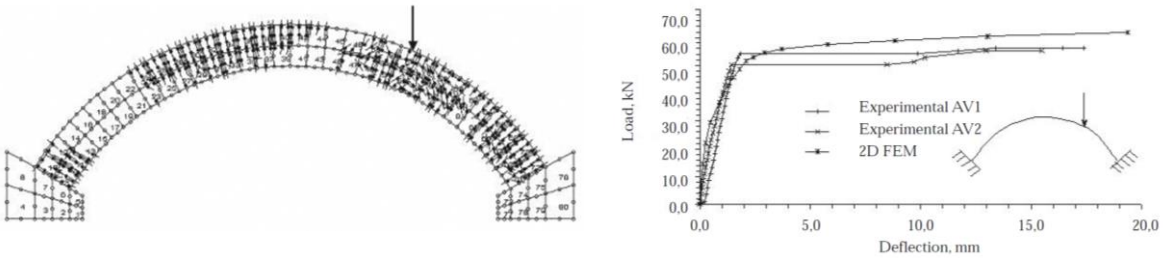

Figure 6 – Masonry arch 2D modelling: crack pattern and comparison of the experimental and analytical load-deflection curve at loading point (Kumar and Bhandari, 2005).

Betti et al. (2008), modelled a single-span masonry barrel arch bridge, loaded vertically at ¼ of the span, using a 2D plane strain elements model, including adaptive unilateral friction-contact interface elements. This means that when in any point between blocks the stress state is not admissible, the corresponding joint is substituted by unilateral contact interface, that allows crack opening. In this case, infill was also modelled. The results obtained showed good accordance with the experimental ones (Figure 7).

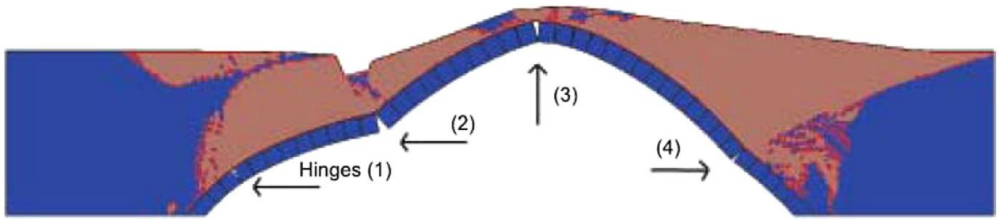

Figure 7 – Collapse mechanism of infilled arch, with adaptive contact-friction interfaces (Betti et al., 2008).

3D models can also be considered, implying the use of tetra-hexa brick elements. Milani and Lourenço (2012) analysed a skew single span masonry arch, tested at Bolton Institute, UK, and a multi span bridge of five semi-circular arches, both loaded by an eccentric vertical load. This was carried out by means of 3D FE models with rigid eight-noded parallelepiped elements, with non-linear interfaces. This type of FE modelling has shown results in compliance with limit analysis ones and with the pre-existing results (Figure 8), obtained on the same example. In particular, it is much suggested for unusually shaped structures, such as skew arches, that need a 3D approach to be modelled and to well interpret their behaviour.

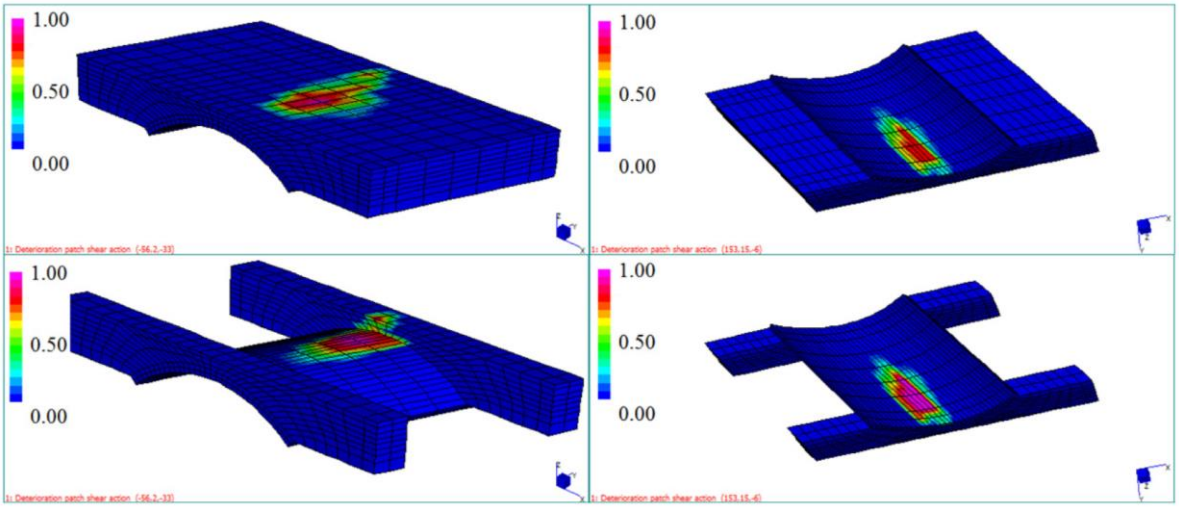

Figure 8 – Bolton Institute skew arch. Degraded interface patch, obtained through the non-linear homogenized FE code. (Milani and Lourenço, 2012).

2.2.2 Discrete Element Models

Typically, Discrete Element Models are based on the separate representation of the mechanical behaviour of the units and the interaction between them (Lemos, 2007). They usually comply with these assumptions:

- Rigid blocks with deformability concentrated at joints. Nevertheless, deformable blocks formulations are also available;

- Interaction between blocks is represented through point contacts, or edge-to-edge contacts, with no attempt to get a continuous distribution of stress through contact surfaces;
- Separation of blocks and large displacements analysis are typically allowed.

By definition, the Discrete Element Method applies to a computational approach only if it permits finite rotations and displacements of discrete units, and is able to compute new contacts between elements as the analysis proceeds (Roca et al., 2010)

Constitutive behaviour of contacts can be *rigid*, with forced no overlapping between blocks, or *soft*, allowing finite axial and shear contact stiffness. In the latter, stress depends on the relative displacement between blocks. Several 2D programs, implementing DE models, are available, such as UDEC (Itasca, Minneapolis, MN, USA), 3DEC (Cundall, 1988; Hart et al., 1988) and CICE (Hocking et al., 1992).

DE models have been largely used for masonry arches modelling, in particular by Gilbert and Melbourne (1995), who investigated the problem of ring separation between multi-ring block arches (Figure 9).

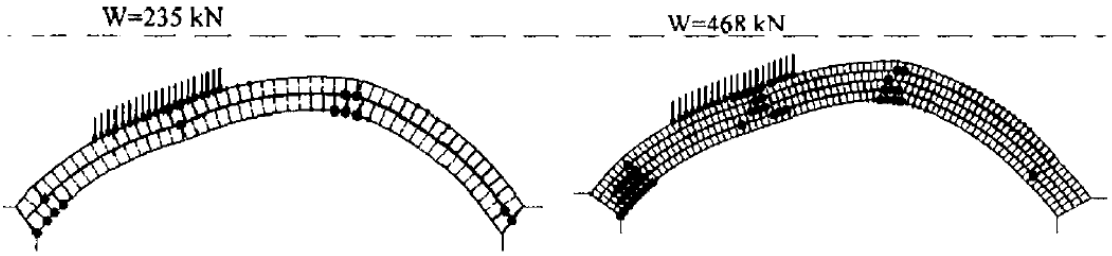

Figure 9 – Discrete Element multi-ring arches failure analysis, Gilbert and Melbourne (1995).

A more recent type of DE model is also available, combining FE and DE: the Discontinuous Deformation Analysis (DDE). This method is based on an assumed deformation field, within distinct domains of ordinary shapes. These type of model, derived from rock mechanics, allows to perform analysis of rigid block motion and block deformation, simultaneously. A DDA analysis of a masonry arch, with which the back-fill represented by a system of deformable blocks (Figure 10), created by a random pattern of joints, was carried out by Bicanic et al. (2001).

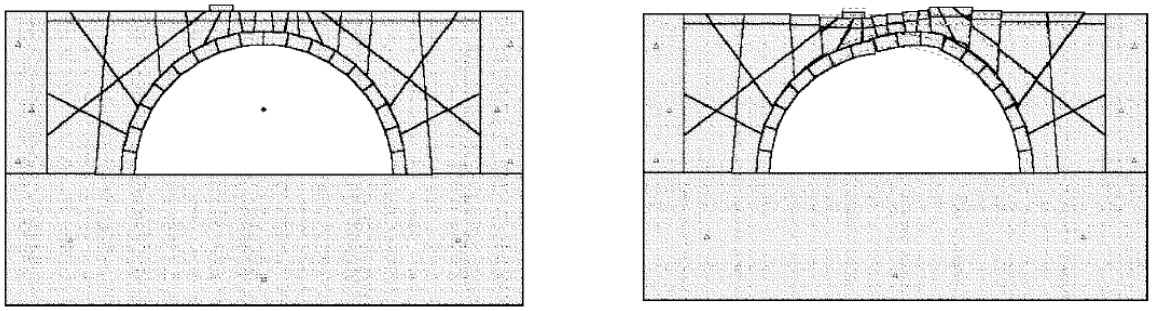

Figure 10 - DDA of Edinburgh University model arch bridge (Bicanic et al., 2001).

Another approach for discontinuous modelling, suitable for arches infill, is the use of Particle Flow models (PFC). These models are based on the discretization of materials through spherical elements, in contact one to another.

Thavalingam et al. (2001) analysed the case of an experimental infilled masonry bridge model, tested at Cambridge University, using three different models: Finite Element (DIANA), PFC and DDA. The results are shown in Figure 11, also in a graph for comparing the capacity curve obtained.

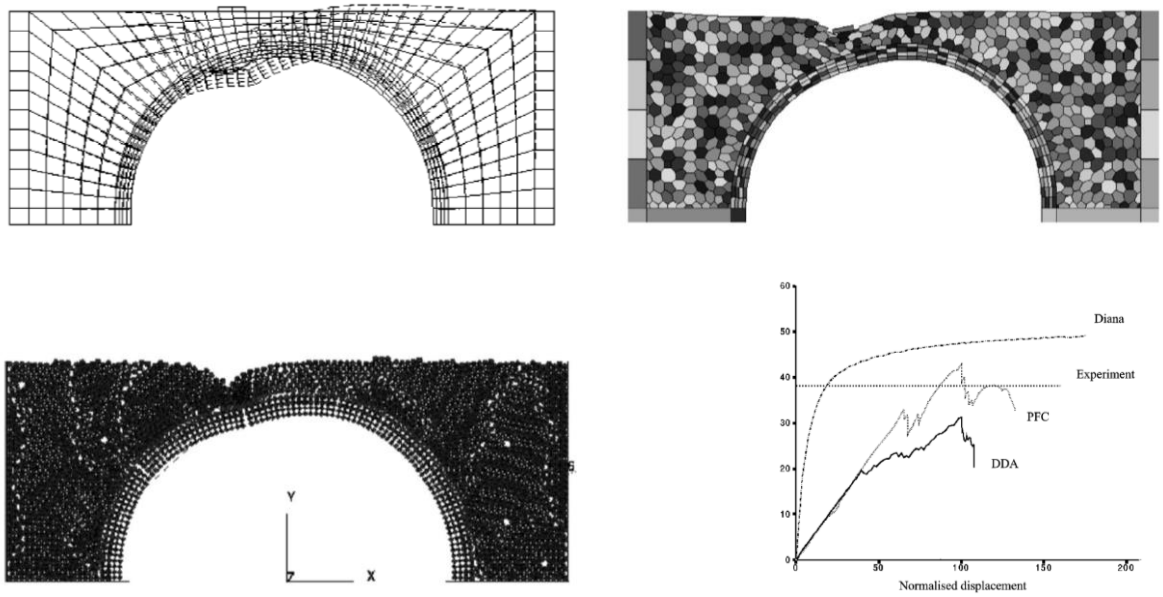

Figure 11 – Different 2D modelling approaches of an infilled masonry bridge. Clockwise from bottom-left: PFC model, FE model (DIANA), DDA model, comparison of results, (Thavalingam et al., 2001).

2.2.3 Alternative Approach: One Dimensional Elements

To discretise masonry arches, a possible alternative to Finite Element models, based on 2D or 3D elements, is the usage of one-dimensional beam elements. This procedure is rather unusual, because

of the predominance of FE programs, even though it shows many positive outcomes, such as low computing demand and the possibility to display directly the value of internal forces. Molins and Roca (1998) proposed a curved members elements model with variable cross section and non-linear material behaviour (elastoplastic under shear and compression and linear elastic-perfectly brittle in tension, with Mohr-Coulomb-like dependence of shear resistance from compressive stress). Moreover, non-linear geometry condition is included. The results obtained on a masonry arch, loaded at quarter-span, are presented in Figure 12. These results have been compared with limit analysis and laboratory tests ones, showing the reliability of these kind of models.

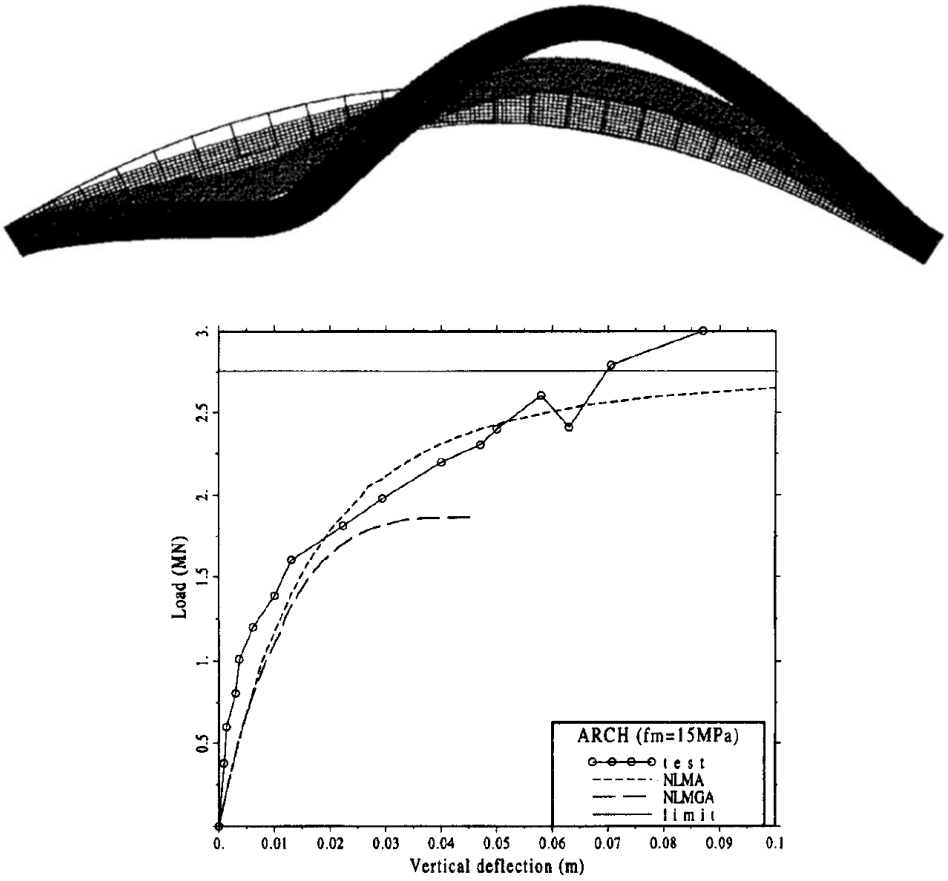

Figure 12 – Collapse configuration of a masonry arch and comparison between numerical model results (Non-Linear Material Analysis and Non-Linear Material and Geometry Analysis) experimental and limit analysis one. (Molins and Roca, 1998).

3. THE REINFORCED ARCH METHOD

Masonry arch is one of the most diffused architectonical element in historical structures, since the Roman period. Most of the heritage buildings and constructions present nowadays, built before the advent of reinforced concrete at the end of the 19th century, are based on the presence of arched and vaulted structures. Arches are especially suitable to withstand vertical uniform loads, because of their ability to work only in compression, that is particularly suitable for masonry, which typically has a relevant compressive strength, but a poor tensile capacity. For this reason, arches can suffer from the presence of horizontal loads (e.g. seism) or non-uniform vertical ones (Figure 13), especially if the amount of compression between the arch element is low, because of the uprising of tensile stresses. These aspects typically cause hinges opening, that can lead to relevant permanent deformations or even to the collapse of the structure, when the maximum number of hinges is reached and the mechanism is activated.

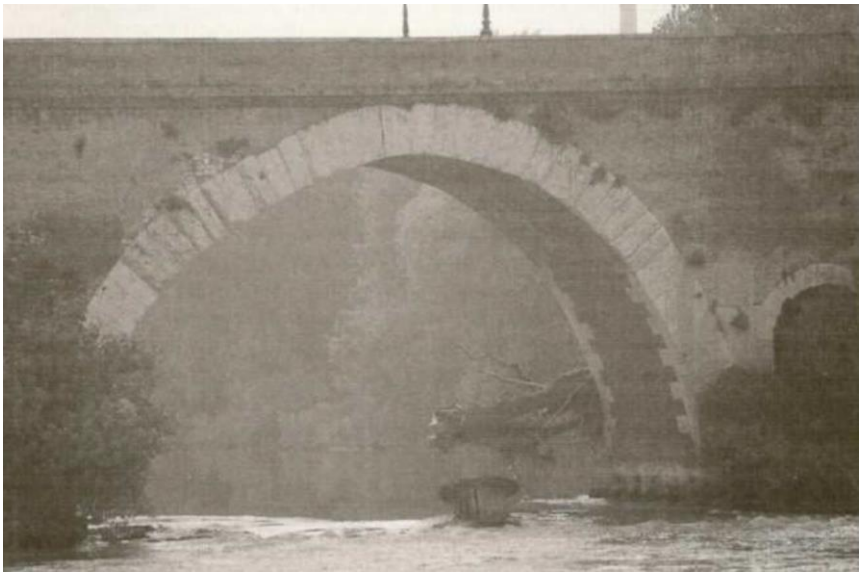

Figure 13 – Deformed masonry arch in the roman Milvio bridge in Rome. (Giglio, 2008).

3.1 Features of the R.A.M. Strengthening Technique

The Reinforced Arch Method is a rather recent strengthening technique, developed by Prof. Lorenzo Jurina at Polytechnic University of Milan (IT), based on the application of steel post-tensioned cables at the extrados or the intrados of masonry arches and vaults (Jurina, 2012). This technique improves the response of the structure because of:

- Providing tensile resistance on one side of the structure, so as to contrast the opening of some hinges, preventing the full formation of the complete mechanism;

- Applying an additional state of uniform compression that is able to re-centre the thrust line and therefore increases the geometrical safety factor of the arch or the vault;
- Improving the resistance to shear failure between blocks (sliding), due to the increment of compression inside the structure.

All of these aspects have been proving, through both experimental tests and actual interventions on real structures (Figure 14), the great suitability of this procedure for the consolidation of historical masonry structures. In fact, tests have shown that both resisting capacity and ductility are significantly improved.

Figure 14 – Examples of strengthening interventions through the RAM: a masonry arch at Villa Borromeo, Senago (MI), IT, (Jurina, 2003) and a ribbed vault in St. Caterina church in Lucca, IT, (Jurina, 2014).

The RAM can also be interpreted as both a *passive* and an *active* strengthening technique. The first definition is due to the passive capability of providing extra strength, connected with the high tensile resistance of the steel cables. This is aimed at suppling the typical extremely low value of this parameter in masonry. This aspect is the principle of most of the strengthening techniques used nowadays, even the most recent ones, such as FRP and FRCM application. Nevertheless, the RAM has the peculiar characteristic of being also an *active* technique. In fact, the post-tensioning of cables induces suddenly an additional compressive state to the masonry, that increases immediately the safety of the structure, by re-centring the line of thrust. The effect of post-tension is, in other words, an active confinement applied to the arch. If we consider a semi-circular arch, the action induced at the structure is a constant radial distributed load, that depends on the arch radius (Figure 15). The active attitude of the RAM entails also the possibility to re-calibrate the post-tension in case of loss of tension, or when the conditions of the structure require it. The permanent presence on the cables of anchors for tensioning allows that. This is a highly remarkable aspect, since in other strengthening procedures this possibility

is not granted. These characteristics make this technique particularly suitable for a possible *incremental approach* to the strengthening intervention, that requires the possibility to rearrange the amount of reinforcement by checking the response of the structure through direct measuring or even monitoring systems. The incremental approach is highly cutting-edge in strengthening of historical structures: this makes the RAM an updated procedure, despite it encompasses the usage of mainly traditional materials, such as steel.

Moreover, the absence of bonding, besides its low invasiveness, permits also sliding between steel cables and the underlying structure during external loading (e.g. seism): this avoids unwanted de-bonding failure, which usually happens in other strengthening systems that require a certain amount of static shear resistance between the original structure and the reinforcement. In fact, the RAM transfers the confinement load mainly in the radial direction. The presence of shear is connected only with friction between cables and masonry, but usually sliding is allowed. This permits also a redistribution of forces between structure and reinforcement during external loading.

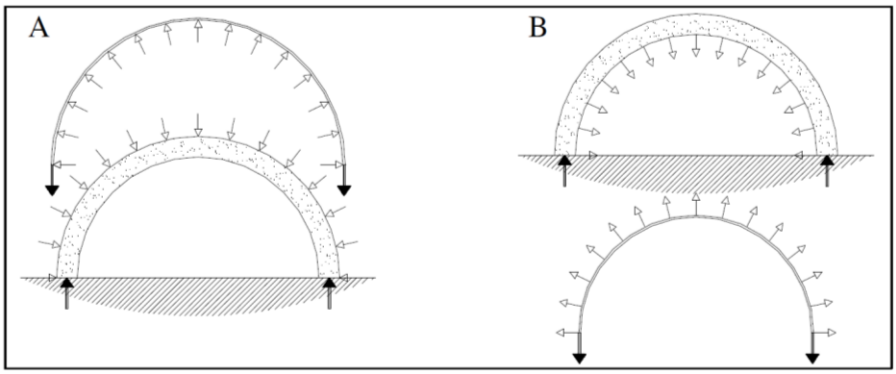

Figure 15 – Interaction forces, between arch and steel cables, applied at the extrados (A) or at the intrados (B), induced by post-tensioning. (Jurina, 2012).

As shown in Figure 15, this technique can be applied at the e*xtrados* or at the *intrados* of the arch. The first case is the most common one, since is the less aesthetically invasive when the visible part of the structure is the intrados, as in most of the cases (e.g. arch-bridges, church vaults, etc.). The second case, instead, is applied mostly when the extrados is not accessible, or it is too complex or invasive for the rest of the structure (e.g. infilled vaults that need a deep dismantling to reach the extrados). Obviously, when the cables are applied at the intrados, proper anchorage must be realized to transfer the radial load at the masonry structure, while in the case of cables at the extrados the load is transferred by simple contact. In the case of relatively small arches and vaults, the anchoring of cables is carried out through the application of steel devices in the lateral masonry walls. In the case of arch bridges, instead, the anchors can be applied even by means of micro-piles in the surrounding soil. Often cables are not in direct contact with masonry, but, especially when the entity of the post-tension is high, a layer of mortar or other devices (Figure 16) can be applied to create the contact, to distribute better the

confinement action. In some cases, as in the one of cables at the intrados, even some small pulley can be fixed to the masonry, to let the cable slide (Figure 14).

Figure 16 – Monastero degli Ovietani di Nerviano (MI): devices for redistributing the confinement due to cable tension (Jurina, 2002).

One of the main features of the RAM, even in comparison with other strengthening procedures, is its remarkable reversibility. This is probably the most distinguishing feature of this type of technique. In fact, the invasiveness of the interventions, to be carried out to apply the steel cables, is very low. The most damaging practise is limited to some drilling on the masonry units, in the case of application of cables at the intrados, or the casting of some mortar to prepare the surfaces of the arch/vault. Therefore, the permanent damage to the original structure is almost null. All the steel devices can be relatively easily dismantled, bringing again the arch to its original conditions. Also, the steel devices can be easily substituted in case of damage or replaced with better ones in case of the improvement of the technology available.

Figure 17 – Interventions through traditional materials: ring confinement of a stone column (left) and post-tensioned cables at extrados of cross-vaults (right) (Jurina, 2002).

Compatibility is one of the most required feature for intervention on historical structures. The RAM encompasses the usage of manly traditional materials, especially steel. Steel compatibility in this case is high, since there is no chemical bonding between cables and masonry. From this point of view, RAM can be seen not only as an innovative technique, but also as a *traditional* one, comparable to iron and steel confining and tying (Figure 17), that have been among the most diffused and effective ones throughout the history of consolidation and restoration. When the cables are applied at the intrados of the arch or the vault, the invasiveness is higher, especially in terms of visive impact. Nevertheless, this is compliant with the principle of *not hiding the intervention* modifying the integrity of the existing structure. Applying visible reinforcement is sometimes more *respectful* of the historical construction than hiding it. This is in general the case of consolidation through post tensioned-cables, especially when hiding them could compromise the original state of the structure, and therefore its value as heritage.

The RAM can be applied not only to arches and barrel vaults, but also to more complex structures, such as domes or ribbed vaults. The basic principle is the same, with the addition of the possibility to apply confinement force even in the horizontal plane. It is well-known that domes are affected from cracking along the meridians, due to the natural presence of a tensile stress state along the parallels at the base. These cracks can be contrasted by applying post tensioned cables along the parallels (Figure 18). The addition of confinement along the meridians contributes to stabilize the dome, for the same reasons of the case of an arch, explained above.

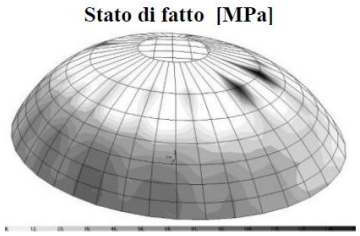

Figura 4. Tensioni massime all'intradosso della cupola per sisma (+Y + 0,3X).

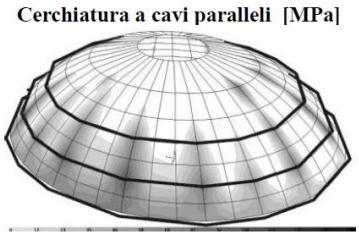

Figura 5. Tensioni massime all'intradosso della cupola per sisma (+Y + 0,3X).

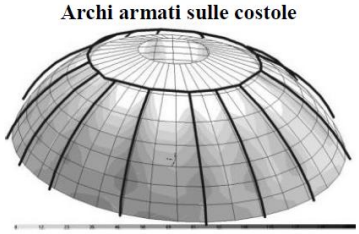

Figura 6. Tensioni massime all'intradosso della cupola per sisma (+Y + 0,3X).

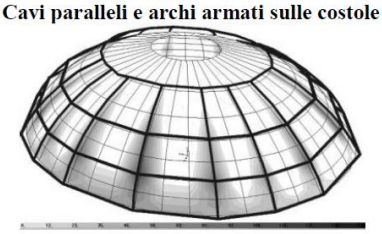

Figura 7. Tensioni massime all'intradosso della cupola per sisma (+Y + 0,3X).

Figure 18 – Santa Caterina's church dome: FE simulation of the intervention with post-tensioned cables at the extrados along meridians, parallels and both (Jurina, 2014).

Post-tensioned cables are suitable also for other applications, such as for instance consolidation of curtain walls and towers (Figure 19). In these cases, the tensioned tendons act to stabilize the structure, thanks to the extra compression provided, but especially for the increase of horizontal global stiffness. This last aspect is important to prevent large displacement at top of slender structures, in particular due to seismic actions.

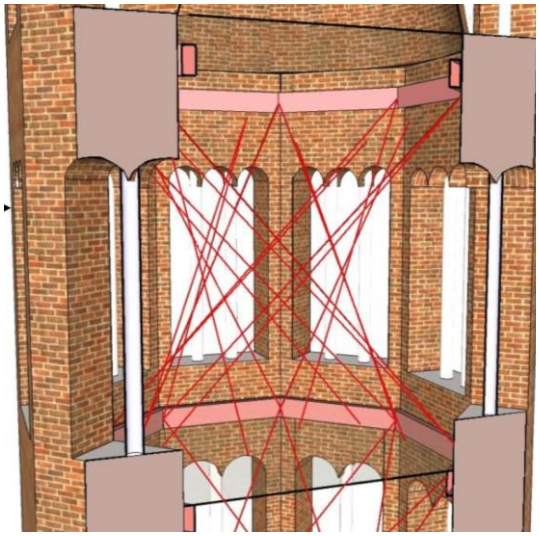

Figure 19 – Examples of alternative use of post-tensioned cables: consolidation of a bell tower (left), (Jurina, 2015) and of a free-standing wall (right) (Jurina, 2003).

3.2 Experimental Results on Scale Models

The effectiveness of the RAM strengthening technique has been broadly tested and proved by a great number of experimental tests. More than 500 tests on different scale models have been carried out by Prof. Lorenzo Jurina, from the Polytechnic University of Milan, showing a wide improvement of the response of arches due to the application of the RAM. This in terms of increase of load capacity, especially against horizontal actions, and even in terms of ductility, that is an increase of the displacement that the structure can withstand before collapsing.

The first campaign, supervised by Prof. Jurina, was performed on real scale brick-mortar arches in 1996. Semi-circular arches of 2 m span, 12 cm of depth and 25 cm of width were tested under vertical punctual loading at one quarter of the span, by means of hydraulic jacks (Figure 20). Displacements were measured in different points of the arch during the tests. Four types of arches were tested:

- Unreinforced;
- Reinforced with a not connected reinforced concrete layer;
- Reinforced with a connected reinforced concrete layer;
- Reinforced with post-tensioned cables (RAM).

Results shown a relevant increase of load capacity, comparable with the ones of arches reinforced with reinforced concrete, but ductility is much higher. Load capacity increases with the post-tension level. Collapse occurred due to compressive failure at hinges (Jurina, 1999).

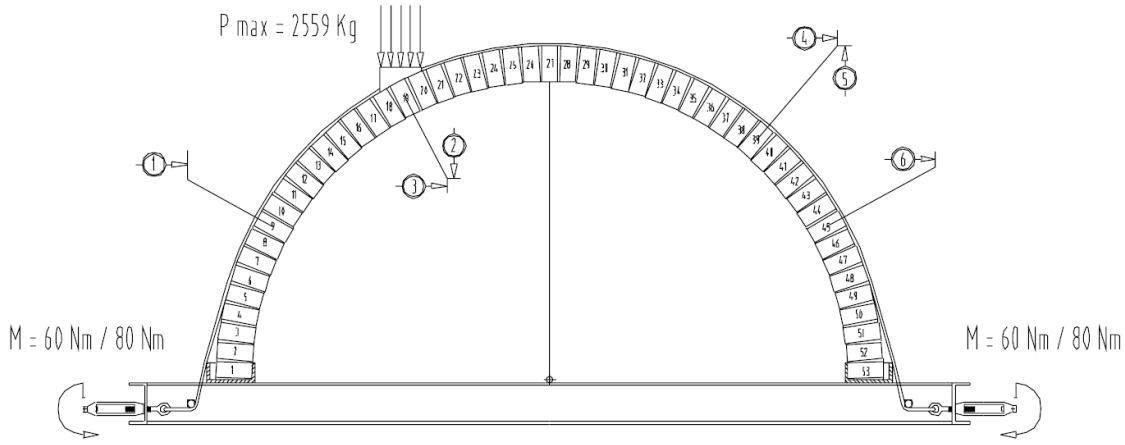

Figure 20 – Test campaign on real scale masonry arches. (Jurina, 1999).

Several other experimental campaigns have been performed on many other models by Prof. Jurina. A more recent campaign, on reduced-scale dry-joints wooden models, is presented. The results of this campaign have been used to validate numerical models, presented in the following chapters of this work. Arches of different geometries have been tested, under punctual vertical load, at different rates of the span: a semi-circular one, a gothic one, two flattened at the top, a camber arch and one with different curvatures. In the following treatise, for the sake of brevity, only the semi-circular one will be presented.

The arch concerned has a 1200 mm net span, 100 mm of depth and 100 mm of width. It is made of 77 beechwood elements, of density equal to 600 kg/m^3. The vertical incremental load was applied by means of a wire connected to a steel device at the centre of the blocks, at different fractions of the span: 1/12, 1/6, 1/4, 1/3, 5/12, 1/2 (Figure 21). To allow this, steel bars were previously inserted in correspondence with the loading blocks, so as to enable the loading device to be connected to the structure.

The reinforcement was applied by means of two steel cables of 2 mm of diameter, positioned either at the extrados or at the intrados. While the cables at the extrados could transfer the load by simple contact, the ones applied at the intrados needed steel loops, screwed to the wooden elements, to ensure the confinement effect (Figure 22). These loops slightly enlarged the effective depth of the arch. Nevertheless, this has not been considered in the numerical modelling phase.

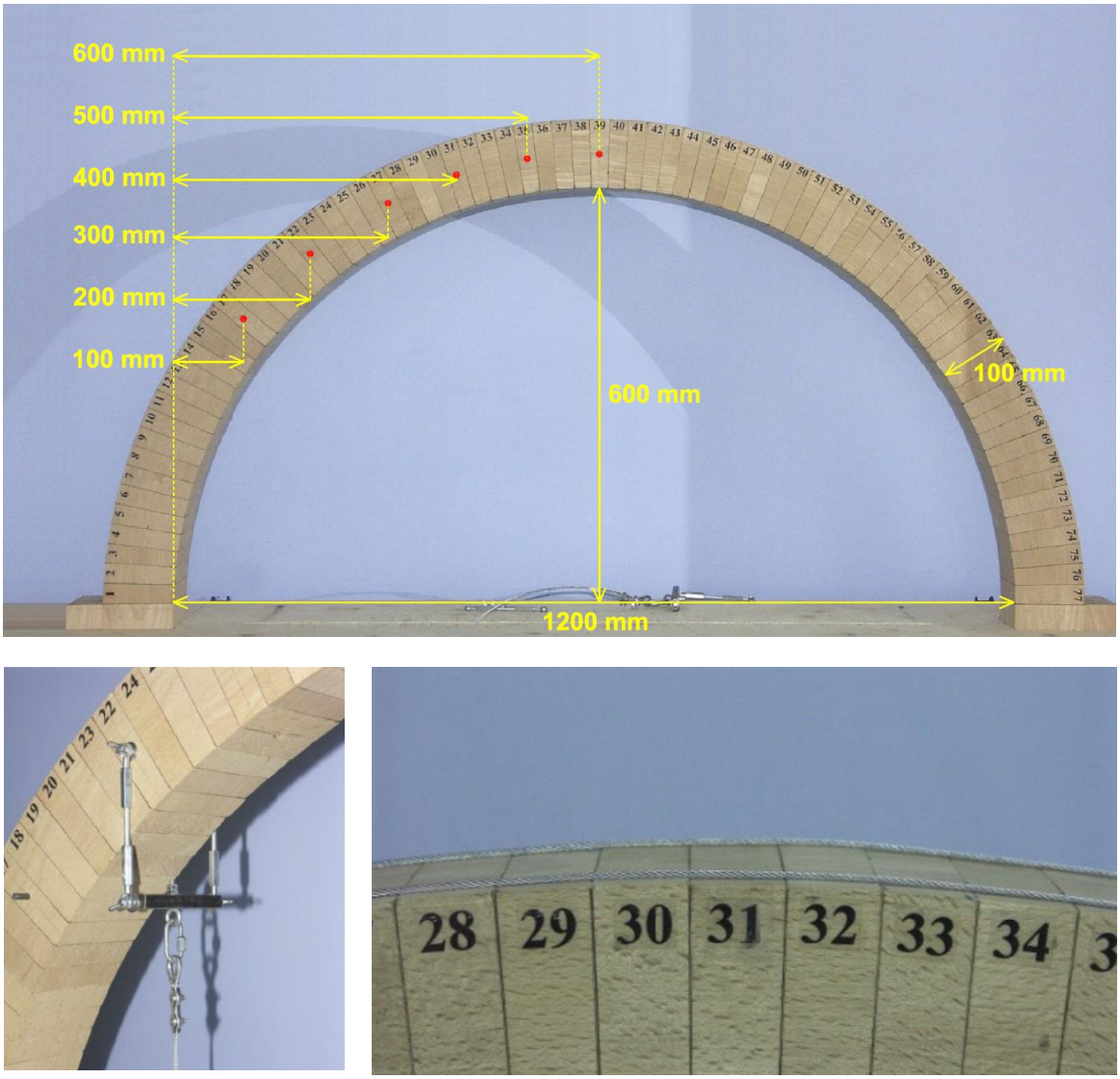

Figure 21 – Top: semi-circular arch tested for vertical incremental load applied at different positions, highlighted with a red circle. Bottom: details of the loading device (left) and cables at the extrados (right). (Giglio, 2008).

During the tests, that consisted on applying an external incremental load by means of controlled wire force, the loading point moved both vertically and horizontally. To ensure that the cable would keep exactly vertical, a slot was cut on the table along the span. All the tests were filmed with a camera, to capture the exact hinged configuration at collapse.

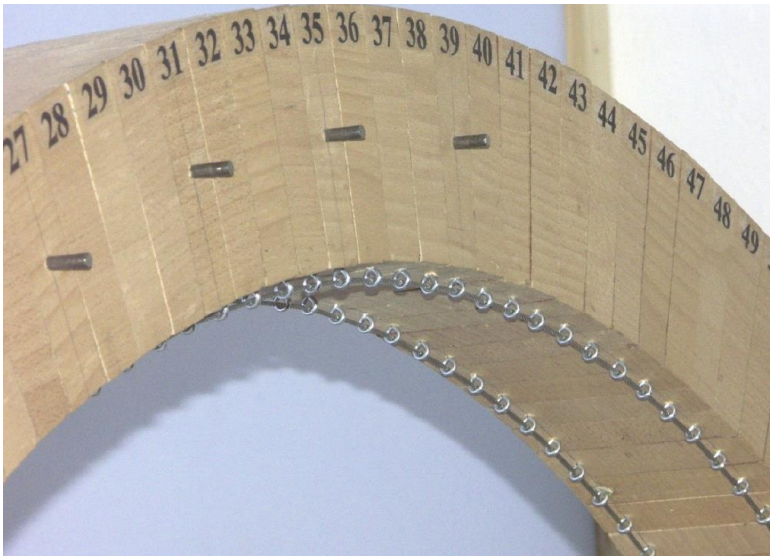

Figure 22 – Detail of the cables applied at the intrados. (Giglio, 2008).

Two main types of application of the reinforcement were produced: one with cables able to slide all along the edges of the arch during the external loading phase, to maintain the cable tension constant (and therefore the confinement pressure on the arch), and another with the cables anchored to the supporting table after the tensioning, to simulate the actual condition of post-tensioning. Different levels of cable tension were tested, as reported in Table 1, that summarises the tests setups.

Cables force [N]	Sliding cables		Anchored cables
	Extrados	Intrados	Extrados
	Load positions [mm]	Load positions [mm]	Load positions [mm]
0	100, 200, 300, 400, 500, 600	100, 200, 300, 400, 500, 600	300, 600
20	100, 200, 300, 400, 500, 600	-	-
39	100, 200, 300, 400, 500, 600	-	-
59	100, 200, 300, 400, 500, 600	-	-
79	100, 200, 300, 400, 500, 600	-	-
98	100, 200, 300, 400, 500, 600	100, 200, 300, 400, 500, 600	300, 600
196	100, 200, 300, 400, 500, 600	100, 200, 300, 400, 500, 600	300, 600
294	100, 200, 300, 400, 500, 600	100, 200, 300, 400, 500, 600	300, 600

Table 1 – Semi-circular arch tests setups. (Giglio, 2008).

No failure due to sliding between blocks was observed in all the tests. Collapse always occurred due to the achievement of the maximum number of admissible hinges, with the consequent mechanism formation and loss of equilibrium.

Figure 23 – Collapse mechanisms for arches loaded at ¼ of the span, with the formation of four hinges: cables at the extrados (top) and cables at the intrados (bottom). (Giglio, 2008).

In the case of sliding cables, therefore with a constant confinement force applied to the arch (neglecting significant curvature variations due to the deformations), results showed a great improvement of the load capacity of the arch (Table 2 and Table 3), in both the reinforcement arrangements (at the intrados and at the extrados). The increase of the capacity has revealed a quasi-linear dependence on the entity of the cable force, that can be noticed in Figure 24 and Figure 25. In these figures is highlighted the decrease of the capacity when the load position moves towards the cable centre, saving a slight increase in at half span. In most of the cases, it was noticed a slightly higher improvement of the capacity in the case of the reinforcement at the intrados, as visible in Figure 26.

Collapse load [N] - sliding cables at the extrados						
Cables force [N]	Load position [mm]					
	100	200	300	400	500	600
0	51	23	10	8	6	7
20	108	59	37	31	26	31
39	152	86	59	51	51	53
59	188	112	85	75	74	80
79	231	139	108	98	97	106
98	258	160	126	119	118	126
196	434	284	235	220	230	241
294	603	411	341	333	335	364

Table 2 – Collapse load for sliding cables at the extrados. (Giglio, 2008).

Collapse load [N] - sliding cables at the intrados						
Cables force [N]	Load position [mm]					
	100	200	300	400	500	600
0	51	23	10	8	6	7
98	267	163	119	108	109	137
196	452	315	244	235	247	259
294	704	486	363	344	366	431

Table 3 – Collapse load for sliding cables at the intrados. (Giglio, 2008).

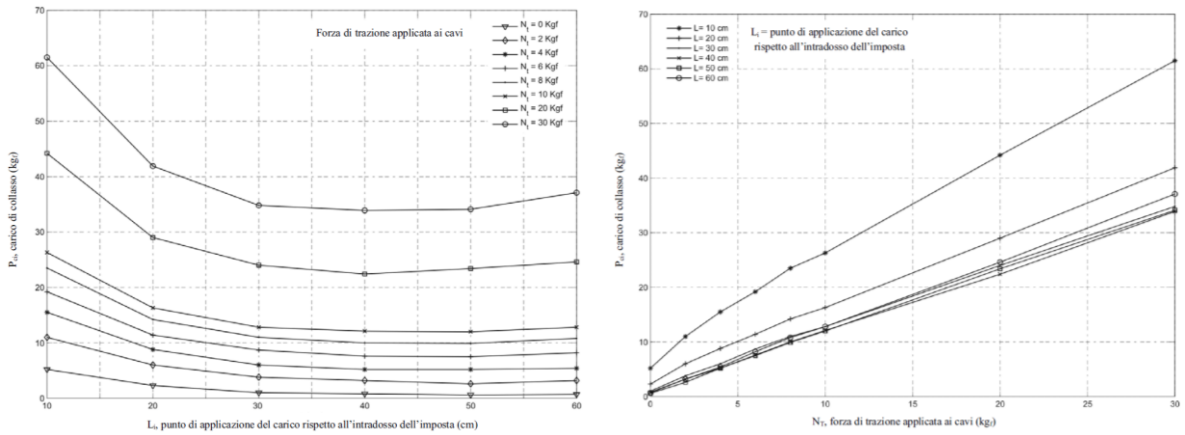

Figure 24 – Sliding cables, reinforcement at the extrados: collapse load vs load position (left), collapse load vs cable force. (Giglio, 2008).

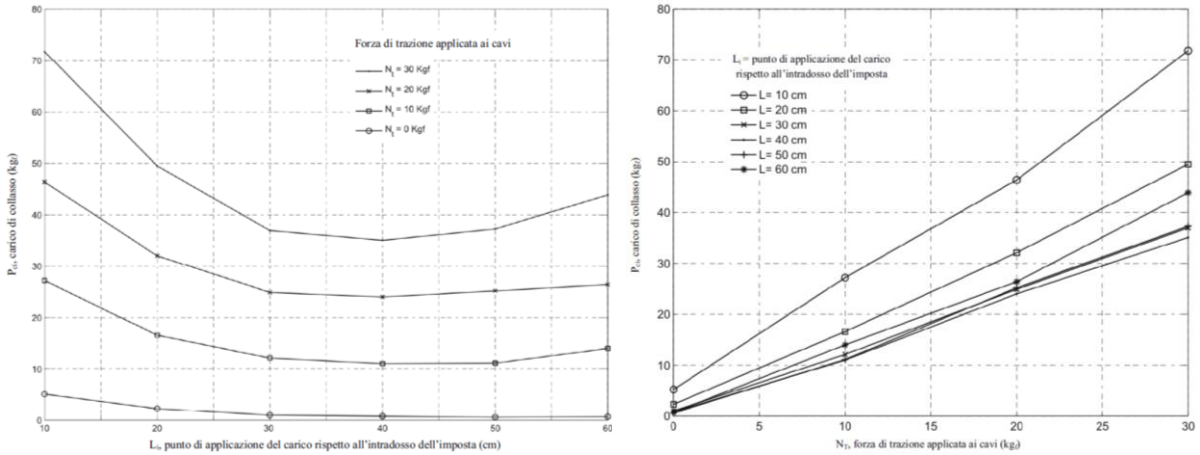

Figure 25 - Sliding cables, reinforcement at the intrados: collapse load VS load position (left), collapse load VS cable force. (Giglio, 2008).

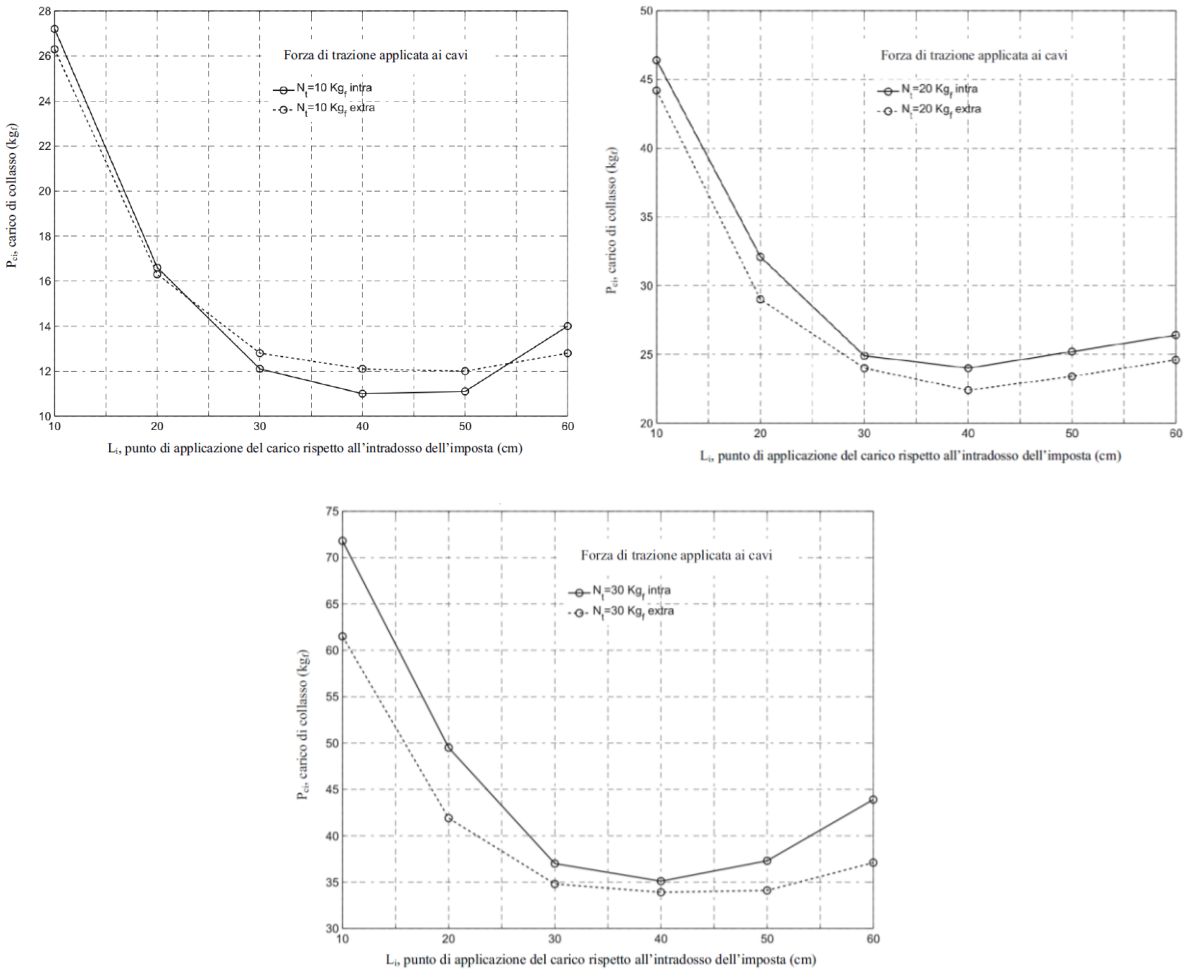

Figure 26 – Sliding cables, collapse load VS application point: comparison of results from reinforcement at the extrados and the intrados, for different cable force (from top left, clockwise: 98.1 N, 196.2, 294.3 N). (Giglio, 2008).

Experiments with the reinforcement cables anchored to the supporting table have also been performed. In the previous cases, in fact, the cables could slide freely along the arch circumference, during the external loading phase. This permitted to theoretically maintain a uniform confinement force all along the arch during the whole test (neglecting the variation due to curvature changes, as stated above). In this second type of tests, instead, the cable was constrained at both its ends, to provide further rigidity at the whole system. These tests were performed on models of the same geometry described above, with the only addition of anchors underneath the base, to block the cables sliding (Figure 27).

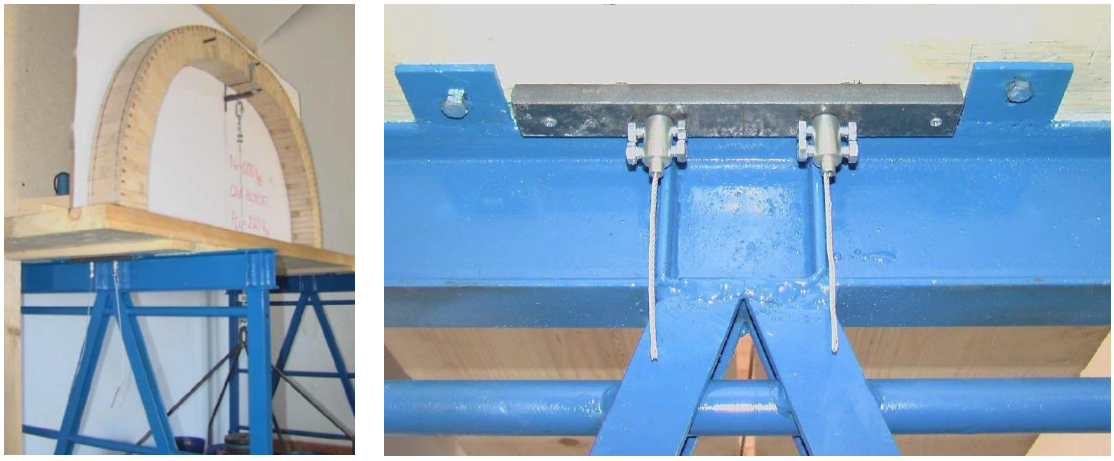

Figure 27 – Details of overall tests setup (left) and anchors detail (right). (Giglio, 2008).

The plan of the tests entailed the application of a punctual load at two positions: ¼ and ½ of the span, with the application of 4 levels of post-tension: 98 N (10 kgf), 196 N (20 kgf) or of 294 N (30 kgf). The reinforcement cables were applied only at the extrados.

The collapse was not reached in any test, showing a dramatic increase of the capacity of the arch. The loading phase was carried out by increasing of 392 N (40 kgf) stepwise the punctual load, until 2354 N (240 kgf), and then unloading with the same load step size. In every step, the amount of displacement in some significant points of the arch was measured, so as to enable the possibility to trace some load/displacements curves (Figure 29 and Figure 30). The deformed shape of the arch was also monitored graphically, by means of special pens connected to the system, able to follow the arch deformation and trace lines on a vertical paper support (Figure 28). With these traces, it was also possible to measure the cable elongation (Table 4) and the hinges opening at the point of maximum load applied (Table 5), for the case loaded at ¼ of the span.

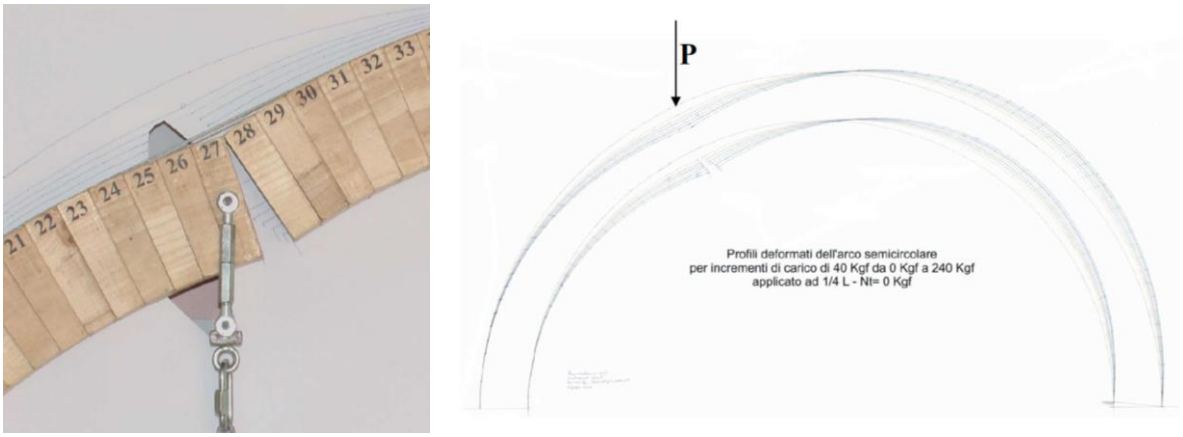

Figure 28 – Details of the traces of the deformed shapes taken. (Giglio, 2008).

For the sake of brevity, only results concerning vertical displacements of the cases of no post-tension and 294 N are reported. Both load positions have been considered.

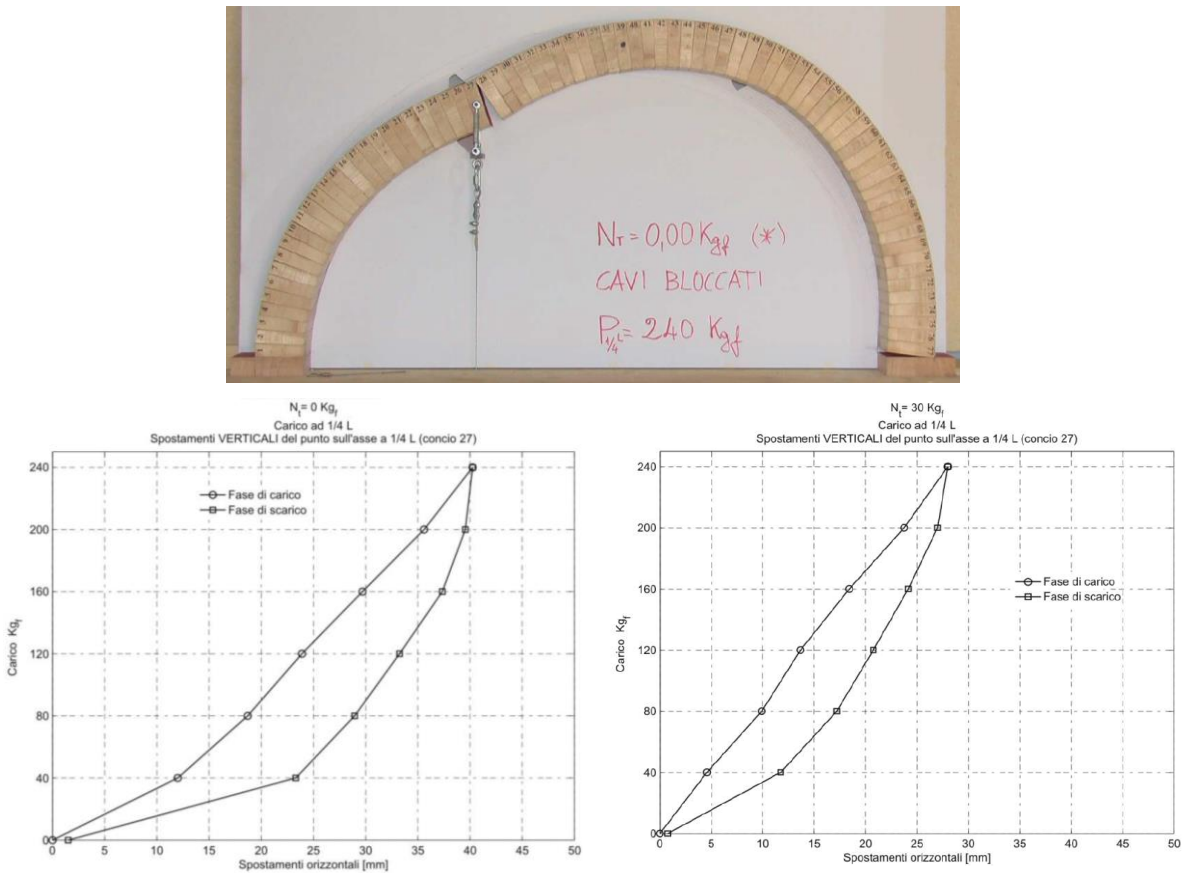

Figure 29 – Anchored cables tests, load at 1/4 of the span. Top: Configuration at maximum load applied, no post-tension case. Bottom: load/vertical displacements curves at loaded point, no post-tension case (left) and 294 N post-tension case (right). (Giglio, 2008).

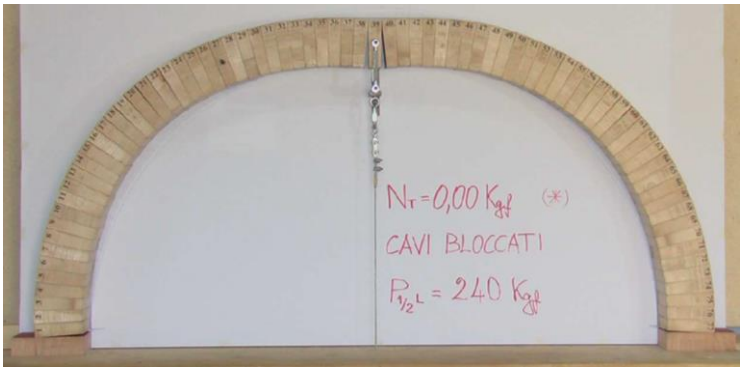

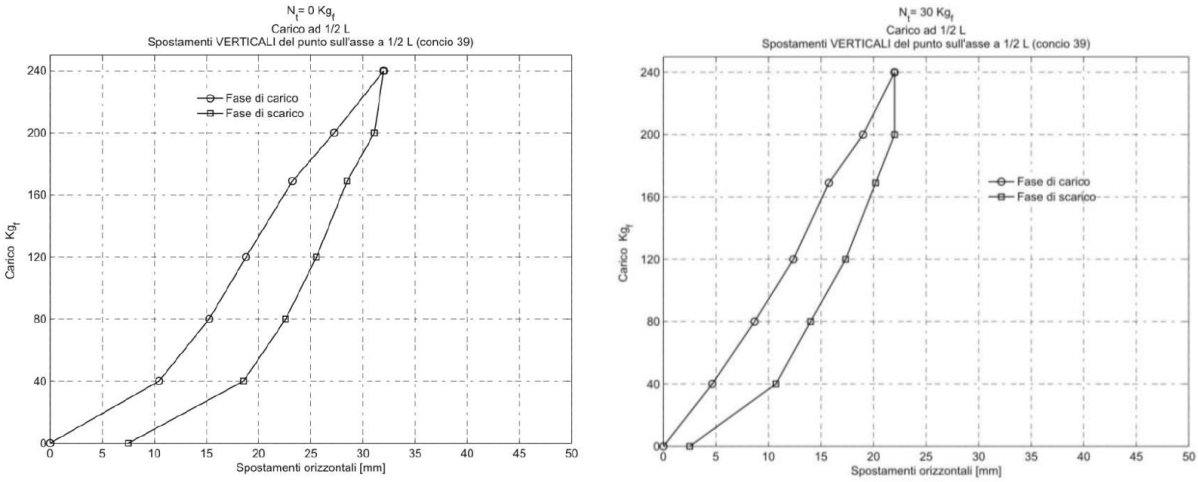

Figure 30 - Anchored cables tests, load at 1/2 of the span. Top: Configuration at maximum load applied, no post-tension case. Bottom: load/vertical displacements curves at loaded point, no post-tension case (left) and 294 N post-tension case (right). (Giglio, 2008).

N_T = 0,00 kg_f	Δ_l = 23,00 mm
N_T = 10,00 kg_f	Δ_l = 18,00 mm
N_T = 20,00 kg_f	Δ_l = 15,00 mm
N_T = 30,00 kg_f	Δ_l = 13,00 mm

Table 4 – Cable elongation at maximum external loading for each prestress level (load at ¼ of the span). (Giglio, 2008).

Nt = 0 kgf	5....14 = 10,75 mm	27....28 = 24,38 mm	43....63 = 21,69 mm	77.. = 10,22 mm
Nt = 10 kgf	1....19 = 13,92 mm	27....28 = 20,26 mm	43....64 = 20,82 mm	77.. = 8,67 mm
Nt = 20 kgf	4....20 = 11,53 mm	27....28 = 17,93 mm	44....63 = 18,43 mm	77.. = 7,61 mm
Nt = 30 kgf	5....17 = 9.60 mm	27....28 = 16,00 mm	43....63 = 17,70 mm	77.. = 7,52 mm

Table 5 – Hinge opening at maximum external loading for each prestress level (load at ¼ of the span). (Giglio, 2008).

4. MODELS USED

Numerical models have been used for the aim of this work. They have been used to simulate the experimental results presented above. The results obtained have been double-checked also in comparison with limit analysis, both with static and kinematic approaches, by means of computer programs. The tools used are:

- Finite element macro-models;
- Finite element micro-model, with interfaces;
- Kinematic limit analysis with a commercial program (Ring);
- Static limit analysis with an Excel spreadsheet.

4.1 Finite Element Models

Finite element models have been used for simulating the experimental campaign described in the previous chapter. Macro-models entail the application of one only material for the arch body, based on masonry materials characteristics, calibrated so as to capture the results from the wooden blocks experiments. Even micro-models, with perfectly elastic blocks and opening interfaces, have been produced. All the Finite Element models have been developed through the software Diana FEA.

The elements used for discretizing the arch body are 4 or 8-noded plane stress elements (Q8MEM or CQ16M), with two DOF per node (Figure 31). Plane stress elements permitted to assign the real thickness of 100 mm to the arch. These plane elements present, in the regular setup, 2x2 Gauss integration points. The number of elements used to discretize the arch depth varies from 12 to 16, for a size of about 6 to 8 mm, depending on the case analysed.

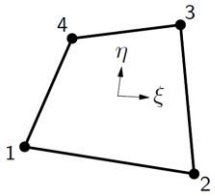

$$u_i(\xi,\eta) = a_0 + a_1\xi + a_2\eta + a_3\xi\eta$$

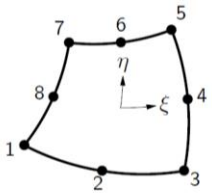

$$u_i(\xi,\eta) = a_0 + a_1\xi + a_2\eta + a_3\xi\eta + a_4\xi^2 + a_5\eta^2 + a_6\xi^2\eta + a_7\xi\eta^2$$

Figure 31 – Q8MEM plane element (left) and CQ16M plane element (right). (DIANA FEA User's Manual Release 10.1, 2016).

All the models have in common the application of gravity load as a volume force in the -Y direction. The external incremental load was applied in terms of an imposed vertical displacement in -Y direction, at the centre of the depth, for different span fractions. Supports were applied as horizontal and vertical translational constraints at the impost (Figure 32). The analysis carried out is a non-linear static one, even in some cases with non-linear geometry (Total or Updated Lagrange). First the gravity was applied in 4 steps, then also the vertical incremental displacements were applied in a variable number of steps,

depending on the case analysed. Newton-Raphson method was used for solving the equilibrium at any load step, with a maximum number of iteration variable between 50 and 200. Control of convergence was applied in terms of energy, force and displacement, with tolerances respectively of $10^{-4} \div 10^{-2}$, 10^{-2}, 10^{-2}.

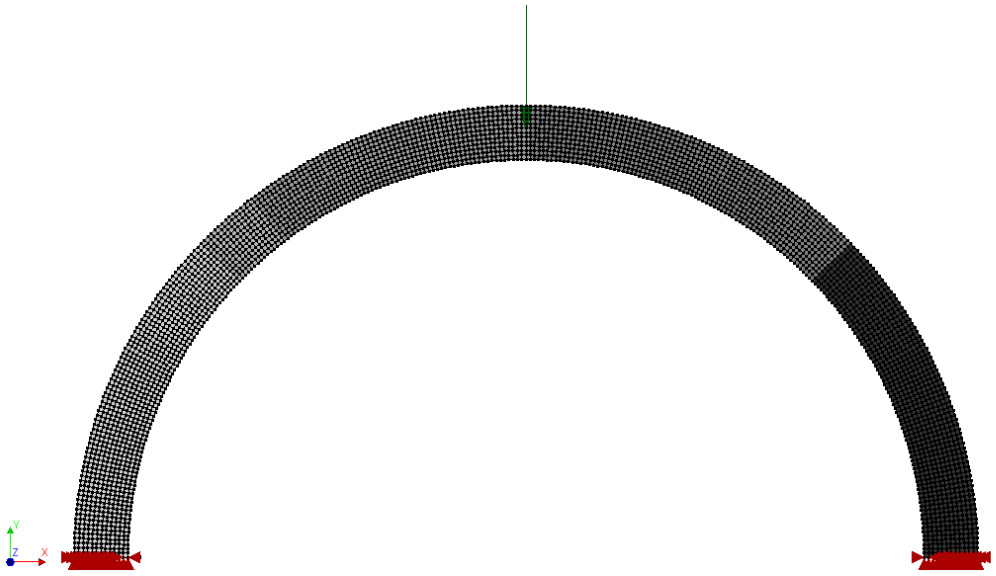

Figure 32 – Typical finite element discretization, load and supports used.

4.1.1 Macro-Models - Unreinforced

The macro-models used present on only material on the overall body of the arch. It has been modelled with the *Total Strain crack* approach (Vecchio and Collins, 1993), based on the smeared crack model, suitable especially for masonry and concrete. This mainly because, despite trying to simulate the behaviour of a rigid-block and dry-joints experimental model, this paper looks forward at the application of the RAM to the real masonry arches case. The total strain crack model is based on the assumption that the stress is evaluated in the directions which are given by cracks. Rotating cracks approach has been chosen: this means that the stress–strain relations are evaluated in the principal directions of the strain vector. The constitutive stress-strain law is different in compression and in tension, and unloading is secant. Concerning the tensile behaviour, linear-crack energy approach has been chosen, while for the compressive one, the parabolic is used (Figure 33).

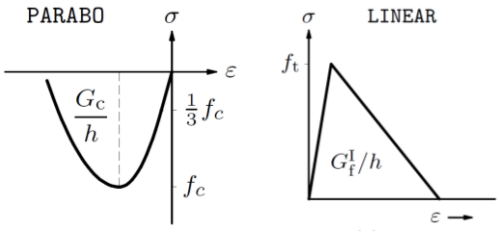

Figure 33 – Stress-strain paths chosen. (DIANA FEA User's Manual Release 10.1, 2016).

The value of the parameters used, listed in Table 6, are presented in the following chapters. These values were chosen in order to accomplish the peculiar case of dry joints (no tensile strength) and very resistant blocks (infinite compressive strength).

	Parameter	Notation	Unit SI
Linear	Young Modulus	E	N/m^2
	Poisson Ratio	υ	-
	Density	ρ	kg/m^3
Tensile	Tensile Strength	f_t	N/m^2
	Tensile Fracture Energy	G_f	N/m
	Residual Tensile Strength	f_{f_res}	N/m^2
Compressive	Compressive Strength	f_c	N/m^2
	Compressive Fracture Energy	G_c	N/m
	Residual Compressive Strength	f_{c_res}	N/m^2

Table 6 – Parameters of masonry due to total strain crack material in the macro-models.

Since the external load, consisting on imposed vertical displacements, was applied at the centre of the arch depth, to avoid unwanted local cracking, a limited area around the loading point was modelled with a higher tensile strength.

4.1.2 Macro-Models – Reinforced

Two main types of reinforcement have been applied:

- confinement as equivalent radial load;
- actual modelling of steel cables as reinforcement.

The first case simply consists on the addition of an equivalent radial load to the unreinforced macro-model described above (Figure 34 and Figure 35). This load depends on the entity of cables-post tension and the curvature of the cables.

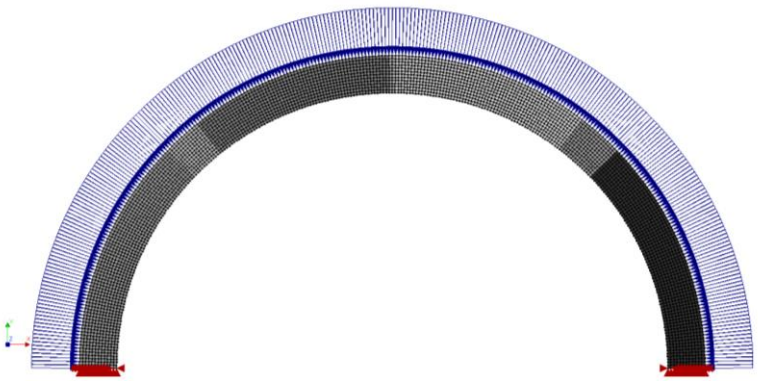

Figure 34 –Model with equivalent radial load reinforcement at the extrados.

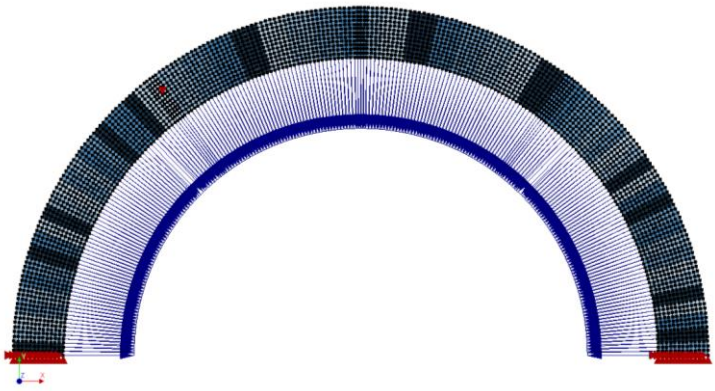

Figure 35 - Model with equivalent radial load reinforcement at the intrados.

As stated above, cables were also modelled. The cables were introduced in the phased analysis after the application of the gravity load, and the gradually post-tensioned by means or simple punctual force (Figure 36).

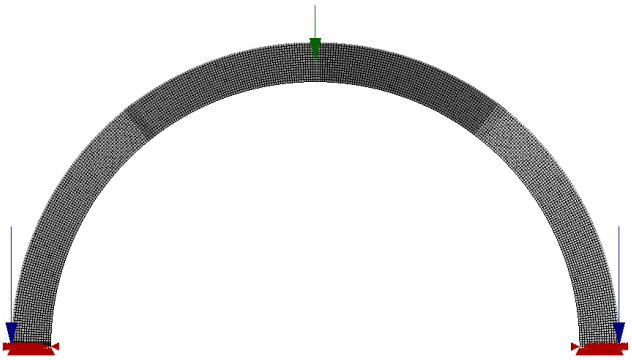

Figure 36 – Macro-model with physical cables at the extrados (notice the application of post-tension).

These macro-models entail the use of one dimensional elements to discretise the cables. The element used to ensure compatibility with the linear plane ones, are 2-noded enhanced 2D trusses (L4TRU). These are essentially 2D truss elements, with the addition, compared to the regular ones, of the degrees of freedom perpendicular to the truss axis (Figure 37). The integration is direct (1 point). The use of truss elements, instead of cable ones, does not affect the results, since compression was never obtained in any result.

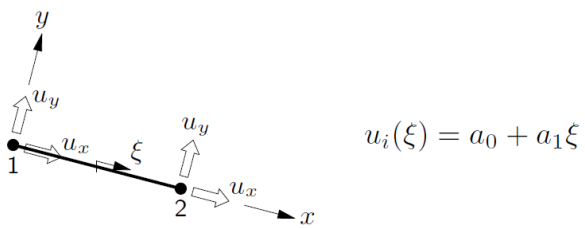

Figure 37 – L4TRU enhanced 2D truss elements (DIANA FEA User's Manual Release 10.1, 2016).

The truss elements were connected by means of interface elements. These elements are named L8IF. The thickness of these elements has been set equal to 0.1 mm, simulating a reasonable contact thickness between cables and arch underneath or above. The basic variables of these elements are the 4 nodal displacements of the two lines connected by the element. From these variables, relative displacements and tractions are derived, depending on the constitutive law assigned. Regular integration entails 2 Newton-Cotes integration points.

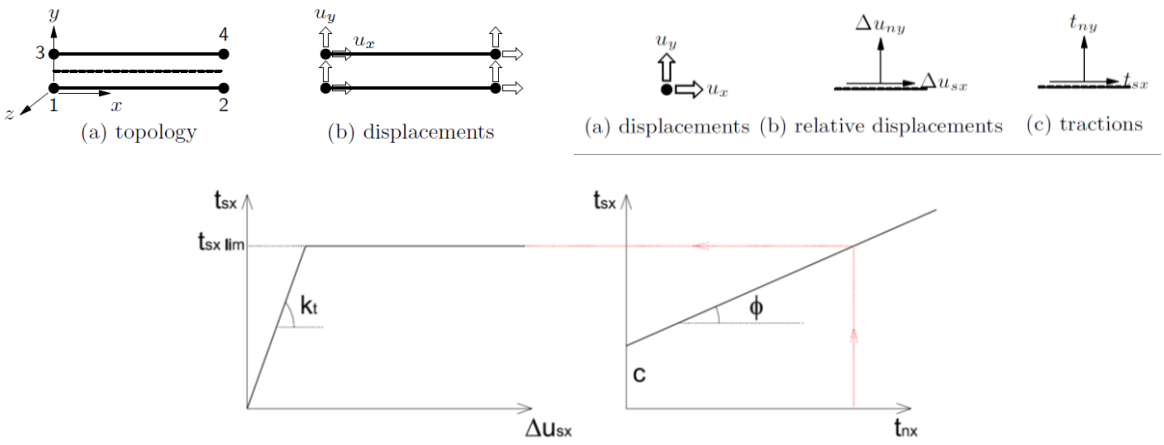

Figure 38 – 2D line interface element L8IF: geometry and variables (top) and Coulomb friction law (bottom) (DIANA FEA User's Manual Release 10.1, 2016).

The constitutive law chosen is a Coulomb friction (Table 7). In the case of cables at the extrados, gap opening was enabled. This means that the behaviour in the direction normal to the connection length (y) is governed by linear elasticity in compression, and free displacement with no resistance in tension. Shear sliding along the connection length (x), instead, is governed by the Mohr-Coulomb law (Figure 38). Therefore, the yield value of shear stress depends on the normal stress state.

	Parameter	Notation	Unit SI
Linear	Normal stiffness	K_n	N/m^3
	Shear stiffness	K_s	N/m^3
Friction	Cohesion	c	N/m^2
	Friction angle	ϕ	rad
	Dilatancy angle	ψ	N/m^2
Gap opening	Tensile strength	f_t	N/m^2

Table 7 – Interface modelling: Coulomb friction parameters to set.

The cables were modelled by simple linear elastic steel material (Table 8).

Parameter	Notation	Unit SI
Young Modulus	E	N/m^2
Poisson Ratio	υ	-
Density	ρ	kg/m^3

Table 8 – Linear elastic material properties.

4.1.3 Micro-Models - Unreinforced

To compare the results coming from macro-models, micro-models were also produced (Figure 39). This was done especially because micro-models are particularly suitable to simulate the behaviour of the experimental wooden arch. In fact, in the experiments the arch has no tensile strength and a very high compressive one. Micro-models allow to use discrete blocks with no resistance to hinge opening.

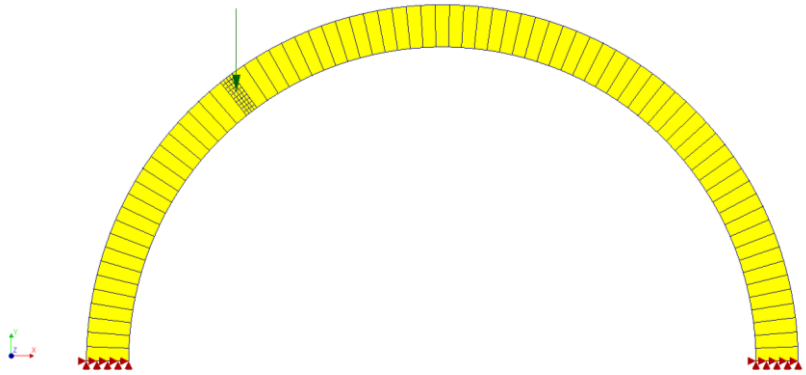

Figure 39 – Micro-models' geometry.

The model entails the presence of stiff linear elastic blocks, modelled with 2D linear plane stress elements (Q8MEM), and structural 2D linear interface elements (L8IF, explained above) along the edges of the voussoirs, oriented towards the arch depth. In this case, gap opening was allowed, with no tensile resistance. To avoid shear sliding failure, and simulate only rotational hinge opening, high values of friction angle and cohesion were chosen. Even a high value of normal stiffness was applied, to avoid relevant blocks superposition.

4.1.4 Micro-Models – Reinforced

The reinforced micro-models, as in the case of macro-models, entailed the use of both the reinforcement simulation procedures described above: uniform equivalent radial load and physical cables modelling.
In the case of the radial uniform load, the procedure is the same described above for the macro-models. The models with physical cables were discretized by means of quadratic elements (Figure 40), for both the 2D plane stress ones and the 2D trusses. The steel cables were represented by means of 2D truss-cable elements (CL6TR). These quadratic elements have two planar degrees of freedom (translations)

for each of the three nodes that compose them. The ordinary integration scheme used is based on 2 Gauss points.

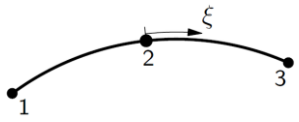

$$u_i(\xi) = a_0 + a_1\xi + a_2\xi^2$$

Figure 40 – 2D quadratic cable truss elements (CL6TR). (DIANA FEA User's Manual Release 10.1, 2016).

The interface elements, both for cable/arch friction and contact between voussoirs, have been chosen consequently to the quadratic order of the elements involved. Therefore, quadratic interface elements, named CL12I were applied (Figure 41). The principles are the same as for linear ones, despite having 3 + 3 nodes with 2 planar displacements each, and a 3 Gauss points integration scheme.

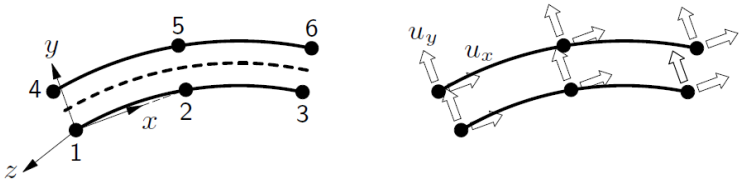

Figure 41 – CL12I interface elements. (DIANA FEA User's Manual Release 10.1, 2016).

Material features and analysis performed are exactly the same as for the macro-models.

4.2 Models based on Limit Analysis

With the aim of validating the results form FE models, simple tools based on limit analysis were used. These tools were able to determine the limit load by means of the safe theorem and the kinematic analysis (upper-bound theorem). The one based on the safe theorem consists on an Excel spreadsheet that determines the thrust line by changing manually some input data, so as to capture after some attempts the one corresponding to the limit load (Figure 42). The input data are the geometric characteristics of the semi-circular arch and the density. Then, changing the eccentricities of the thrust line at the impost and the horizontal thrust, the thrust line can be determined, given the punctual external load entity and its position. The spreadsheet permits also to include a radial distributed load, applied at the intrados or at the extrados of the structure, to simulate the effect of confinement due to reinforcement.

The tool based on the upper-bound theorem, instead, is an actual commercial program (Ring, by Limit State), that automatically determines the limit load, by scanning all the possible mechanisms of an arch (Figure 43). Also in this case the geometric data and density are required. For the position and the load inserted, the maximum load multiplier is computed.

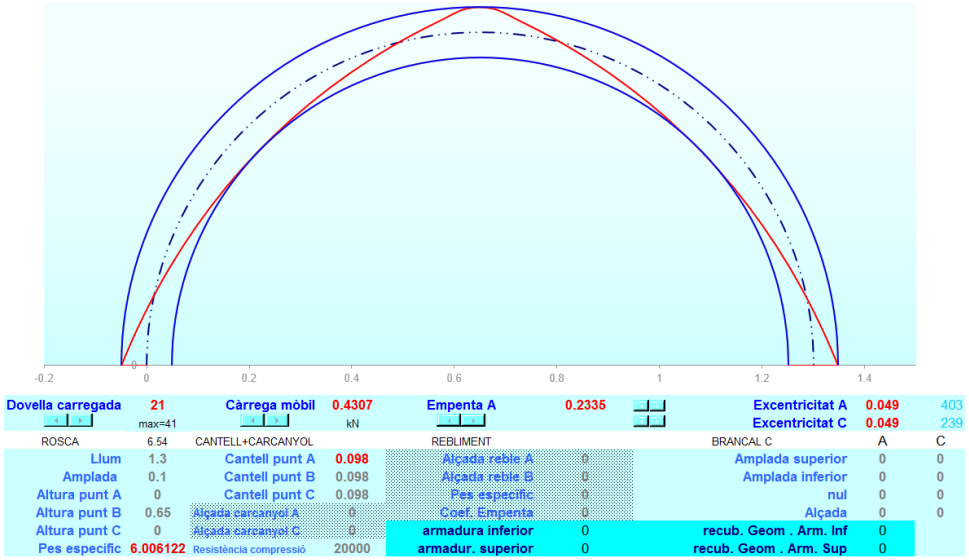

Figure 42 – Excel spreadsheet for graphic statics of semi-circular arches.

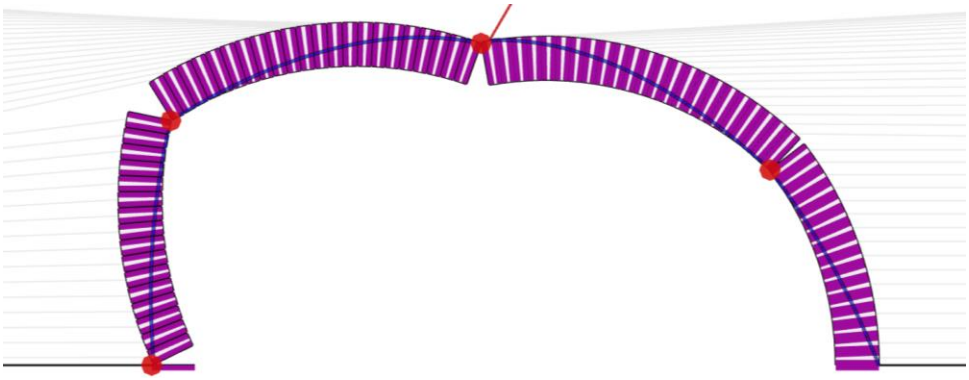

Figure 43 – Ring (Limit State) output configuration.

Unfortunately, the precision of the Excel spreadsheet is limited, especially for positions of the load close to the impost. This is due to the fact that the arch is discretized in a limited number of voussoirs: 41. Then, if the number of voussoirs is higher than 41, as in the case of the experimental arch concerned, the loaded one is not exactly definable. Therefore, results coming from Ring program should be rated as more precise.

5. LIMIT ANALYSIS RESULTS

5.1 Unreinforced Arch

Through the tools described in the previous chapter, firstly the unreinforced semi-circular arch has been analysed, in terms of maximum capacity for punctual loads. For the exact geometry of the experimental arch, both approaches (static and kinematic) showed values close to each other, but sensitively higher than the experimental ones, as shown in Table 9.

Load position (span fraction)	Collapse load [N]			Error	
	Experimental	Static (Excel)	Kinematic (RING)	Static (Excel)	Kinematic (RING)
1/12	51	82	98	60%	91%
1/6	23	37	43	62%	90%
1/4	10	25	26	155%	165%
1/3	8	19	19	140%	145%
5/12	6	16	16	177%	177%
1/2	7	18	18	166%	166%

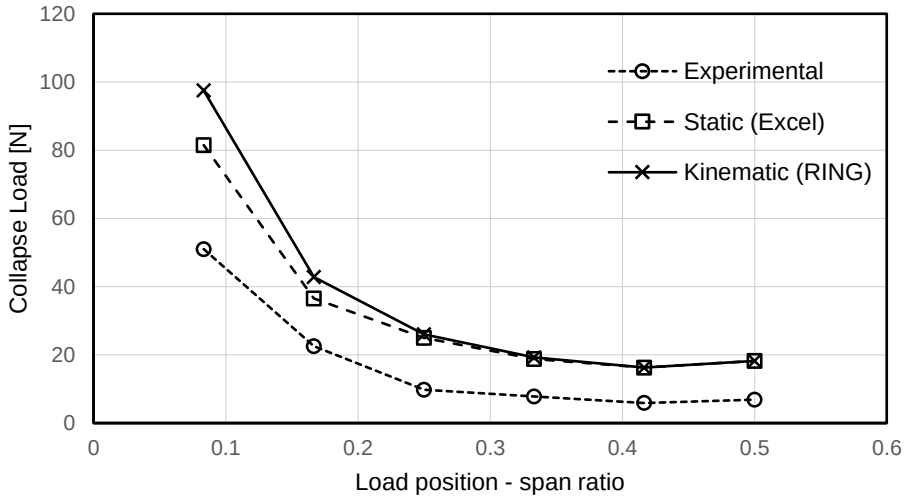

Table 9 – Unreinforced arch, exact geometry: limit analysis results compared to experimental ones, for all the load positions.

This considerable difference has induced further investigations. In particular, the experimental collapse configurations have been compared to the ones derived from limit analysis. It has been noticed a remarkable difference on the hinges distribution. In the limit analysis results, for instance, a hinge was forming, in any load position case, at the loading point, while in the experimental arch they were forming far from it (Figure 44).

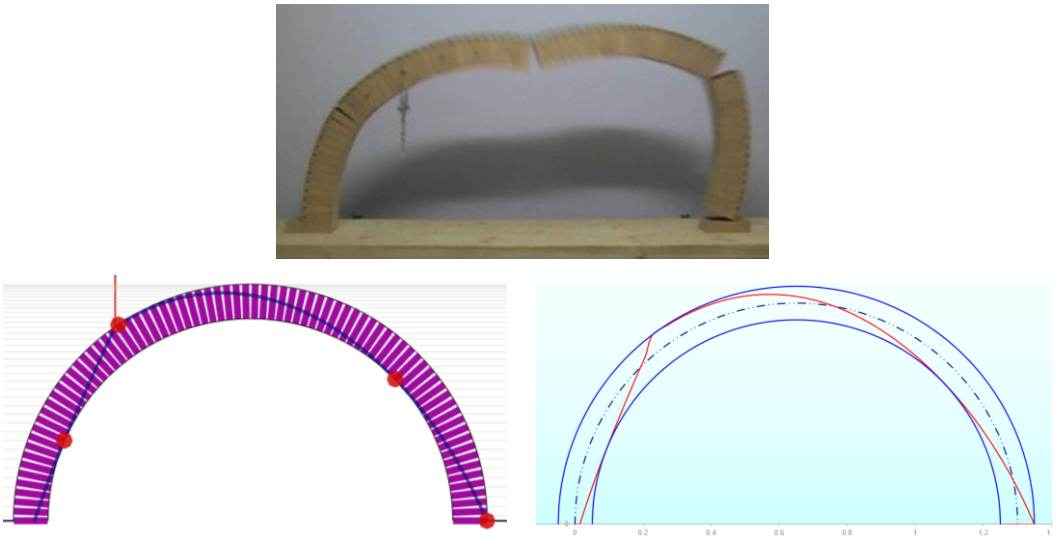

Figure 44 – Original unreinforced arch geometry, load at 1/6 span, collapse configurations. From top clockwise: experimental, static and kinematic one.

This means that the experimental thrust line at collapse was completely different, and the one captured from limit analysis cannot form in the reality. In other words, the theoretical results are unexpectedly less conservative. This impossibility of the thrust line, computed with limit analysis, to take place in the experimental case led to the formulation of the following hypothesis: the theoretical thrust line at collapse cannot be geometrically fitted inside the arch borders, therefore the effective depth of the arch should be reduced. The reason of the impossibility of the formation of the theoretical collapse mechanism is not easy to establish. This can be due to imperfections in the contact of the wooden blocks, or to other unknown factors. Nevertheless, this is out of the aim of this work.

By means of the kinematic approach, always with the double-check from static approach, a back-analysis has been performed to compute the equivalent reduced depths needed to obtain results comparable with the experimental case (Table 10), both in terms of ultimate load and collapse hinged configuration. Together with the reduction of the depth, the density has been proportionally increased, so as to maintain the same overall weight.

Load position (span fraction)	Equivalent model data			Collapse load [N]		Comparison		
	Depth [mm]	Density [kg/m^3]	Clear span [mm]	Static (Excel)	Kinematic (RING)	Experiment	Error Static	Error Kinematic
1/12	82	732	1218	46	52	51	-10%	2%
1/6	82	732	1218	21	21	23	-6%	-5%
1/4	79	759	1221	10	10	10	-3%	-1%
1/3	82	732	1218	8	9	8	2%	9%
5/12	82	732	1218	6	6	6	8%	9%
1/2	82	732	1218	6	6	7	-6%	-6%

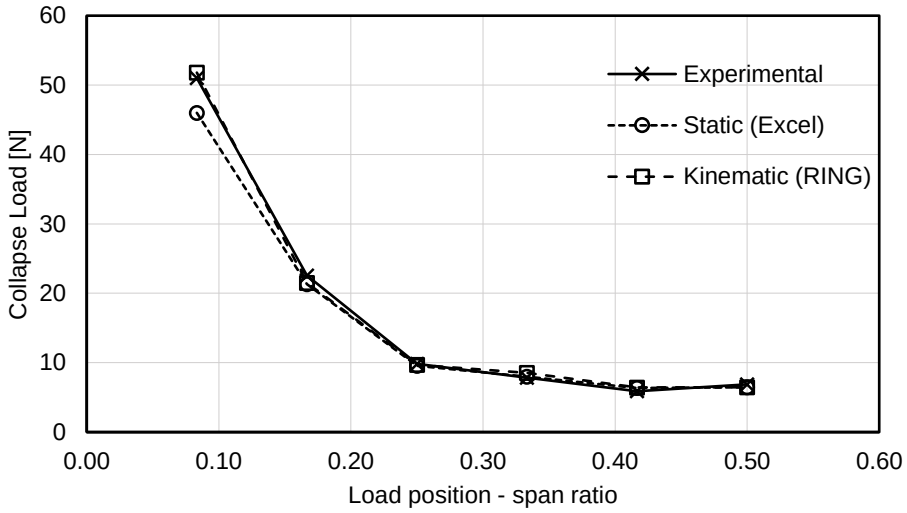

Table 10 – Equivalent models determined by limit analysis. Results and comparison with experimental ones.

The validity of the hypothesis on the impossibility of the cross-section of the arch to react in its entire surface is confirmed. This is also supported by the distribution of hinges obtained with the equivalent models, that is much more coherent with the one of the experimental arch. As is can be noticed in Figure 45, limit analysis shows that there is no hinge forming at the loading point, as it was observed in in Figure 44. The collapse configuration is completely different from the one obtained with limit analysis of the arch with the original geometry, but it highly resembles the experimental one (Figure 45).

Therefore, in the unreinforced numerical models have been shaped with the equivalent depths computed with the back-analysis explained here. This means that the actual geometry has not been modelled, since it has been showing to lead to much more conservative results than the limit analysis ones. Typically, the experimental models show a higher capacity than the one computed with limit analysis, due to the presence of a minimum tensile strength. In this case happens the opposite, due to the absence of tensile strength in the physical model, and the presence of some unknown imperfections that reduce arch cross-section and the global capacity.

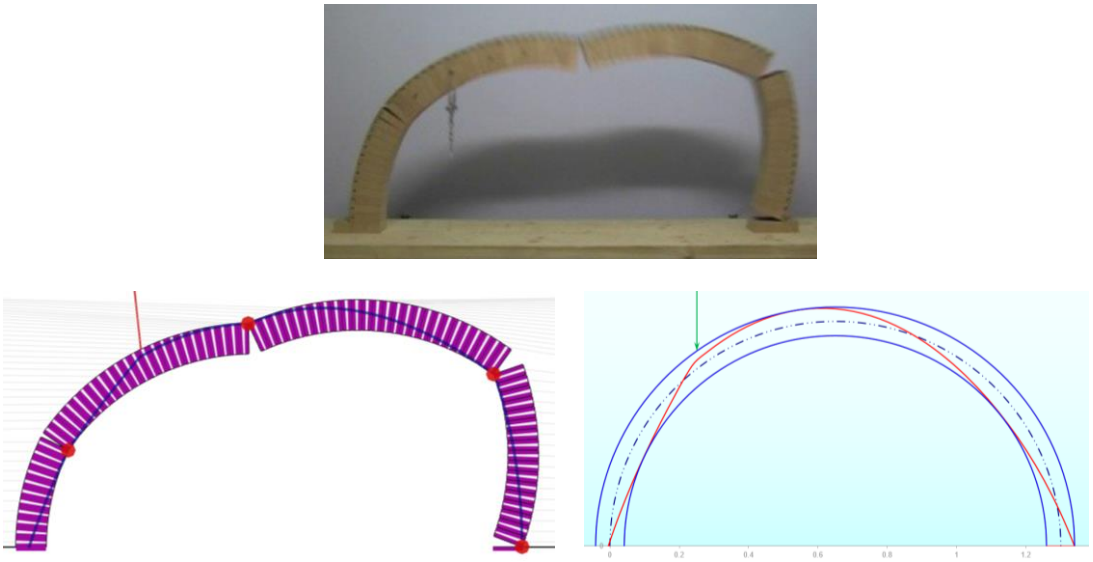

Figure 45 – Comparison of collapse configurations for load at 1/6 of the span. Top: experimental. Bottom: equivalent depth models: static limit analysis (right) and kinematic one (left).

Furthermore, in favour of the assumption concerning the reduced effective depth, it has been tried to vary the original density of 600 kg/m^3, that could have been affected by small errors, keeping the original geometry, including the depth of 100 mm. This means that the overall weight is not kept equal to the original one anymore. Results from limit analysis has shown, for the sample case of punctual load at 1/6 of the span, that the equivalent density to obtain the experimental collapse load, should be of 3 kg/m^3 for the static approach, and 3.16 kg/m^3 in case of the kinematic one. This means that the error on the density should be about 46 ÷ 49 %, that is not plausible. Moreover, the collapse hinged configuration would be considerably different from the real experimental one (Figure 46).

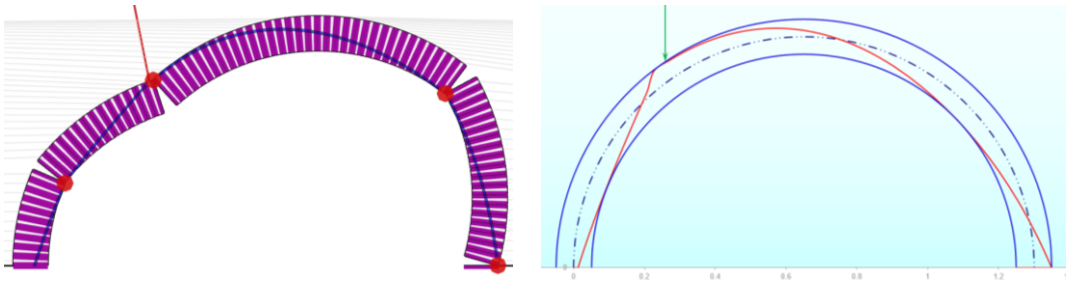

Figure 46 – Collapse configurations of arch loaded at 1/6 of the span, obtained with both limit analysis approaches (kinematic on the left, static on the right), in the case of equivalent density for obtaining the same capacity of the experimental arch.

In the further numerical analysis, for the sake of brevity, the cases of load applied at 1/6 and 1/2 of the span has been analysed. This is a convenient choice, since these two cases present the same equivalent depth of 82 mm (Table 11) for obtaining the experimental behaviour.

Experimental arch Collapse configuration	**Original geometry** Kinematic analysis	**Reduced depth** Kinematic analysis
	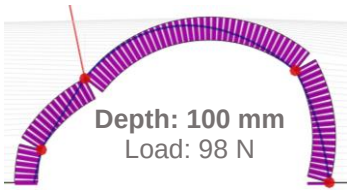	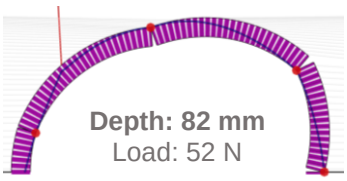
	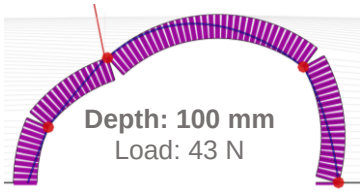	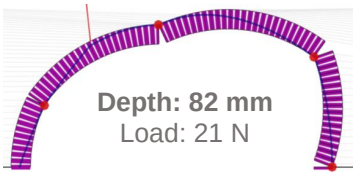
	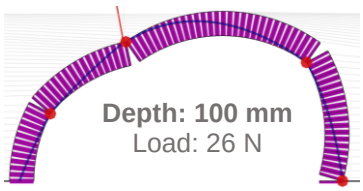	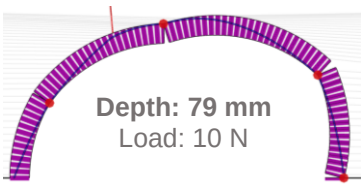
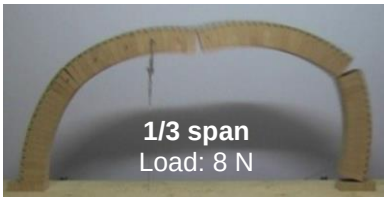	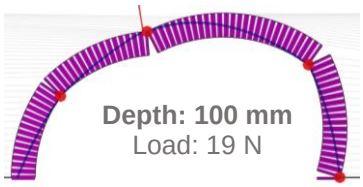	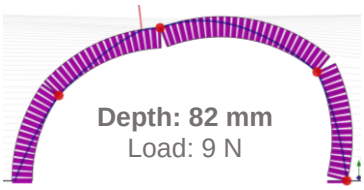
	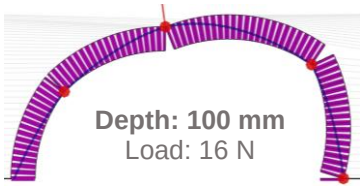	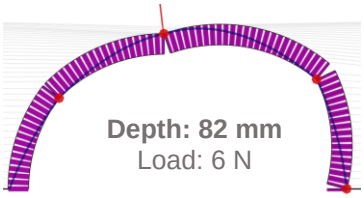
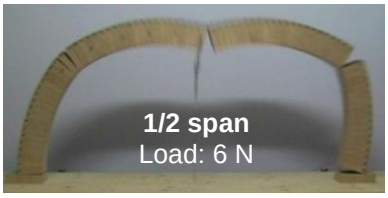	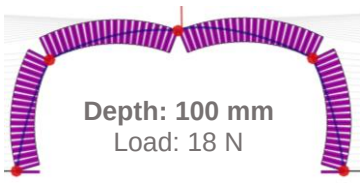	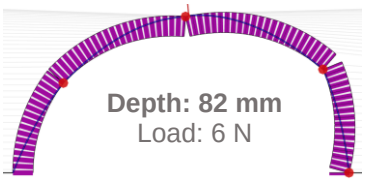

Table 11 – Collapse hinged configurations: experimental arch and kinematic analysis with original and reduced depths.

5.2 Reinforced Arch

Limit analysis has been applied also to the cases of reinforced arches. The kinematic analysis was not possible in this case, since the program Ring does not include the option of such reinforcement, so only the Excel spreadsheet for graphic statics has been used. In fact, this tool provides the possibility to find the line of thrusts including a uniform radial confinement load, applied at the intrados or at the extrados of the arch. The confinement radial load was calculated with the simple relation involving the curvature, explained in Figure 47.

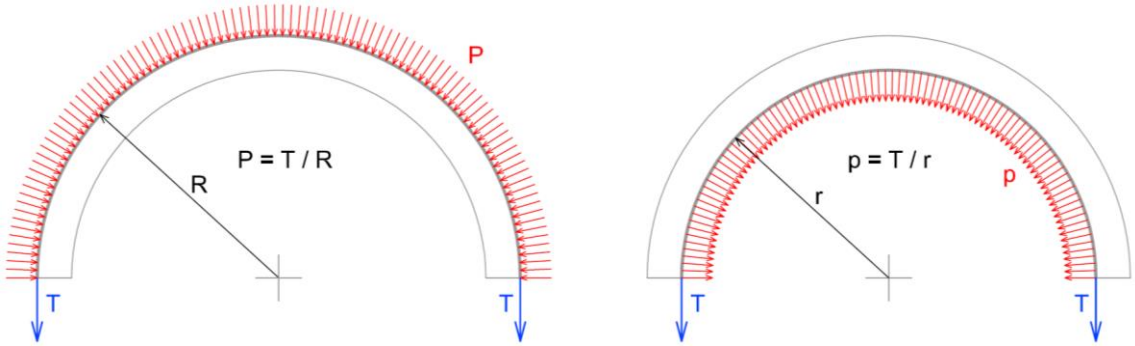

Figure 47 – Equivalent confinement radial load due to post-tensioned cables, applied at the extrados (left) or at the intrados (right). R, r: the radius of the arches, T: cable post-tension.

The cases of punctual load at 1/6 and half span have been analysed, for all the post-tension levels. Same problem arose in unreinforced case has been rising also in the reinforced one: the resistance calculated with limit analysis is sensitively higher than the one obtained experimentally, for low post-tension levels (Figure 48). Nevertheless, it increases with the post-tension level (Table 12 and Table 13), approaching the experimental values for the maximum ones, especially in the case of cable at the intrados. Therefore, the same equivalent depth used for analysing the unreinforced case cannot be applied for the reinforced arch cases. Not even a unique depth can be established for all the post-tension levels. This has been interpreted as a tendency of the cables presence to restore the original depth, the more post-tension confinement is applied (Figure 49).

Collapse Load [N] - Cables at the Extrados						
Post tension [N]	Load at 1/6 span			Load at 1/2 span		
	Experimental	Limit Analysis	Error	Experimental	Limit Analysis	Error
20	59	72	23%	31	48	53%
39	86	102	18%	53	78	46%
59	112	130	16%	80	106	32%
78	139	158	13%	106	133	26%
98	160	183	15%	126	162	29%
196	284	318	12%	241	310	28%
294	411	451	10%	364	452	24%

Table 12 – Comparison of collapse load for different post tension levels between experimental results and limit analysis with original geometry arch. Cable at the extrados.

Collapse Load - Cables at the Intrados						
Post tension [N]	Load at 1/6 span			Load at 1/2 span		
	Experimental	Limit Analysis	Error	Experimental	Limit Analysis	Error
98	163	186	14%	137	160	16%
196	315	324	3%	259	305	18%
294	486	456	-6%	431	440	2%

Table 13 - Comparison of collapse load for different post tension levels between experimental results and limit analysis with original geometry arch. Cable at the intrados.

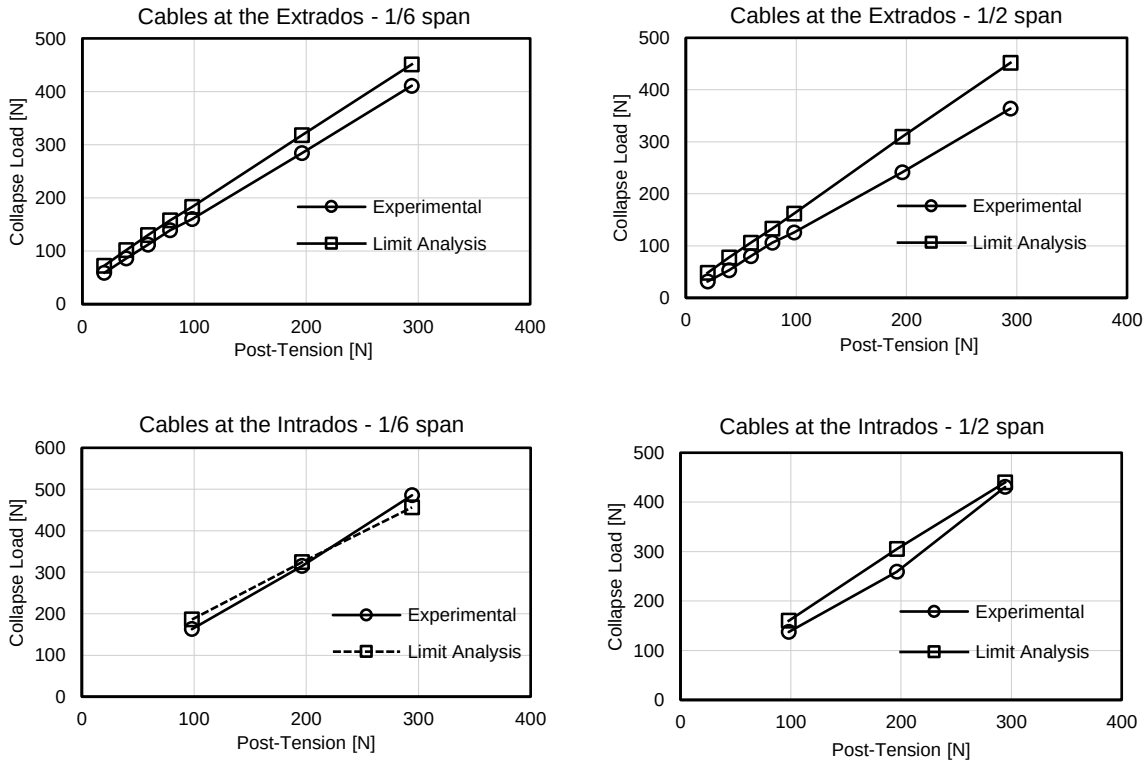

Figure 48 – Comparison of experimental and limit analysis results for the reinforced arch.

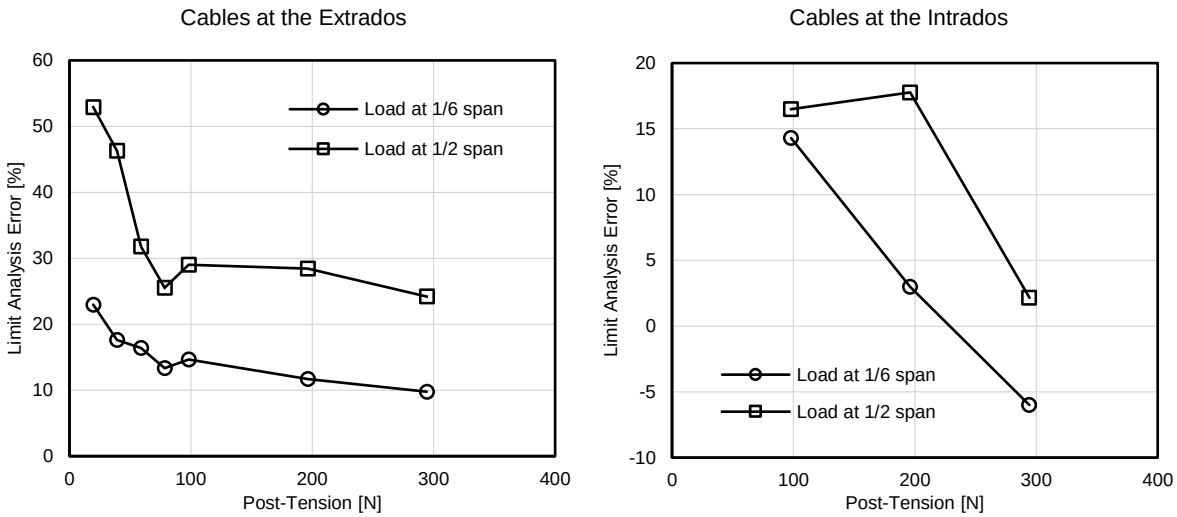

Figure 49 – Percentage errors on collapse load computed with limit analysis to the experimental results.

The values of the equivalent depths have been computed through the Excel spreadsheet for graphic statics, with the same procedure described for the unreinforced arch, for each post-tension level. For this back-analysis, the case of load at half span has been chosen. This because the static limit analysis tool is more reliable for load positions closer to the mid-point, than for the ones closer to the impost, because of the arch discretization. It must be underlined that the value of the equivalent depth computed is affected from a rounding error (1 mm) that is not always totally negligible. This is the reason why, presenting the numerical results, both experimental and limit analysis results will be included. Nevertheless, the results obtained confirm the increase of the effective depth with the increment of the post-tension rate (Table 14).

Post tension [N]	Equivalent Depth [mm]	
	Cables at the Extrados	Cables at the Intrados
20	85	
39	85	
59	87	
78	88	
98	88	91
196	89	92
294	90	100

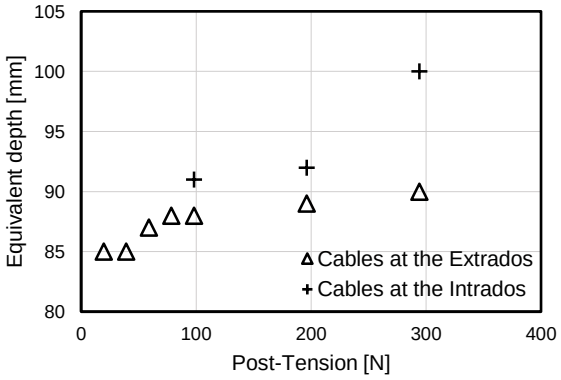

Table 14 – Equivalent depths, computed by static limit analysis, for obtaining the same collapse load of experiments in the reinforced arch cases (load at half span).

For the sake of brevity, in the next sections concerning numerical analysis, only the cases with maximum post-tension force will be presented, therefore the models will have 90 mm of depth for the case with the cables at the extrados, and 100 mm (full depth) for the ones with the cables at the intrados.

The results of this back-analysis for determining the equivalent depth, performed by attempts with Ring, are affected from an approximation error. In fact, the sensitivity of the arch capacity to the geometrical depth is significant. Therefore, the approximation of ±0.5 mm could propagate in a not negligible error on the limit load. To prove this, a model representing the experimental unreinforced arch, with a punctual load at half span, has been produced in RING. Variating the depth from 80 mm to 90 mm, and applying consequently the equivalent density, for keeping the overall weight constant, the capacity of the arch has been computed (Table 15).

Depth [mm]	Density [kg/m^3]	Span [mm]	Rise [mm]	Ultimate Load [N]
80	750	1220	610.0	5.3
81	741	1219	609.5	5.9
82	732	1218	609.0	6.5
83	723	1217	608.5	7.0
84	714	1216	608.0	7.6
85	706	1215	607.5	8.2
86	698	1214	607.0	8.8
87	690	1213	606.5	9.3
88	682	1212	606.0	9.9
89	674	1211	605.5	10.5
90	667	1210	605.0	11.2

Table 15 – Sensitivity analysis of ultimate load to the depth of the arch in RING.

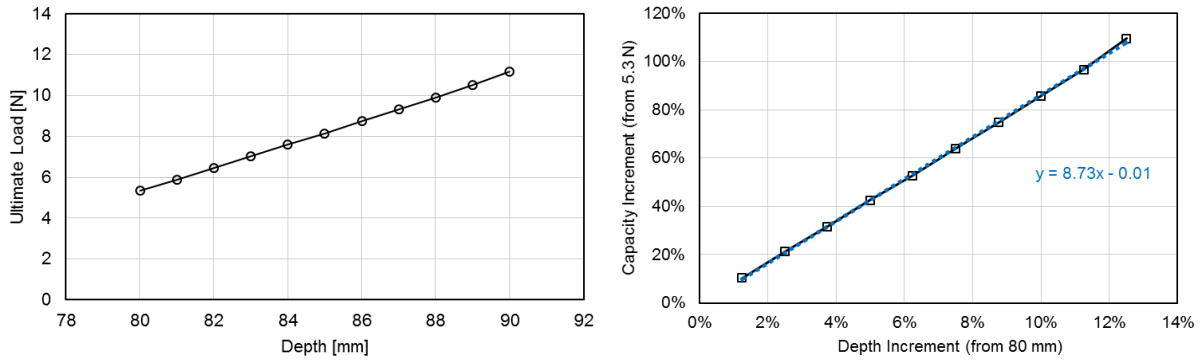

Figure 50 – RING sensitivity to depth (left) and depth increment (right).

In Figure 50 is shown a relative increment of load capacity 9 times greater than the relative increment of depth (to an original value of 80 mm).

6. NUMERICAL ANALYSIS: MICRO-MODELS

6.1 Hypothesis and Arch Body Material Parameters

The micro-models produced are aimed at simulating as faithfully as possible the actual condition of the experimental arches, in terms of stiff wooden units, simply in contact one to each other, with no tensile strength at their interface. Therefore, linear elastic material has been chosen for modelling the blocks, with material parameters as equal as possible to the ones of the beechwood used for shaping the voussoirs (Table 16). Wood is a composite orthotropic material, nevertheless the behaviour inside the block is not relevant for our analysis, because no compressive failure has happened during the experiments. The collapse behaviour observed, that these models aim at capturing, is the rotational hinges opening. Then, the only fundamental material parameter in this case is the density, but also the elastic ones have been applied carefully. In the reinforced cases, the cable weight has been neglected in all the analysis carried out.

Wooden Blocks - Elastic parameters				
Parameter		Notation	Value	Unit
Young Modulus		E	15000	MPa
Poisson's ratio		υ	0.3	-
Density*	82 mm depth models	ρ	732	kg/m^3
	90 mm depth models	ρ	667	kg/m^3
	100 mm depth models	ρ	600	kg/m^3

*Table 16 – Wooden blocks linear elastic parameters. *Equivalent density has been used to keep constant the overall weight of the experimental arch.*

Most of the capacity and the deformability of the model are due to the presence of interface elements. The values of the parameters of the Coulomb friction material assigned at these elements are aimed at preventing shear sliding, and providing no tensile resistance to hinges opening. Moreover, the normal elastic stiffness of the interface has been chosen relatively high, so as to minimise blocks superpositions, simulating as much as possible a rigid contact, while the shear one has been chosen reasonably, compared with the ones suggested for masonry (Lourenço, 2002), in absence of more specific data (Table 17).

Blocks Interface - Parameters				
	Parameter	Notation	Value	Unit
Linear	Normal stiffness	K_n	10000	N/mm^3
	Shear stiffness	K_s	2000	N/mm^3
Friction	Cohesion	c	0	MPa
	Friction angle	φ	1.55	rad
	Dilatancy angle	ψ	0	rad
Gap opening	Tensile strength	f_t	0	MPa

Table 17 – Coulomb friction interface parameters between blocks.

6.2 Unreinforced Arch - Results

As stated above, for the unreinforced arch a depth of 82 mm has been computed with limit analysis to comply the experimental results. Equivalent density is therefore 732 kg/m^3. For the two load positions concerned, both linear and non-linear geometry analysis (Total Lagrange approach) have been performed, for sake of comparison. Analysis setup is reported in Table 18.

Element Type	4-noded
Element Size	6 mm
Steps increment of Displacement	0.001 mm
Iterative Method	Full Newton-Raphson
Convergence Control	Energy, Force, Displacements
Tolerance	0.01

Table 18 – Unreinforced arch: analysis setup details.

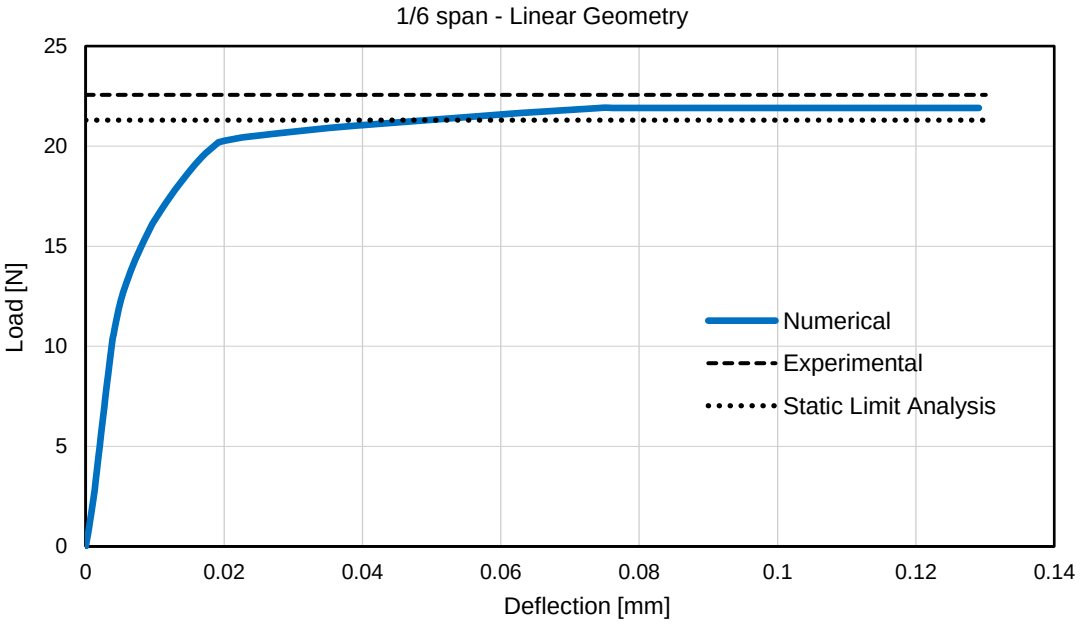

Figure 51 – Micro-model, unreinforced arch (82 mm depth), load at 1/6 of the span, linear geometry, deflection of loaded point vs load applied.

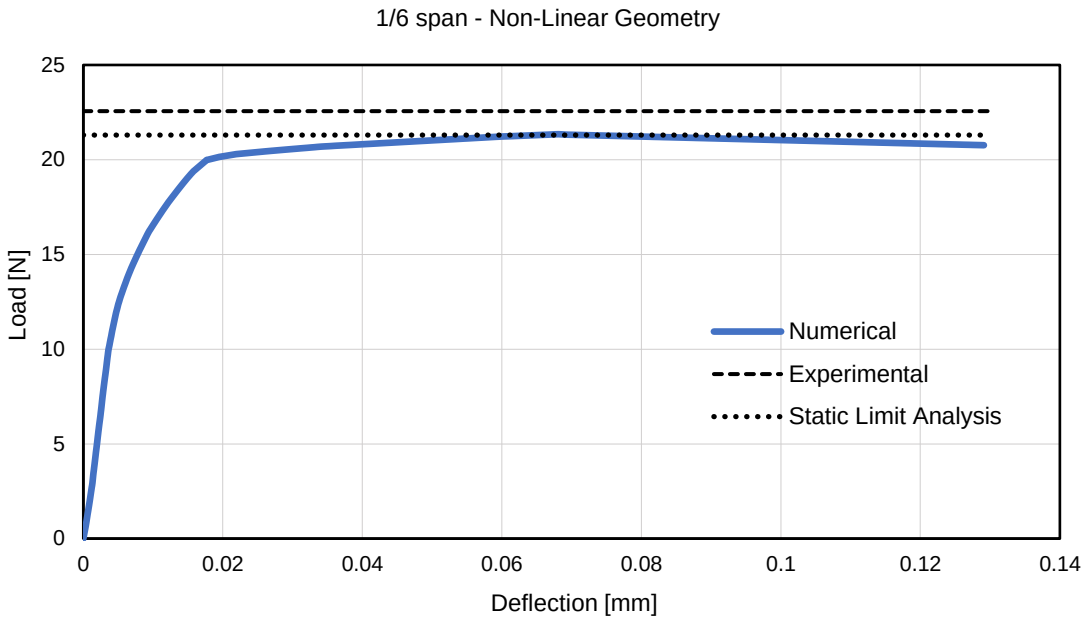

Figure 52 – Micro-model, unreinforced arch (82 mm depth), load at 1/6 of the span, non-linear geometry, deflection of loaded point vs load applied.

The results of limit analysis have been also reported, since the depth computed and applied is not the exact one to get the experimental value, due to approximation that affects the back-analysis performed with the kinematic approach by means of Ring.

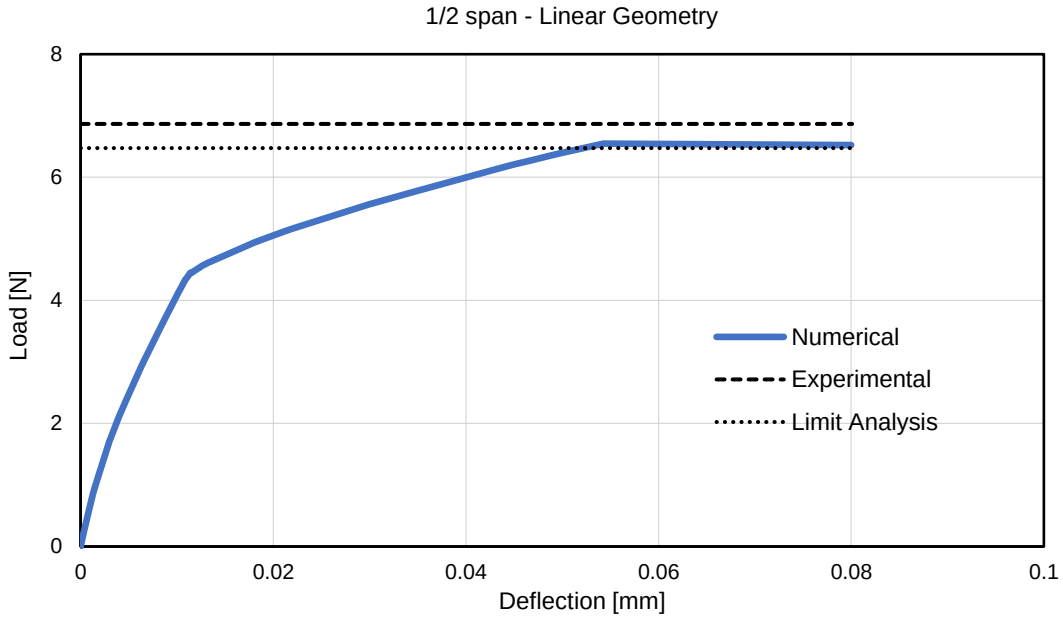

Figure 53 - Micro-model, unreinforced arch (82 mm depth), load at 1/2 of the span, linear geometry, deflection of loaded point vs load applied.

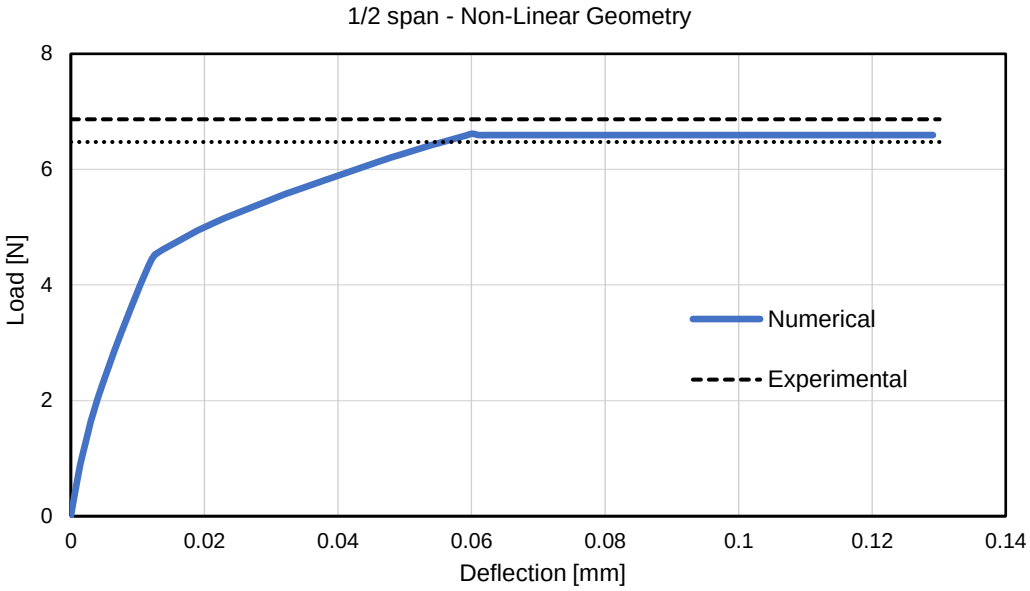

Figure 54 - Micro-model, unreinforced arch (82 mm depth), load at 1/2 of the span, non-linear geometry, deflection of loaded point vs load applied.

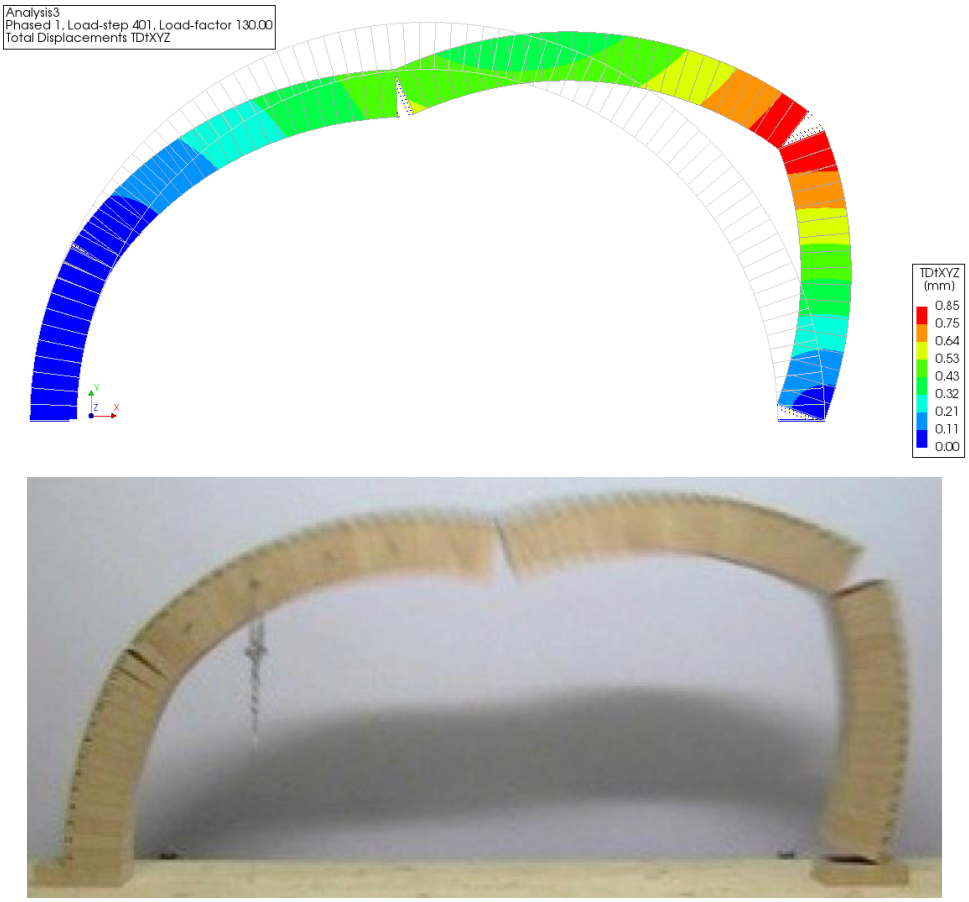

Figure 55 – Top: micro-model unreinforced, 82 mm depth, non-linear geometry, load at 1/6 of the span, norm of displacements at collapse deformed configuration (x200 amplification). Bottom: experimental collapse configuration.

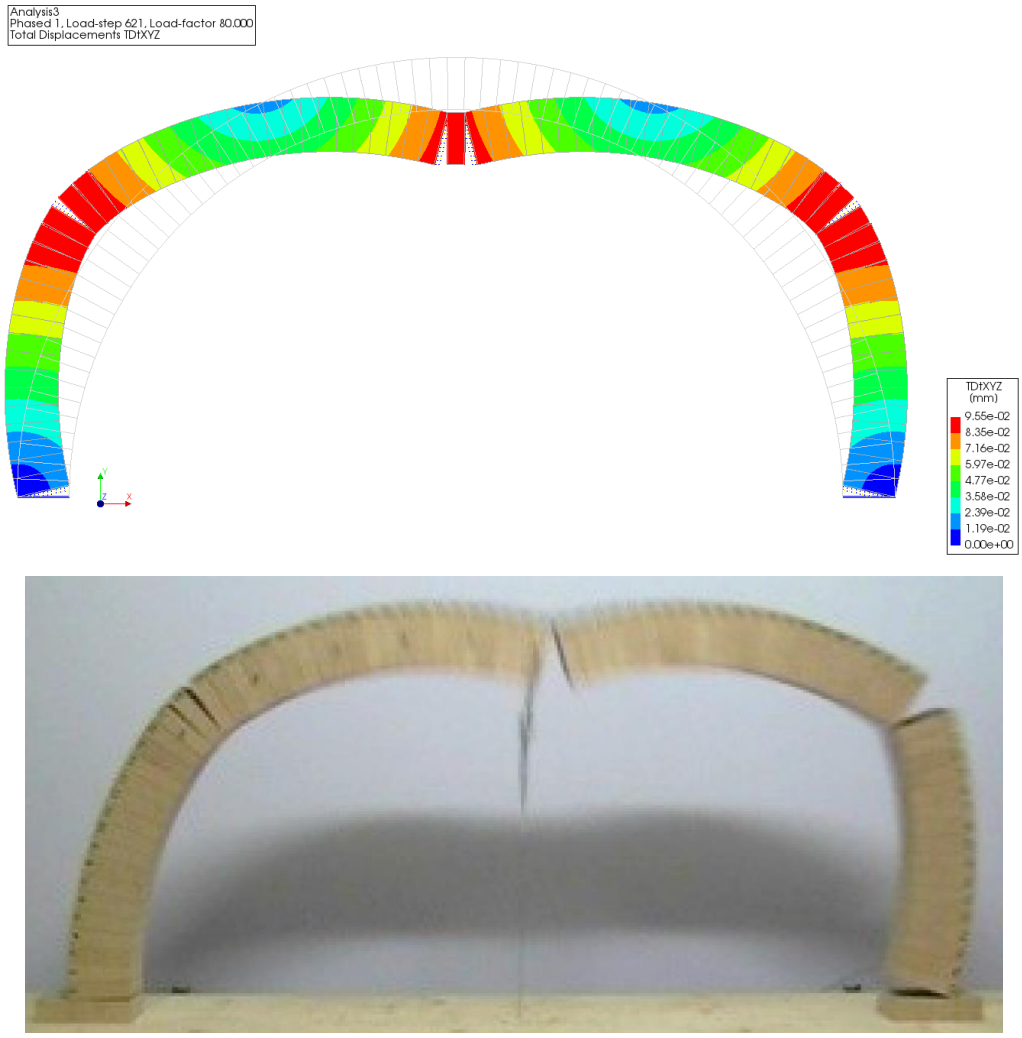

Figure 56 - Top: micro-model unreinforced arch, 82 mm depth, non-linear geometry, load at 1/2 of the span, norm of displacements at collapse deformed configuration (x1000 amplification). Bottom: experimental collapse configuration.

Load position (span fraction)	Non-Linear geometry	Collapse load [N]				Error to Numerical		
		Numerical	Static (Excel)	Kinematic (RING)	Experim.	Static	Kinem.	Experim.
1/6	No	21.9	21.3	21.5	22.6	3%	2%	-3%
1/6	Yes	21.3	21.3	21.5	22.6	0%	-1%	-5%
1/2	No	6.5	6.5	6.5	6.9	1%	1%	-5%
1/2	Yes	6.6	6.5	6.5	6.9	2%	2%	-4%

Table 19 – Micro-model unreinforced, 82 mm depth, numerical results compared.

In general, it can be stated that the results give values slightly lower than the experimental ones. Nevertheless, they comply relatively well to the limit analysis ones. This is due to the fact that the depth was calculated with a certain approximation (1 mm) by means of Ring, and it has been proven that even small variations of the depth much affect the overall capacity of the arch. Therefore, the errors cannot

be ascribed to numerical issues, but to previously accepted approximations. The collapse hinged configurations are fully compatible with the experimental ones, and with the ones obtained from limit analysis (Figure 55 and Figure 56). Despite capturing reliably the ultimate capacity, the deformation obtained are highly limited, as it can be noticed on the screenshots presented, but deformability analysis is out of the purpose of this document. In the non-linear geometry analysis, it can be noticed a post-peak softening behaviour, especially in the case loaded at 1/6 of the span (Figure 52, Figure 54), while in the linear geometry case the curve is essentially flat (Figure 51, Figure 53).

6.3 Reinforced Arch with Equivalent Radial Load - Results

Micro-model analysis has been performed also for the case of radial uniform load reinforcement, applied either the extrados or at the intrados, with the criterion explained in Figure 47. As explained above, the models used for the reinforced cases have been provided of an increased equivalent depth, computed by means of a back-analysis, performed with the Excel spreadsheet for graphic statics. For the sake of brevity, only the case with post-tension equal to 294 N (30 kgf) are presented. Concerning the load position, the same cases as for the unreinforced case have been analysed: 1/6 and half span. The geometrical characteristics and density of the models used are reported in Table 20. In these cases, only linear geometry analysis has been performed.

Parameter	Cables position	
	Extrados	Intrados
Depth [mm]	90	100
Span [mm]	1210	1200
Rise [mm]	605	600
Width [mm]	100	100
Density [kg/m^3]	667	600
Radial Load [N/m]	423	491

Table 20 – Geometrical parameters and density of reinforced arches with radial load equivalent to 294 N of post-tension.

Firstly, the results concerning the cases with the equivalent radial load reinforcement at the extrados are presented. Analysis setup is reported in Table 21.

Element Type	4-noded
Element Size	8 mm
Steps increment of Displacement	0.001 mm
Iterative Method	Full Newton-Raphson
Convergence Control	Energy, Force, Displacements
Tolerance	0.01

Table 21 – Micro-models with equivalent radial load at the extrados, analysis setup.

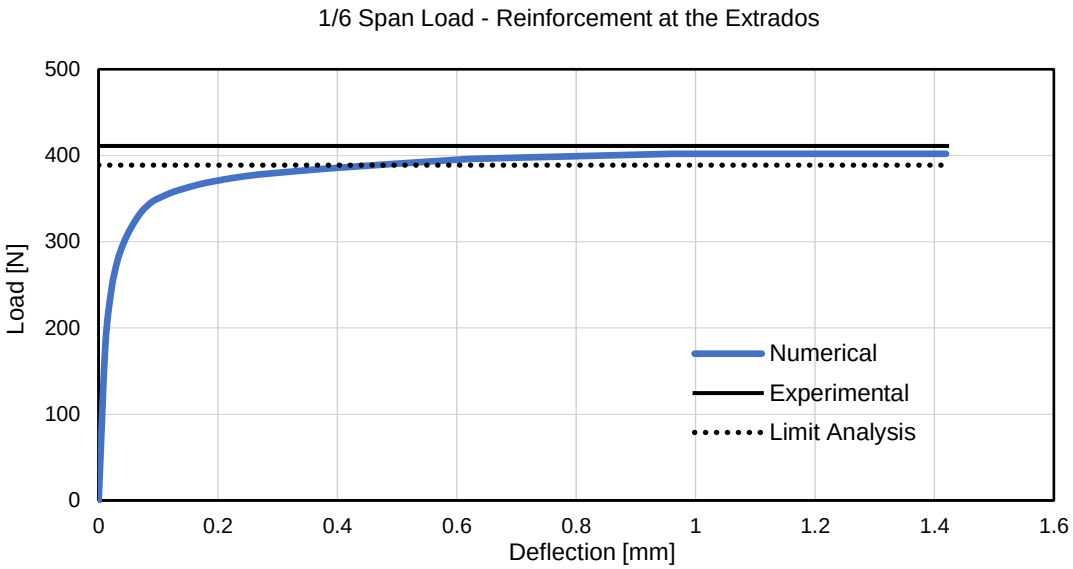

Figure 57 – Arch with equivalent radial reinforcement at the extrados (294 N post-tension), load at 1/6 of the span, deflection of loaded point vs load applied.

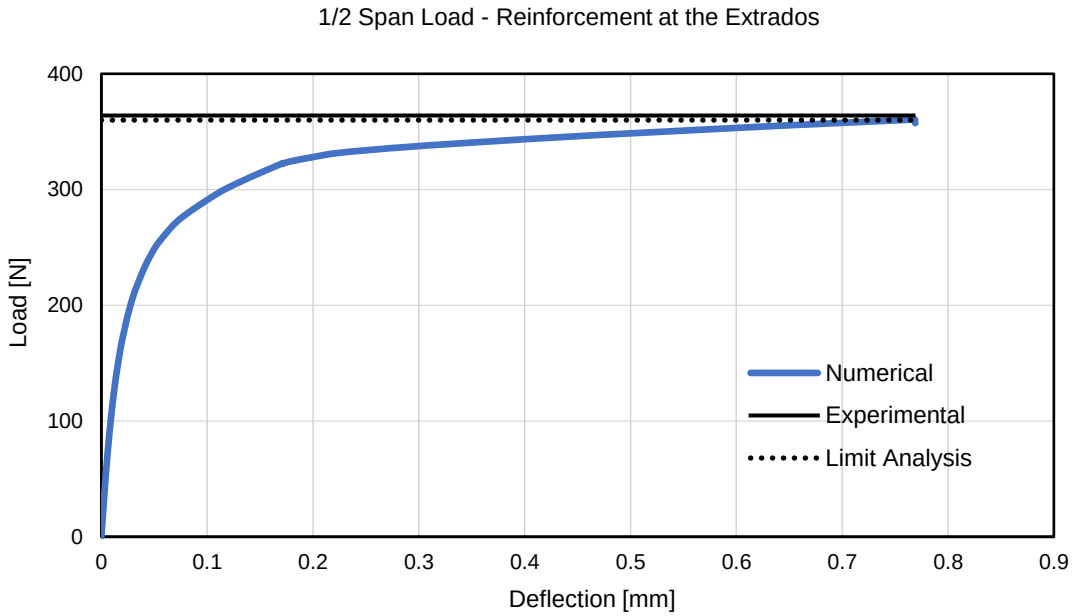

Figure 58 - Arch with equivalent radial reinforcement at the extrados (294 N post-tension), load at 1/2 of the span, deflection of loaded point vs load applied.

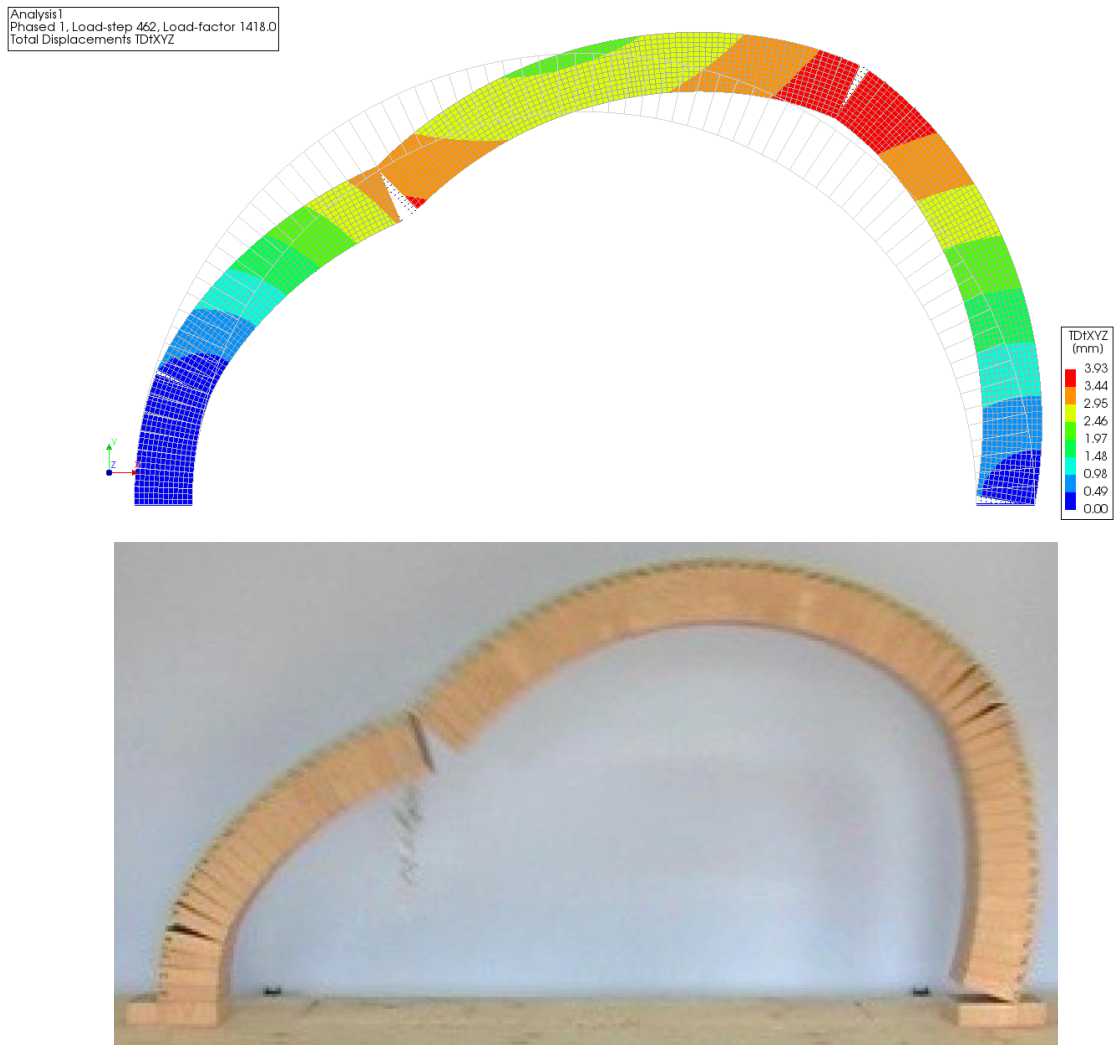

Figure 59 - Top: micro-model with equivalent radial reinforcement at the extrados, 90 mm depth, load at 1/6 of the span, norm of displacements at collapse deformed configuration (x30 amplification). Bottom: experimental collapse configuration.

Load position (span fraction)	Collapse load [N]			Error	
	Numerical	Experim.	Limit Analysis	to Experim.	to L. Analysis
1/6	402	411	389	-2.2%	3.4%
1/2	361	364	360	-0.9%	0.1%

Table 22 – Equivalent radial load reinforcement at the extrados: micro-models results and comparison with experimental ones and limit analysis.

Numerical results, in terms of capacity, show an optimal accordance with the experimental ones (Figure 57 and Figure 58). Also the collapse hinged configurations show a compatible layout (Figure 59, Figure 60). This means that the hypothesis on the reduced depth made were consistent, and also shows the reliability of modelling the reinforcement by means of an equivalent radial load, in the case of the cable at the extrados.

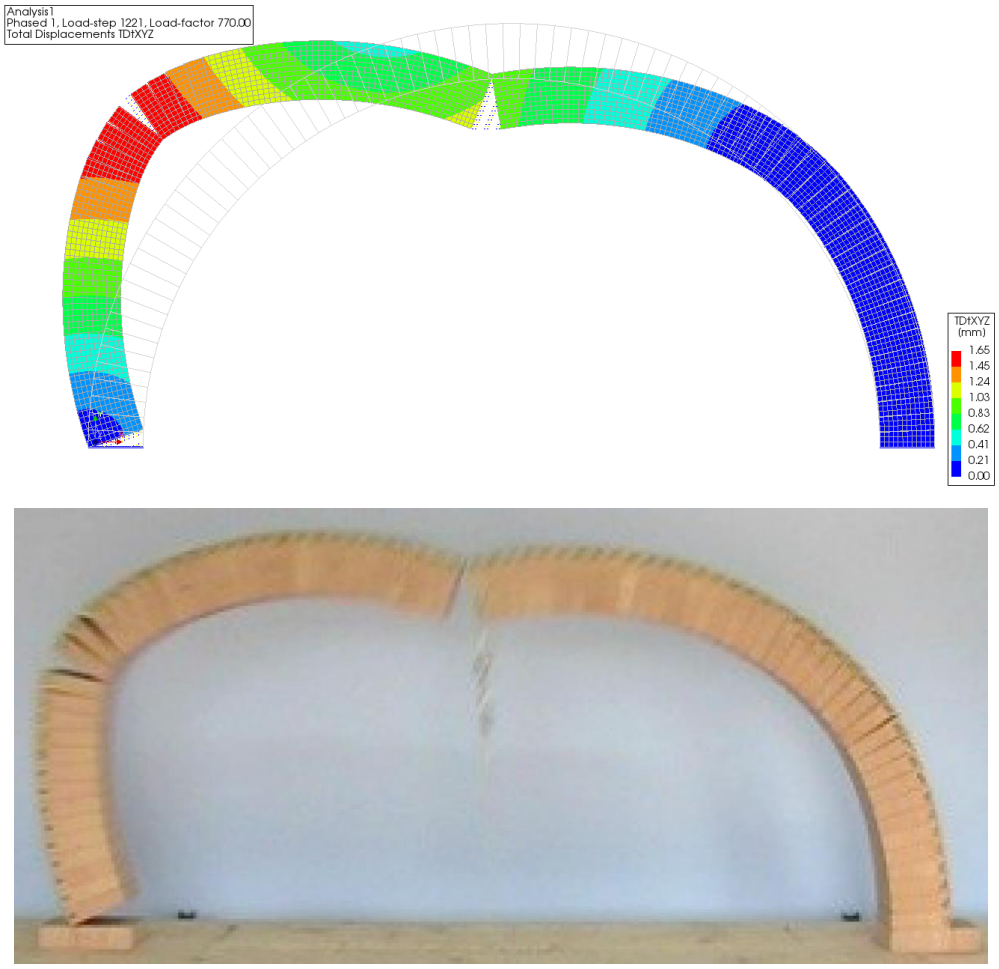

Figure 60 - Top: micro-model with equivalent radial reinforcement at the extrados, 90 mm depth, load at 1/2 of the span, norm of displacements at collapse deformed configuration (x100 amplification). Bottom: experimental collapse configuration.

Also the case of reinforcement at the intrados has been taken into consideration. In this case the depth computed by limit analysis, for the case concerned of 294 N post-tension (30 kg), is the full one of 100 mm. Therefore, the models represent the exact geometry and density (600 kg/m^3) of the real experimental arch. In these cases, non-linear geometry analysis has been performed, to get a better convergence. Analysis setup is reported in Table 23.

Element Type	4-noded
Element Size	8 mm
Steps increment of Displacement	0.001 mm
Iterative Method	Full Newton-Raphson
Convergence Control	Energy, Force, Displacements
Tolerance	0.01
Non-Linear Geometry	Updated Lagrange

Table 23 - Equivalent radial load at the intrados reinforced models, analysis setup.

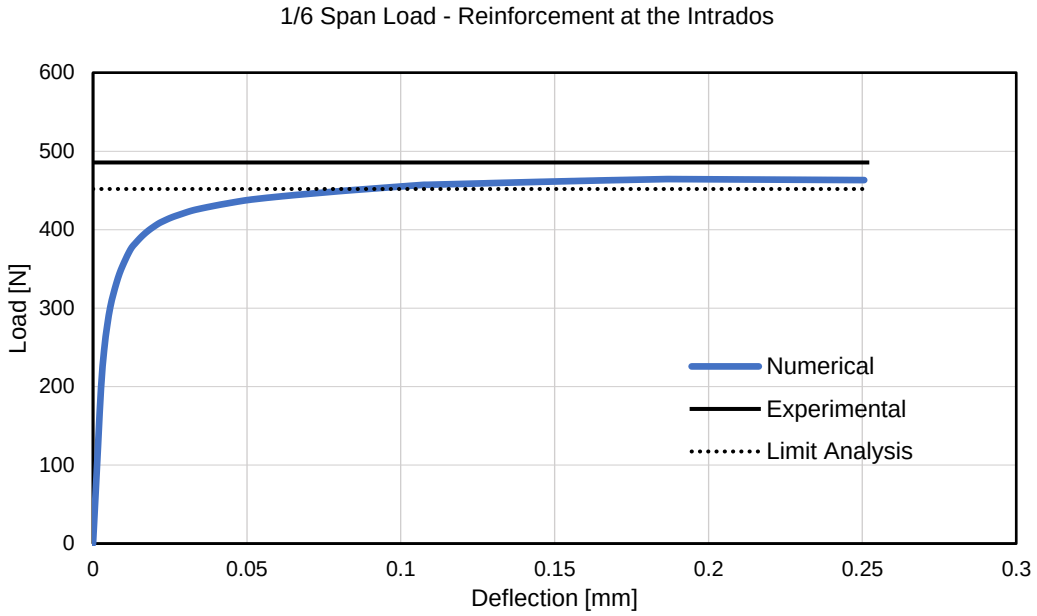

Figure 61 – Arch with equivalent radial reinforcement at the intrados (294 N post-tension), load at 1/6 of the span, deflection of loaded point vs load applied.

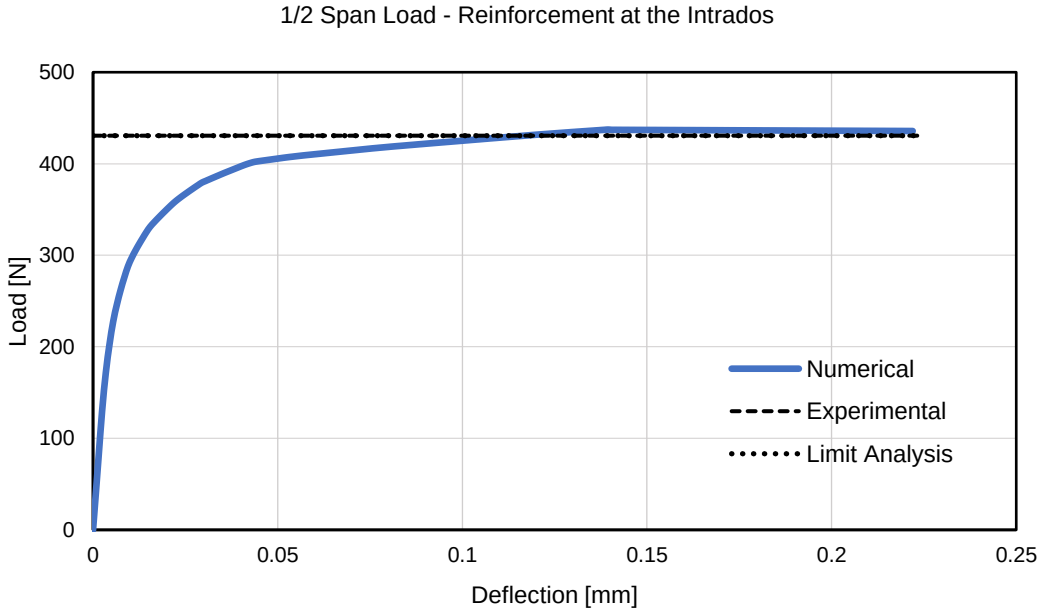

Figure 62 - Arch with equivalent radial reinforcement at the intrados (294 N post-tension), load at 1/2 of the span, deflection of loaded point vs load applied.

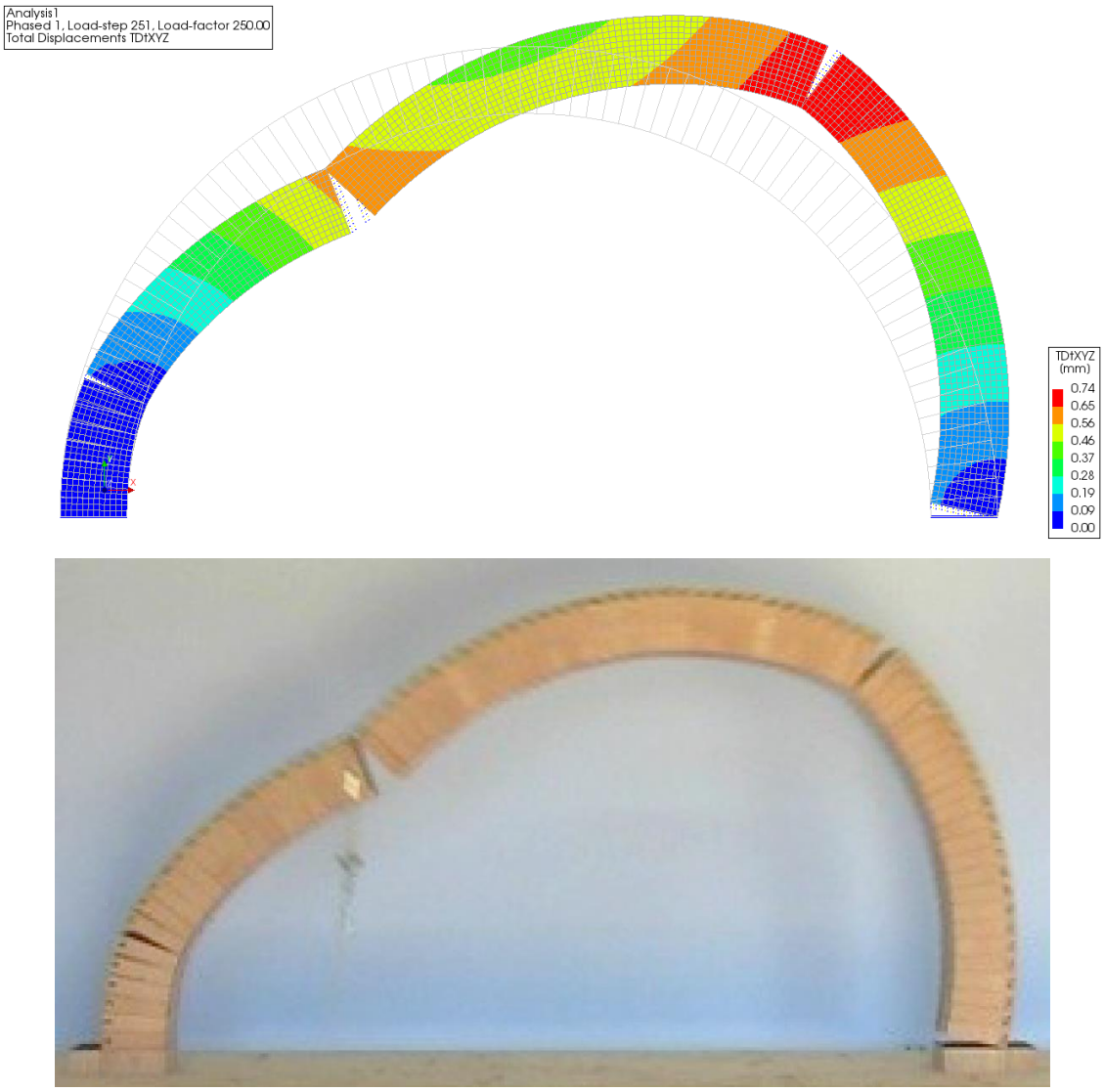

Figure 63 - Top: micro-model with equivalent radial reinforcement at the intrados, 100 mm depth, load at 1/6 of the span, norm of displacements at collapse deformed configuration (x200 amplification). Bottom: experimental collapse configuration.

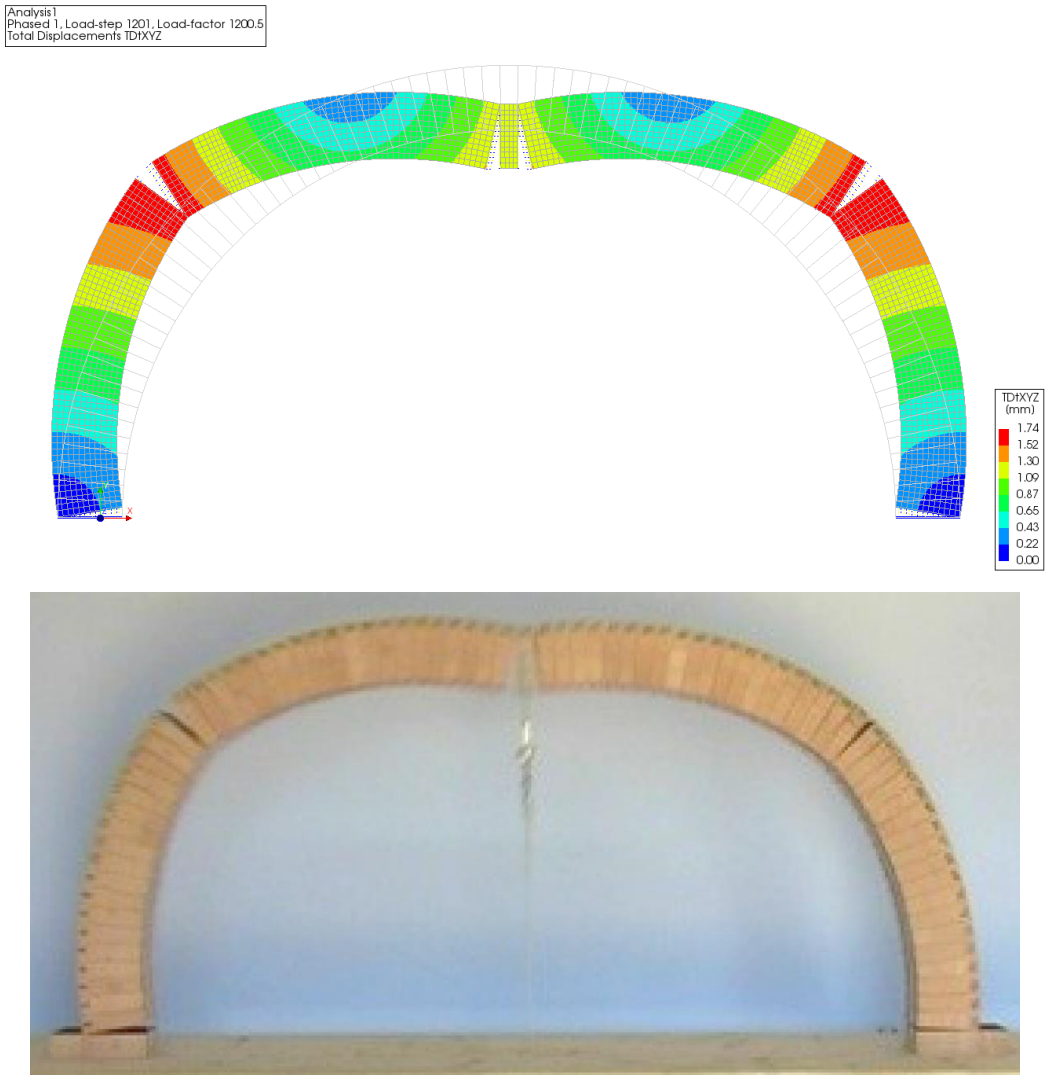

Figure 64 - Top: micro-model with equivalent radial reinforcement at the intrados, 100 mm depth, load at 1/2 of the span, norm of displacements at collapse deformed configuration (x50 amplification). Bottom: experimental collapse configuration.

Load position (span fraction)	Collapse load [N]			Error	
	Numerical	Experim.	Limit Analysis	to Experim.	to L. Analysis
1/6	464	486	452	-4.4%	2.8%
1/2	437	431	431	1.6%	1.6%

Table 24 - Equivalent radial load reinforcement at the intrados: micro-models results and comparison with experimental ones.

Even in this case, the results obtained with the micro-model analysis are in good accordance with the experimental ones (Table 24), with slightly lower values, but they faithfully reproduce the limit analysis ones (Figure 63, Figure 64). It must be reminded that once again results concerning arches loaded at half span have a slightly better coherence with the experimental ones (Figure 62) than the one loaded at 1/6 of the span (Figure 61), for the same reasons of the previous cases, explained above.

6.4 Modelling of Steel Cables Reinforcement

6.4.1 Reinforcement Parameters

One of the main aims of this work is to investigate the behaviour of the steel cable reinforcement (Figure 65), especially in terms of interaction with the arch, during the external loading. Modelling this interaction is not straightforward, since the parameters governing the interaction are not known in general. It is not known also the actual influence of these parameters on the capacity of the arch and on the overall behaviour of the structure.

To simulate this interaction, a model based on Coulomb friction has been chosen. The same interface elements used for the block contact interface have been applied to the cable/arch interfaces, but with completely different parameters. For the sake of brevity, not all the unknown parameters of this interaction mechanism can be fully investigated, so some of them have been estimated with reasonable values. The main one, that has been deeply investigated in the following paragraph, is the friction angle φ. In Table 25 are reported all the parameters involved in these analysis, with their qualitative uncertainty rate: known, estimated or variable. These parameters have been studied to simulate as faithfully as possible the experimental cases concerned. Nevertheless, in possible further developments involving actual masonry structures, they would need a more accurate calibration, considering the materials in contact. The density of the cables has been set as null, so as to neglect their weight, as in the previous analysis. The value of the Young modulus of the cables has been chosen as a reasonable one considering this kind of device. In fact, in the case of cables, usually it is sensitively lower than the common one of pure steel, due to non-elastic deformation phenomena. The interface friction surface width is another source of uncertainty, and it has been estimated as a reasonable vale of 0.1 mm. Nevertheless, its influence can be, at least partially, transferred to the friction angle variability, that has been investigated, since the friction force involves both these parameters in the same formula derived from Coulomb's law (shear stress is integrated in the width).

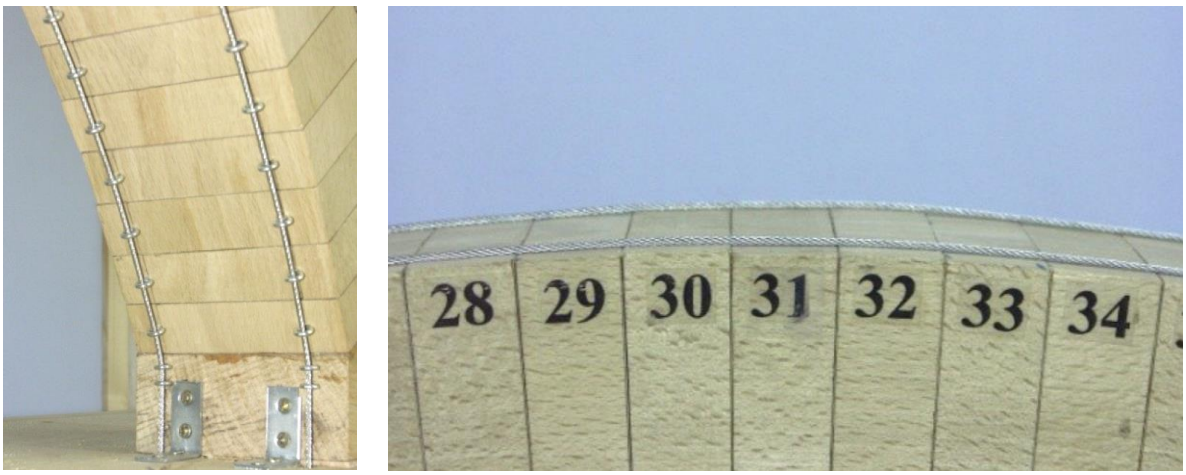

Figure 65 – Details of the cable/wood interface in the experimental arch. (Giglio, 2008).

Steel Cable - Elastic Parameters				
Parameter	Notation	Uncertainty Class	Value	Unit
Young Modulus	E	Estimated	196000	MPa
Poisson's ratio	υ	Estimated	0.3	-
Density	ρ	Known	0	kg/m^3
Steel Cable - Geometric Parameters				
Parameter	Notation	Uncertainty Class	Value	Unit
Cable Diameter	d	Known	2	mm
Cables Section Area	A	Known	6.18	mm^2
Friction Surface Width	t	Estimated	0.1	mm
Cable/Arch Interface - Parameters				
	Parameter	Notation	Uncertainty Class	Value	Unit
Linear	Normal stiffness	K_n	Estimated	10000	N/mm^3
	Shear stiffness	K_s	Estimated	100	N/mm^3
Friction	Cohesion	c	Estimated	0	MPa
	Friction angle	φ	Variable	0.6° - 30°	Deg
	Dilatancy angle	ψ	Estimated	0°	Deg
Gap Opening*	Tensile strength	f_t	Known	0	MPa

*Table 25 – Cables and interface parameters. *Gap opening depends on the position of reinforcement: in the case of reinforcement at the extrados it is activated, in the case of at the intrados it is not.*

6.4.2 Influence of Cable/Arch Friction Angle

Through micro-models, the influence of friction angle on the behaviour of the overall reinforced structure has been studied. For the sake of brevity, the only case of the arch loaded at half span, reinforced at the extrados with a post-tension of 294 N (30 kg), has been investigated, assuming that the results can be extended to all the other cases. The features of the models are the one explained in 4.1.2 and 4.1.4. After the application of gravity load at the unreinforced arch, the cable has been added and consequently the post-tension applied in 10 steps. Then, increments of the external load have been applied. The main advantage of these models is the possibility to investigate the state of stress of the cable and its interaction forces with the arch. As an example, it is reported in Figure 66 the distribution of the axial force all along the steel cable, at the end of the application of the post-tension force, for the case of friction angle φ = 5°. As it can be easily noticed, at the end of the application of the post-tension, the presence of shear stress at the interface (Figure 67) creates a state of non-uniform distribution of the tension inside the cable. The cables should be free to slide, therefore the normal stress (the actual confinement effect) remains constant along the semi-circumference (Figure 68).

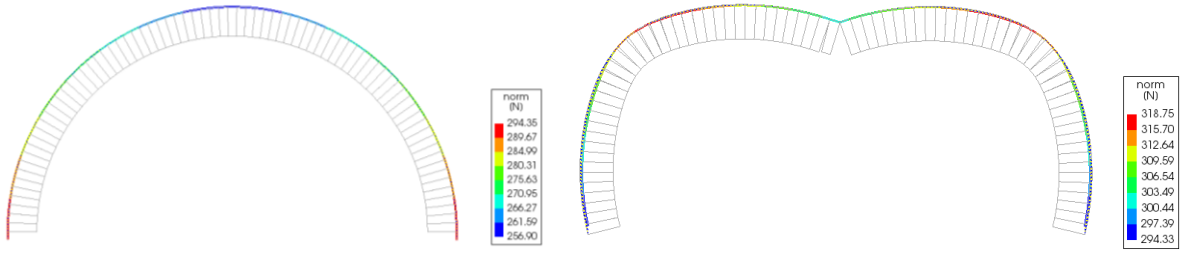

Figure 66 - Cable axial force at the end of the application of the post-tension (left) and at collapse (right). (Micro-model, physical cables, φ=5°, deformation x20).

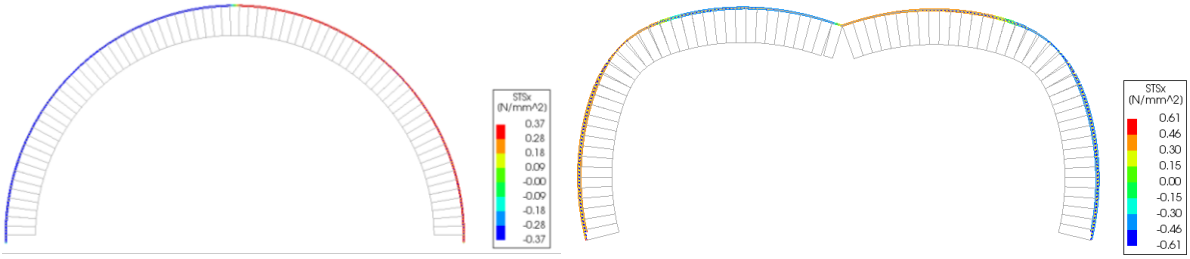

Figure 67 – Shear stress in the interface at the end of the application of the post-tension (left) and at collapse (right). (Micro-model, physical cables, φ=5°, deformation x20).

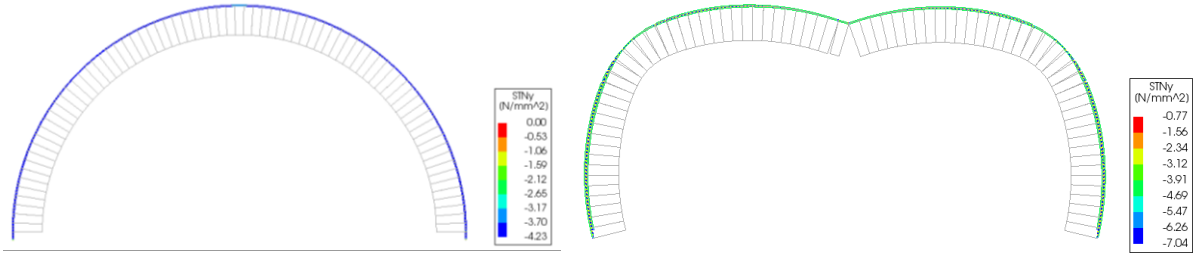

Figure 68 – Normal stress in the interface at the end of the application of the post-tension (left) and at collapse (right). (Micro-model, physical cables, φ=5°, deformation x20).

The aim of this sensitivity analysis is to determine a sufficiently low value of the friction angle, that permits the actual sliding of the cables and guarantees a low shear stress at the interface. Moreover, the effect itself on the arch capacity has been investigated. Four values of friction angle have been considered: 0.6°, 5°, 20°, 30°. The interaction cable/arch has been studied in three representative points of the arch, shown in Figure 69:

- Close to the impost (A);
- At about 45° (B);
- Close to the maximum height point (C).

The points A and C have not been chosen at the very base and tip to avoid disturbance due to local phenomena, such as stress concentrations or changes of sign of the parameters (Figure 69).

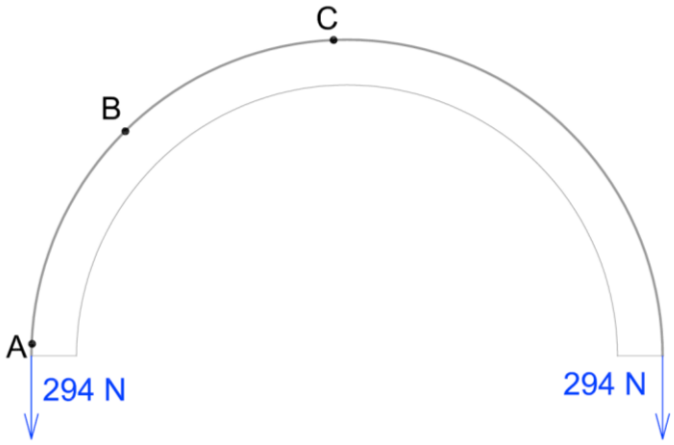

Figure 69 – Three point chosen for investigating the interaction cable/arch.

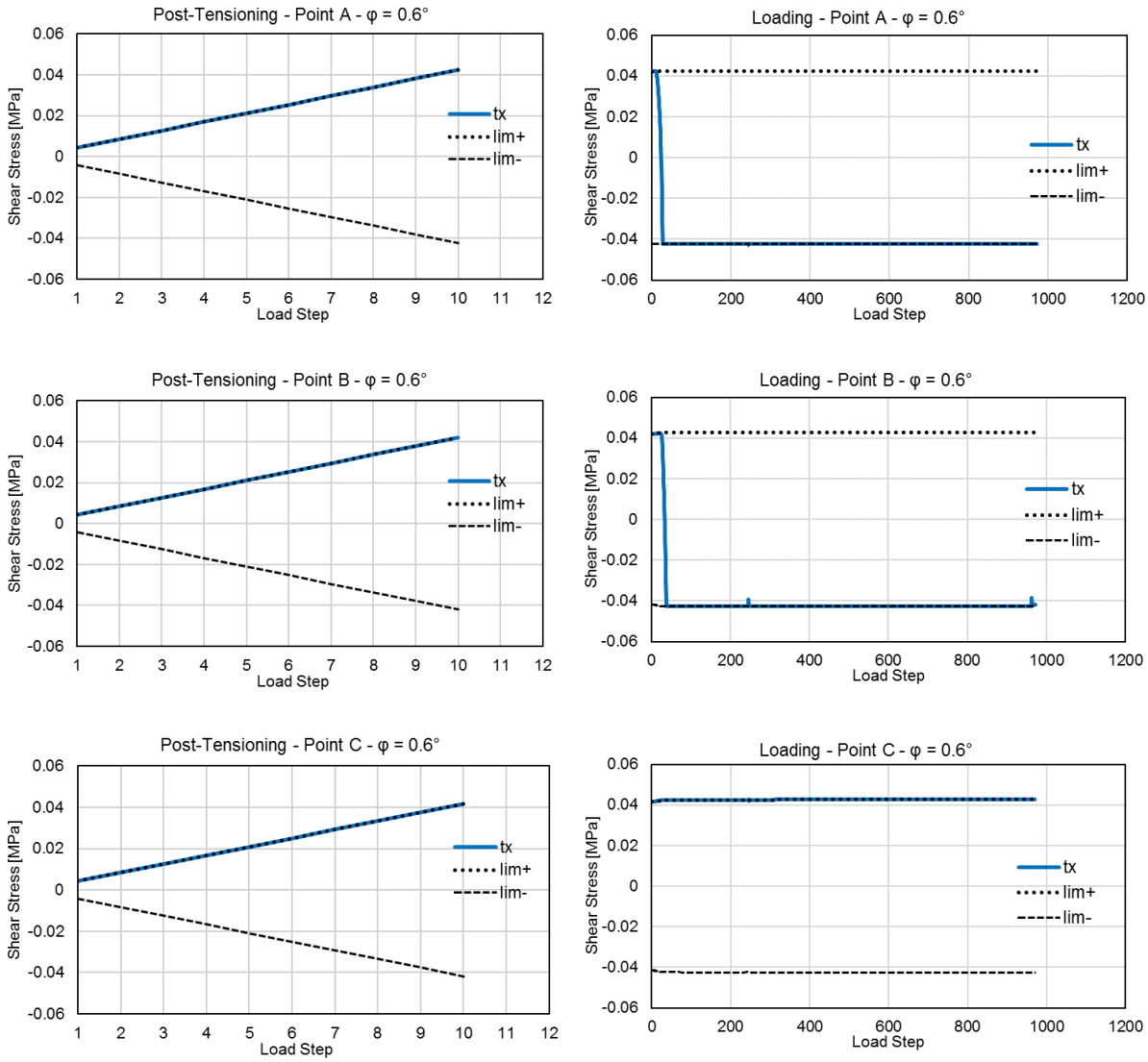

Figure 70 – Friction angle φ = 0.6°. Shear stress trend.

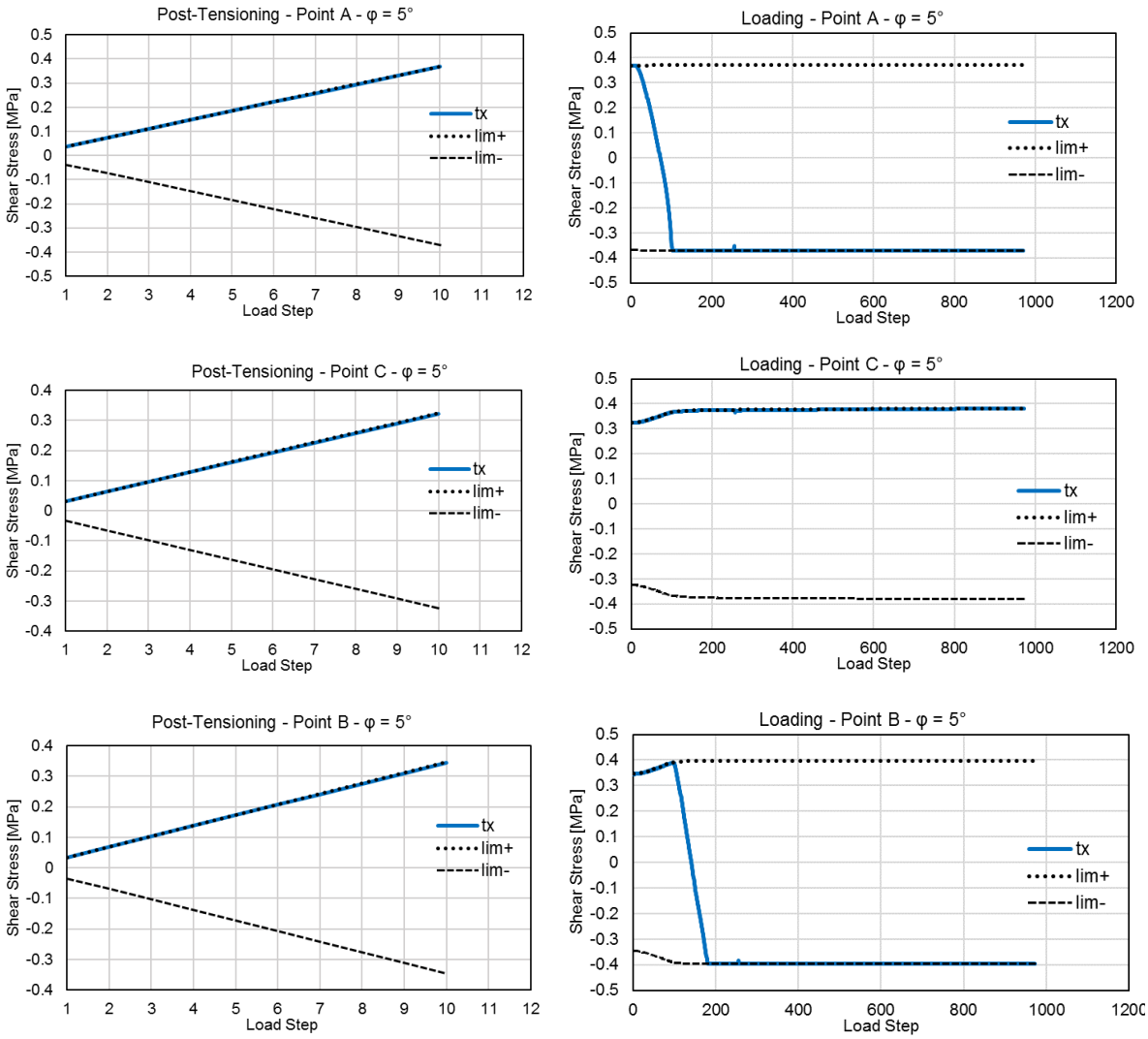

Figure 71 - Friction angle φ = 5°. Shear stress trend.

It can be noticed that, increasing the friction angle from 0.6° to 5°, during all the post-tensioning phase the cable slides, since the value of shear stress is always equal to the limit one, in all the three point considered (Figure 70 and Figure 71). During external loading, instead, at the points A and B, the phase of adherence becomes longer, proportionally to friction angle increase. In both cases, in A and B, the shear stress inverts its sign, due to the inversion of the relative displacement cable/arch from the post-tensioning phase to the external loading one. This can be notice also in Figure 66, from the direction of the displacement of the cable ends, relatively to the arch extrados, in the two phases: during post-tensioning they move downwards, then during external loading they move upwards, causing also the inversion of the friction force direction. Nevertheless, at point C the cable always slides. In addition, during the first phase, it can be noticed that the limit value of the shear stress always increases linearly. This is due to the constant increment of the post-tension applied, whose consequence is the constant increment of the radial normal stress and therefore of the shear resistance, due to Coulomb's friction law.

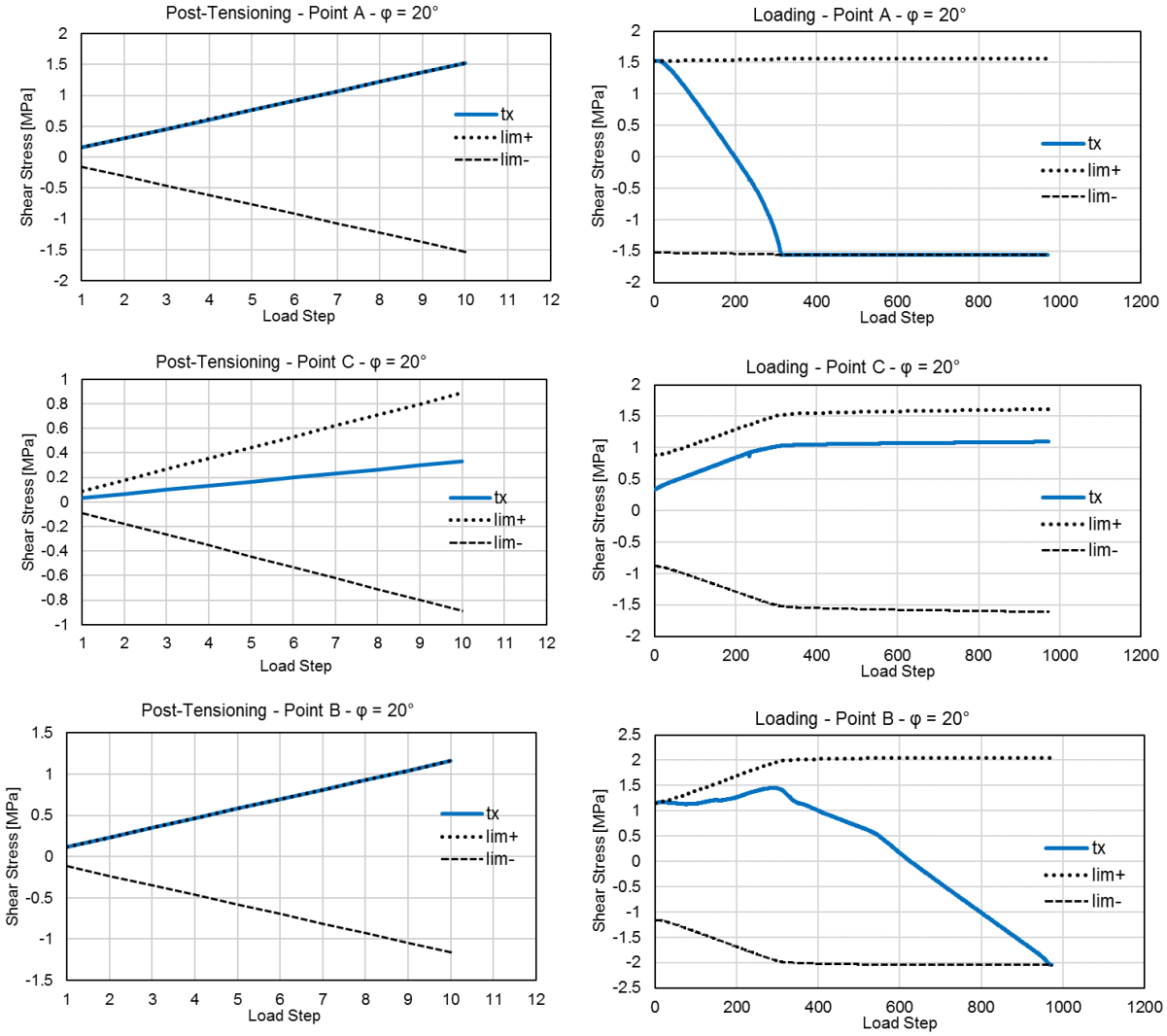

Figure 72 - Friction angle φ = 20°. Shear stress trend.

By further incrementing the friction angle to 20° and 30°, the tendency described is confirmed, and becomes more evident (Figure 72 and Figure 73). In point A, the adherence phase increases. Even, in B and in C full adherence is reached during all the second stage. Also during the post-tensioning phase adherence is enhanced. In both the friction angle cases adherence is obtained even for point C, while in A and B sliding is still present. This is due to greater relative displacement cable/arch activated during the first phase in the points closer to the impost (A and B), compared to the one near the symmetry axis (C). To sum up, as expected, increasing the friction angle adherence is enhanced.

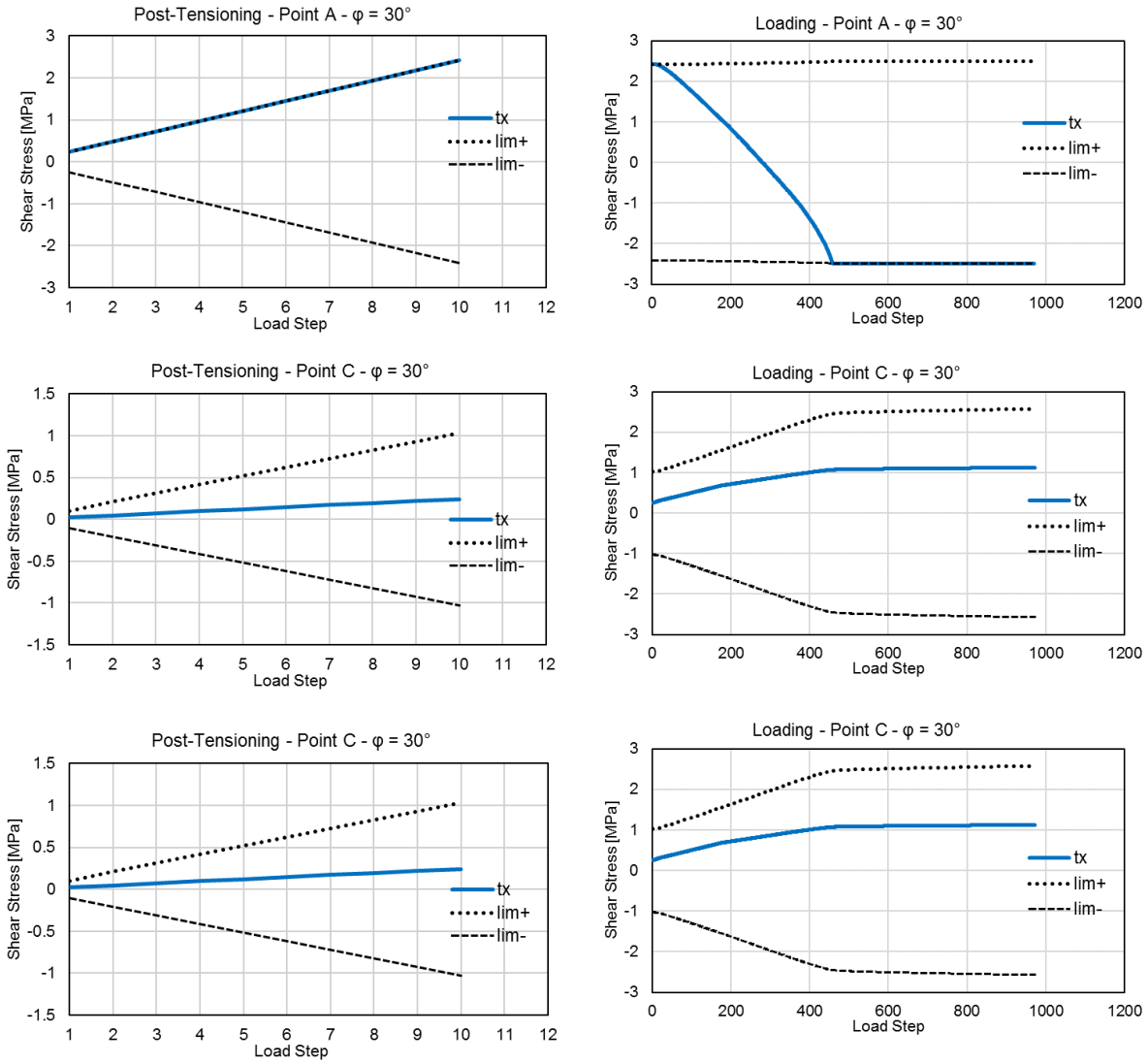

Figure 73 - Friction angle φ = 30°. Shear stress trend.

Even after these analysis, the real value of the friction angle cannot be established. Nevertheless, they can provide a precise indication of the effect of this parameter on the interaction cable/arch, especially in terms of sliding/adherence. More precise indications, to develop further analysis, can be derived, instead, by comparing the overall capacity of the reinforced arch, with different friction angles, with the experimental value (Figure 74).

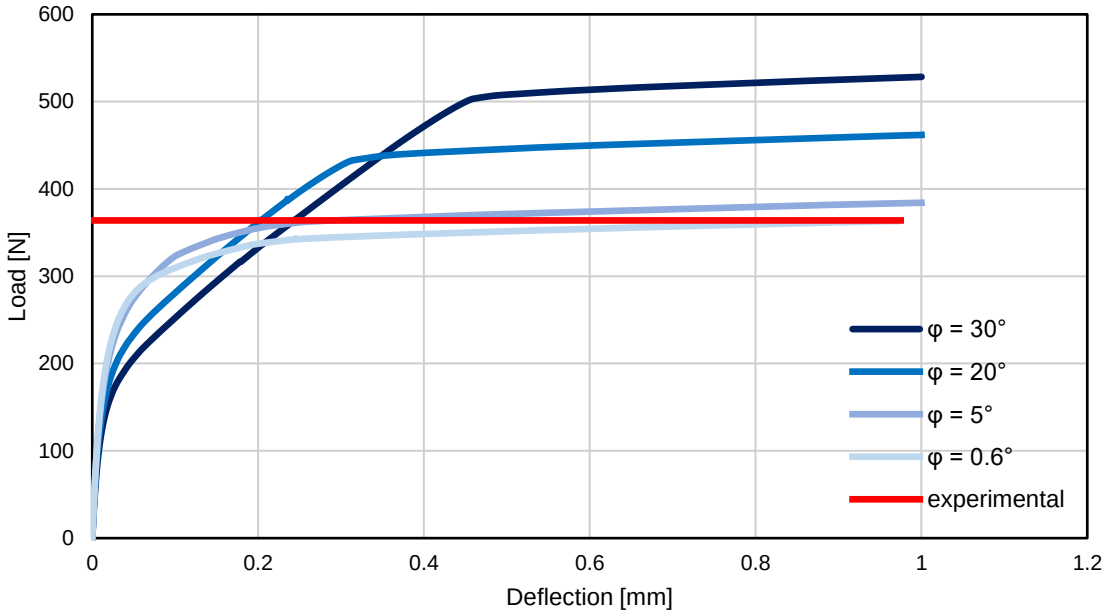

Figure 74 – Micro-model, load at ½ span, physical modelling of cables at the extrados, 294 N post-tension, 90 mm depth: comparison of capacity curve with different friction angles cable/arch.

The curve that better fits the experimental results is the one with the lower friction angle: φ = 0.6°. This means that, even though the real friction angle remains unknown, it is much likely that the cables are able to slide almost freely, and friction is essentially negligible.
This allowed to develop models with physical cables reinforcement able to slide, as it is supposed to be in the reality of the experiments. Therefore, in the further analysis a value of 0.6° has been used for the friction angle.

6.4.3 Free Sliding Cables Models Results

Micro-models with the presence of cable reinforcement were used for simulating the collapse behaviour of the experimental arches. The cases involved are the same of the previous analysis:

- Cable at the extrados (90 mm depth), 294 N of post-tension, load at 1/6 and half of the span;
- Cable at the intrados (100 mm depth), 294 N of post-tension, load at 1/6 and half of the span.

When the cables were applied at the extrados, debonding was allowed (gap opening of the interface), while in the cases with them at the intrados, the interfaces worked both in tension and compression. First, the cases of the reinforcement at the extrados are presented. Linear geometry has been used. The parameters used are the ones described in Table 25, with φ = 0.6°, to obtain free sliding in any phase. Analysis setup is reported in Table 26.

Element Type	8-noded
Element Size	8 mm
Steps increment of Displacement	0.001 mm
Iterative Method	Full Newton-Raphson
Convergence Control	Energy, Force, Displacements
Tolerance	0.01

Table 26 – Free sliding cable at the extrados, reinforced micro-model, analysis setup.

Concerning the post-tension application phase, in Figure 75 are reported the axial force distribution, the normal confinement stress and the shear stress at the interface cable/arch. Notice that the normal stress at the interface, if integrated along the width of the interface (0.1 mm), gives almost exactly the value of the equivalent confinement, calculated with the relation reported in Figure 47.

Equivalent Radial Load → p = T / R = 294 N / 695 mm = 0.423 N/mm

Confinement Effect from Cable Modelling → p' = σ_R x t = 4.24 MPa x 0.1 mm = 0.424 N/mm

T: cable traction, R: external radius, σ_R: radial normal stress, t: interface width.

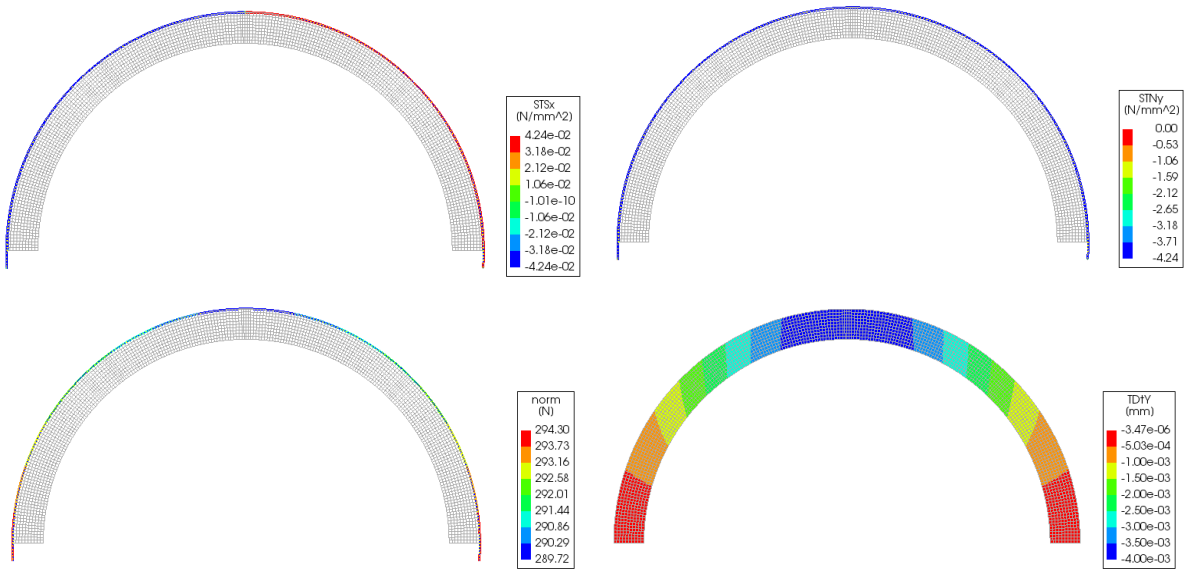

Figure 75 – Micro-model with physical reinforcement at the extrados (90 mm depth): end of the application of post-tension (294 N). Top: shear stress interface distribution (left) and normal stress interface distribution. Bottom: axial load in the reinforcement (left) and vertical displacements of the arch body (right). Deformation scale x200.

The capacity curves are reported in Figure 76 and Figure 77 in comparison with the ones computed for the cases concerning equivalent radial load reinforcement, treated in 6.3.

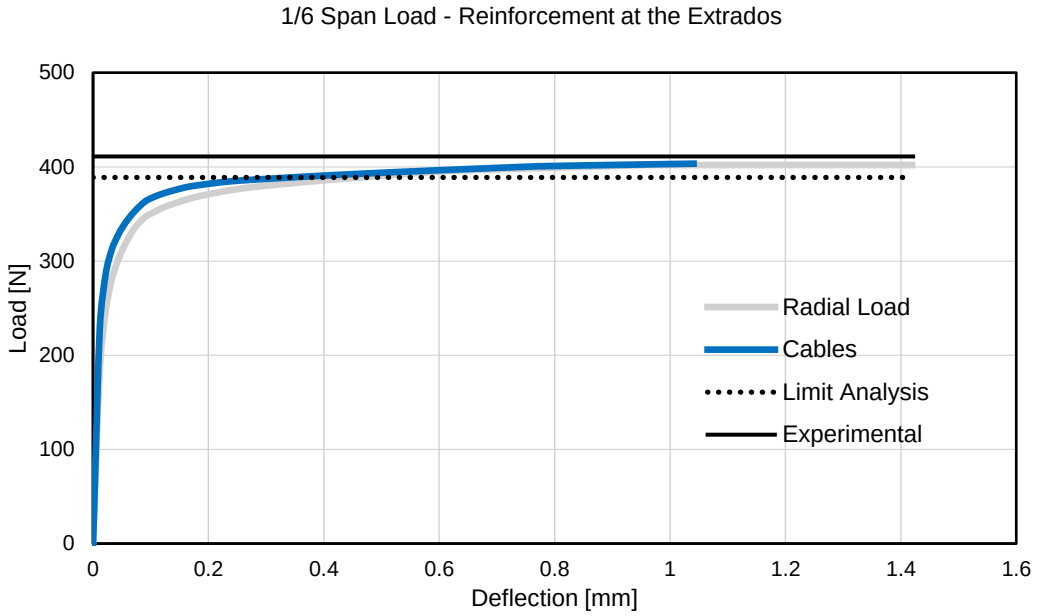

Figure 76 - Arch with physical cable at the extrados (294 N post-tension), load at 1/6 of the span, deflection of loaded point vs load applied, comparison with equivalent load case.

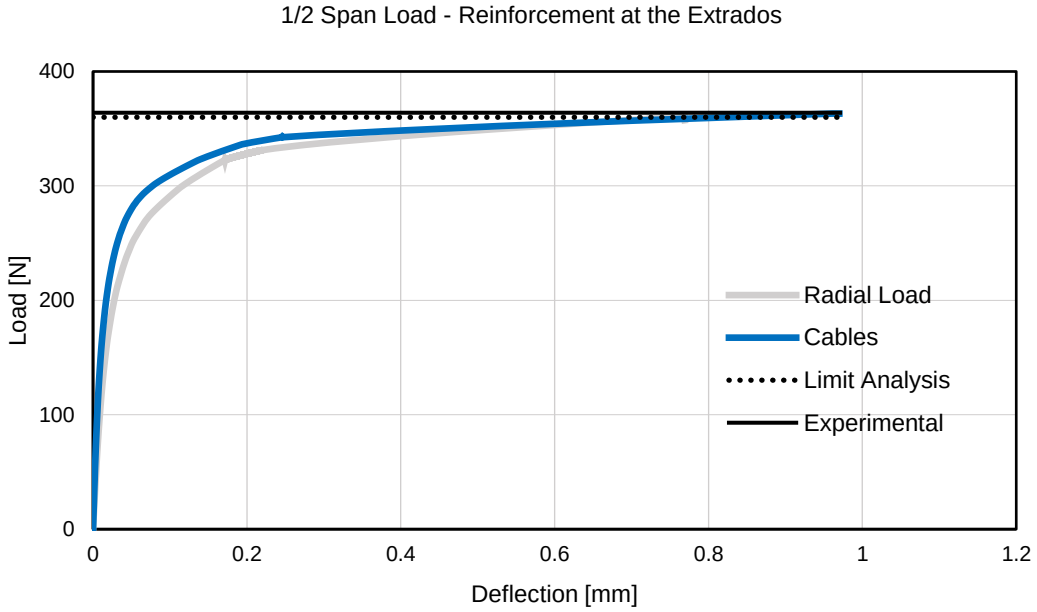

Figure 77 - Arch with physical cable at the extrados (294 N post-tension), load at 1/2 of the span, deflection of loaded point vs load applied, comparison with equivalent load case.

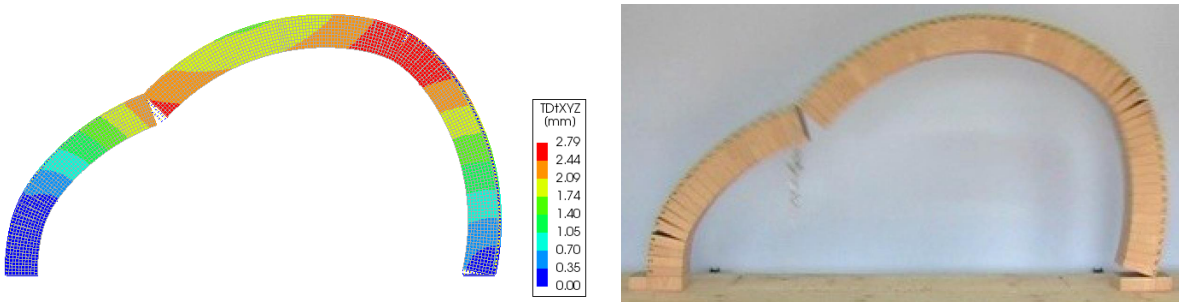

Figure 78 - Left: micro-model with physical reinforcement at the extrados, 90 mm depth, load at 1/6 of the span, norm of displacements at collapse deformed configuration (x50 amplification). Right: experimental collapse configuration.

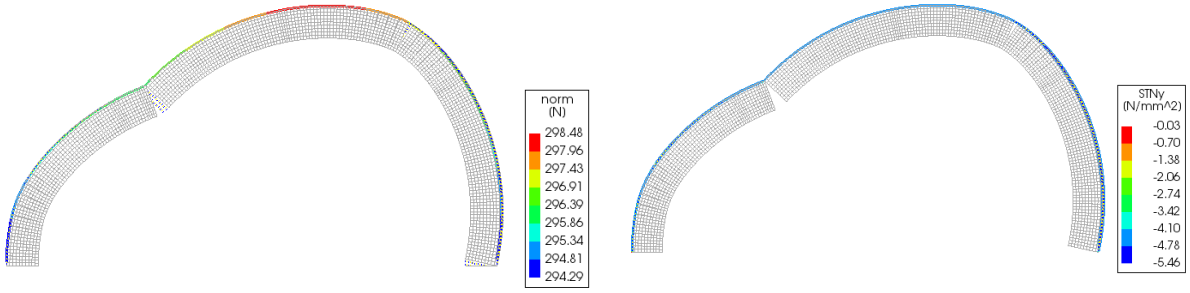

Figure 79 - Micro-model with physical reinforcement at the extrados, 90 mm depth, load at 1/6 of the span, collapse deformed configuration (x50 amplification). Left: axial force in the cable, right: interface normal stress.

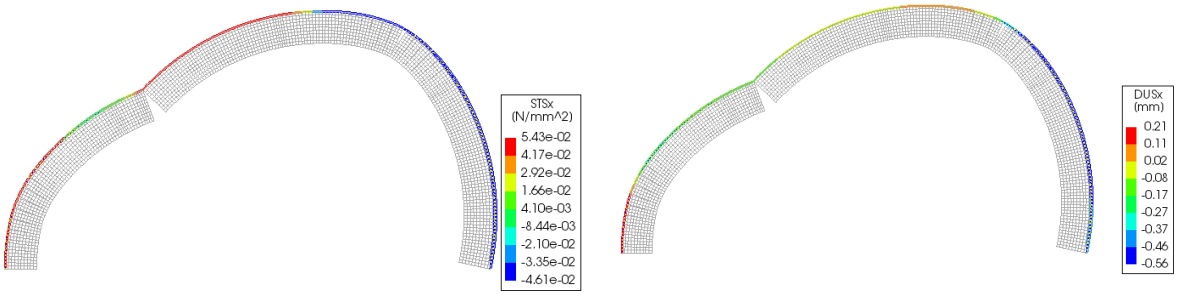

Figure 80 - Micro-model with physical reinforcement at the extrados, 90 mm depth, load at 1/6 of the span, collapse deformed configuration (x50 amplification). Left: shear stress at the interface, right: shear displacements.

The results show a good accordance with the ones derived from the equivalent load reinforcement (Figure 78 and Figure 81), confirming the coherence of the parameters choice, in both the load positions cases (Figure 84). The capacity, in fact, is close to the previously computed one. From contour plots it can be noticed that the tension of the cable is maintaining rather uniform around the post-tension value (Figure 79 and Figure 82), all along the circumference (3÷5 N excursion) and consequently the shear stress value at the interface are relatively low (0.045÷0.07 MPa) and the normal stress remains constant (radial confinement effect). The amount of shear relative displacements is limited and comprised between 0.21 mm and 0.56 mm (Figure 80 and Figure 83).

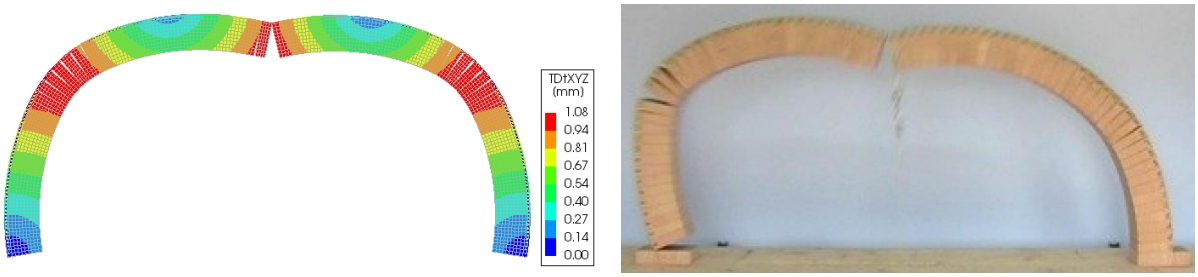

Figure 81 - Left: micro-model with physical reinforcement at the extrados, 90 mm depth, load at 1/2 of the span, norm of displacements at collapse deformed configuration (x70 amplification). Right: experimental collapse configuration.

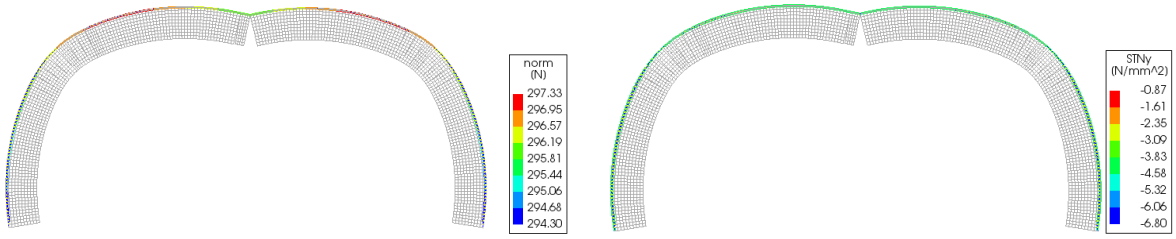

Figure 82 - Micro-model with physical reinforcement at the extrados, 90 mm depth, load at 1/2 of the span, collapse deformed configuration (x70 amplification). Left: axial force in the cable, right: interface normal stress.

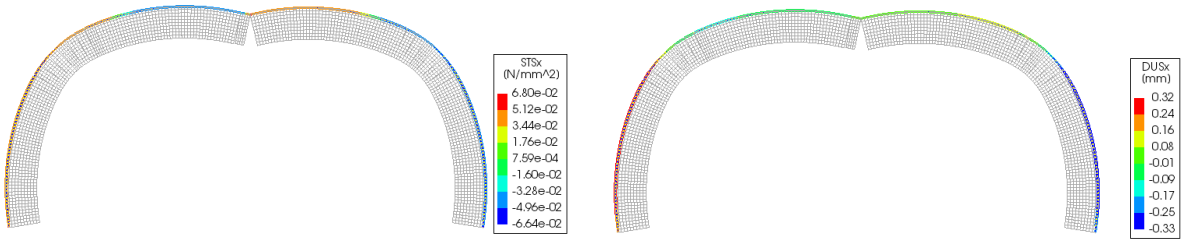

Figure 83 - Micro-model with physical reinforcement at the extrados, 90 mm depth, load at 1/2 of the span, collapse deformed configuration (x70 amplification). Left: shear stress in the interface, right: shear displacements.

Load position (span fraction)	Collapse load [N]				Error		
	Cable Model.	Radial Confinement	Experim.	Limit Analysis	to Radial Confinement	to Experim.	to L. Analysis
1/6	403	402	411	389	0.4%	-1.9%	3.8%
1/2	363	361	364	360	0.8%	-0.2%	0.9%

Figure 84 – Cable at the extrados: micro-models results and comparison with previous results and experimental ones.

Also the case concerning reinforcement at the intrados has been studied. The same considerations of the case at the extrados can be made. The model is the same one used previously, with 100 mm depth, with the addition of the steel cable at the intrados, with no possibility to debond at the interface with the arch. The analysis setup are reported in Table 27.

Element Type	8-noded
Element Size	8 mm
Steps increment of Displacement	0.001 mm
Iterative Method	Full Newton-Raphson
Convergence Control	Energy, Force, Displacements
Tolerance	0.01

Table 27 - Free sliding cable at the extrados, reinforced micro-model, analysis setup.

Also in this case, are reported the axial force distribution, the normal confinement stress and the shear stress at the interface cable/arch, soon after the post-tension application phase (Figure 85). Even in this case, the normal stress at interface, if integrated along the width of the interface (0.1 mm), gives the value of the equivalent confinement, here with a slight variability along the circumference.

Equivalent Radial Load→ p = T / R = 294 N / 600 mm = 0.49 N/mm

Confinement Effect from Cable Modelling→ p' = σ_R x t = 4.83÷4.91 MPa x 0.1 mm = 0.483÷0.491 N/mm

T: cable traction, R: external radius, σ_R: radial normal stress, t: interface width.

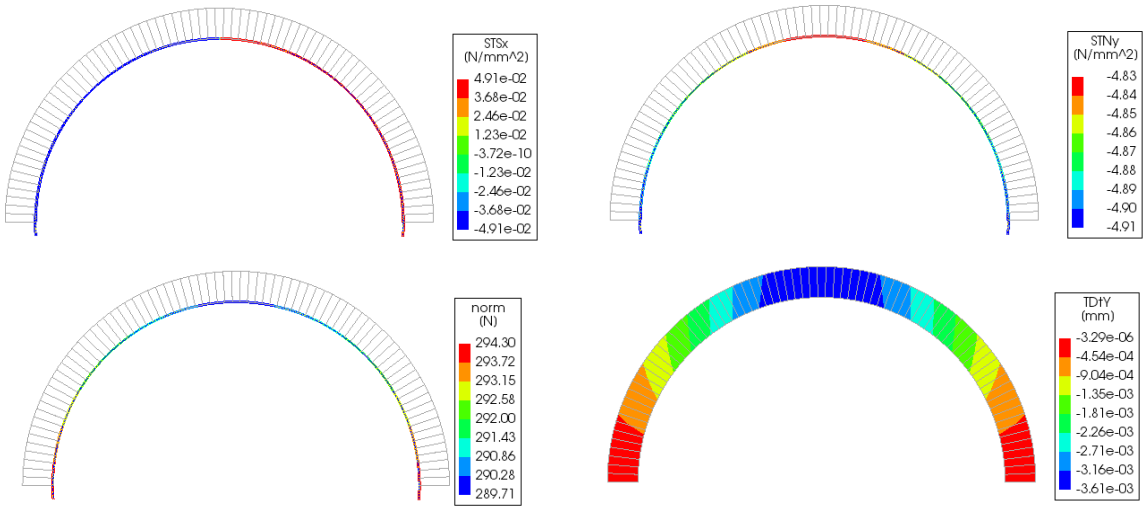

Figure 85 - Micro-model with physical reinforcement at the intrados (100 mm depth): end of the application of post-tension (294 N). Top: shear stress interface distribution (left) and normal stress interface distribution. Bottom: axial load in the reinforcement (left) and vertical displacements of the arch body (right). Deformation scale x200.

Even in this case, the capacity curves are reported in comparison with the ones computed for the cases concerning equivalent radial load reinforcement, treated in 6.3.

It must be underlined that, for the case of cables modelled at the intrados, for load position at ½ span, non-linear geometry has been applied, to get a better convergence.

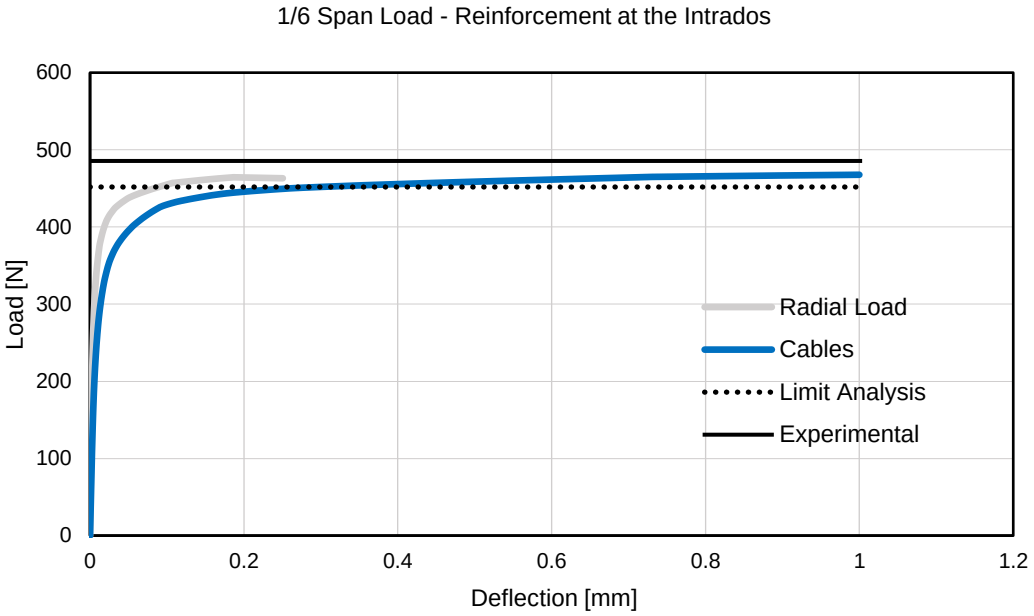

Figure 86 - Arch with physical cable at the intrados (294 N post-tension), load at 1/6 of the span, deflection of loaded point vs load applied, comparison with equivalent load case.

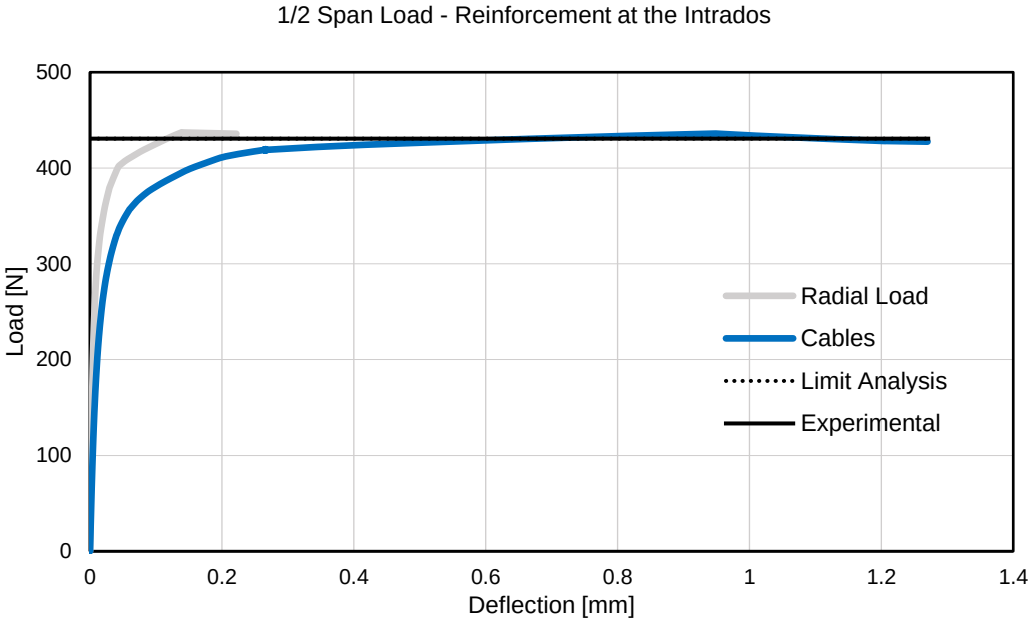

Figure 87 - Arch with physical cable at the intrados (294 N post-tension), load at 1/2 of the span, deflection of loaded point vs load applied, comparison with equivalent load case.

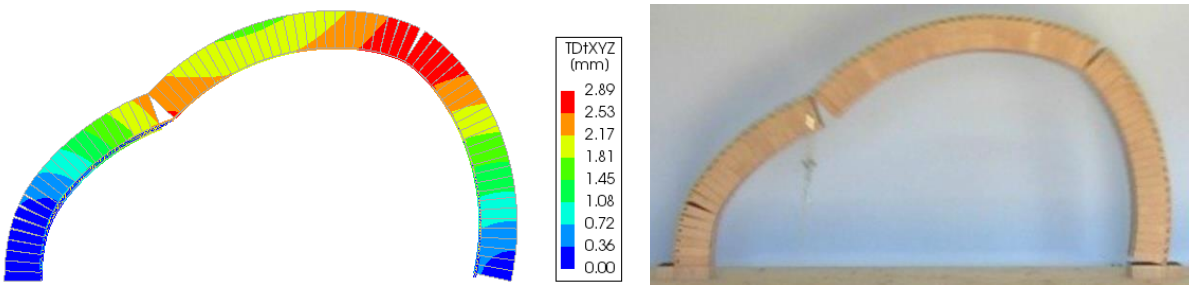

Figure 88 - Left: micro-model with physical reinforcement at the intrados, 100 mm depth, load at 1/6 of the span, norm of displacements at collapse deformed configuration (x50 amplification). Right: experimental collapse configuration.

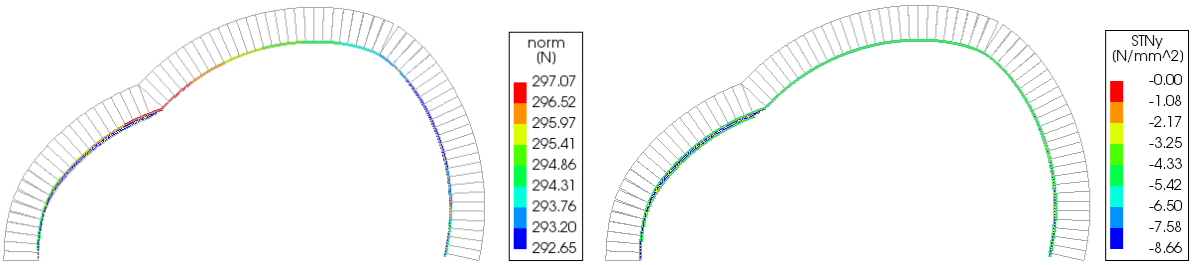

Figure 89 - Micro-model with physical reinforcement at the intrados, 100 mm depth, load at 1/6 of the span, collapse deformed configuration (x50 amplification). Left: axial force in the cable, right: interface normal stress.

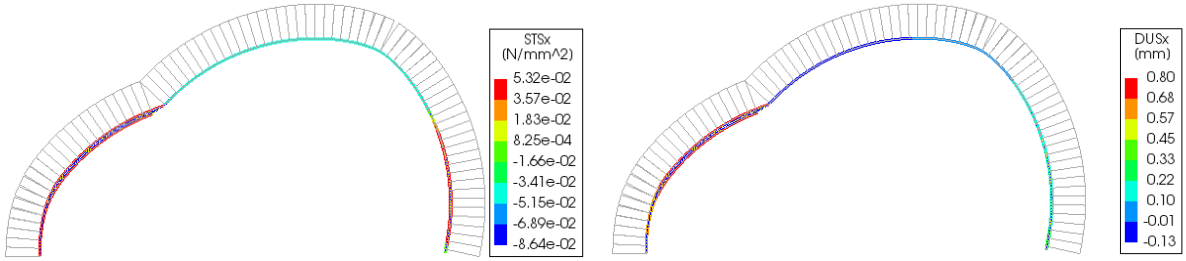

Figure 90 - Micro-model with physical reinforcement at the intrados, 100 mm depth, load at 1/6 of the span, collapse deformed configuration (x50 amplification). Left: shear stress in the interface, right: shear displacements.

Even in the case of cables at the intrados, the results show a good accordance, in terms of capacity (Figure 86 and Figure 87), with the ones derived from the equivalent load reinforcement (Figure 94), in both the load positions (Figure 88 and Figure 91). Again, the tension of the cable is keeping rather uniform around the post-tension value (293÷297 N). The shear stress value at the interface are also relatively low (Figure 90 and Figure 93) (0.05÷0.09 MPa) and the normal stress keeps constant (radial confinement effect) (Figure 89 and Figure 92). The amount of shear relative displacements remains between 0.13 mm and 0.80 mm.

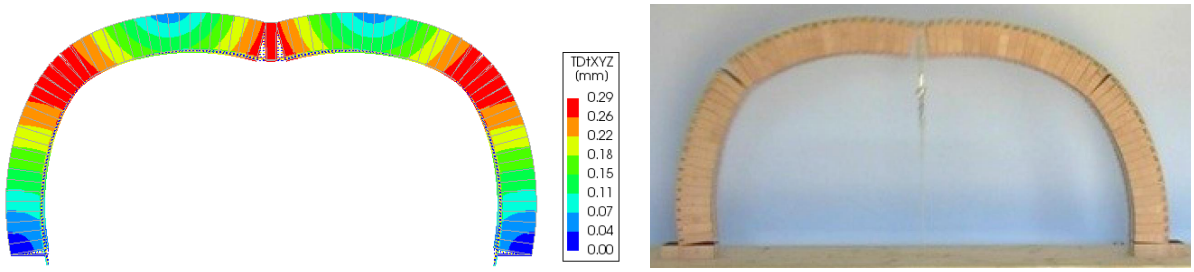

Figure 91 - Left: micro-model with physical reinforcement at the intrados, 100 mm depth, load at 1/2 of the span, norm of displacements at collapse deformed configuration (x300 amplification). Right: experimental collapse configuration.

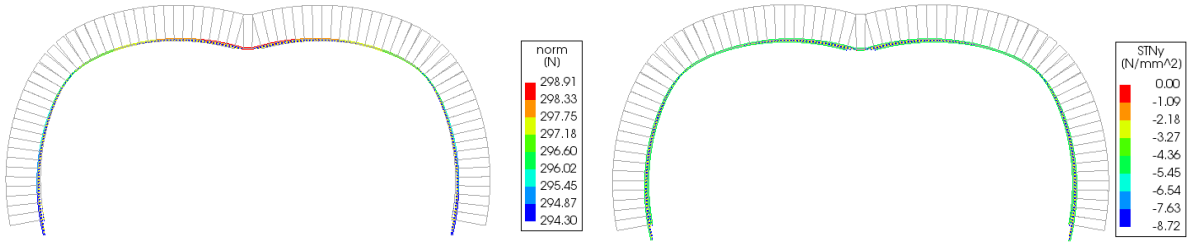

Figure 92 - Micro-model with physical reinforcement at the intrados, 100 mm depth, load at 1/2 of the span, collapse deformed configuration (x300 amplification). Left: axial force in the cable, right: interface normal stress.

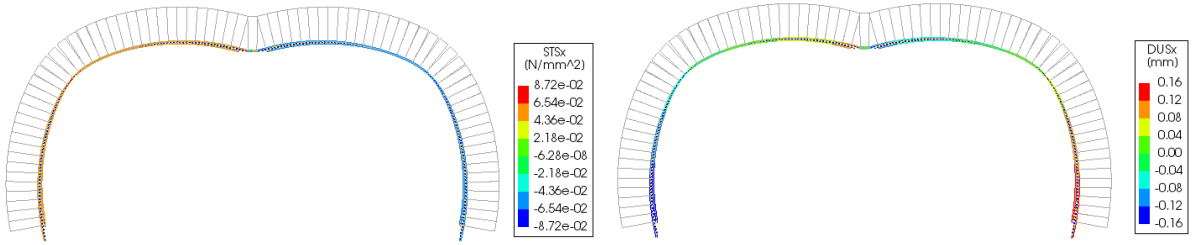

Figure 93 - Micro-model with physical reinforcement at the intrados, 100 mm depth, load at 1/2 of the span, collapse deformed configuration (x300 amplification). Left: shear stress in the interface, right: shear displacements.

Load position (span fraction)	Collapse load [N]				Error		
	Cable Model.	Radial Confinement	Experim.	Limit Analysis	to Radial Confinement	to Experim.	to L. Analysis
1/6	468	464	486	452	0.7%	-3.7%	3.5%
1/2	436	437	431	431	-0.3%	1.2%	1.2%

Figure 94 – Physical cable reinforcement at the intrados: micro-models results and comparison with previous results and experimental ones.

6.4.4 Anchored Cables Models Results

Micro-models have been used to investigate also the behaviour of the reinforced arch in the case of cables anchored at the ends. These cases showed a considerable increase of the capacity of the system, in the experimental tests, as explained in 3.2. For the sake of brevity only the case loaded at half span has been studied, in the cases of reinforcement applied either at the extrados or at the intrados.

Concerning the cable force, only the case with no post-tension and 294 N have been modelled. These models do not claim to capture the deformability of the system, but their aim is just to confirm the overall behaviour of the reinforcement, in terms of capacity and internal force distribution. The material parameters used for the blocks, the cables and the interfaces are the same of the ones used for the sliding cables cases, explained in the previous paragraph, in Table 25, with friction angle again φ = 0.6°. Both linear and non-linear geometry analysis have been performed. Analysis setup is reported in Table 28.

Element Type	8-noded
Element Size	8 mm
Steps increment of Displacement	0.001 mm
Iterative Method	Full Newton-Raphson
Convergence Control	Energy, Force, Displacements
Tolerance	0.01
Non-Linear Geometry	Total Lagrange

Table 28 – Anchored cables reinforced arch micro-models, analysis setup.

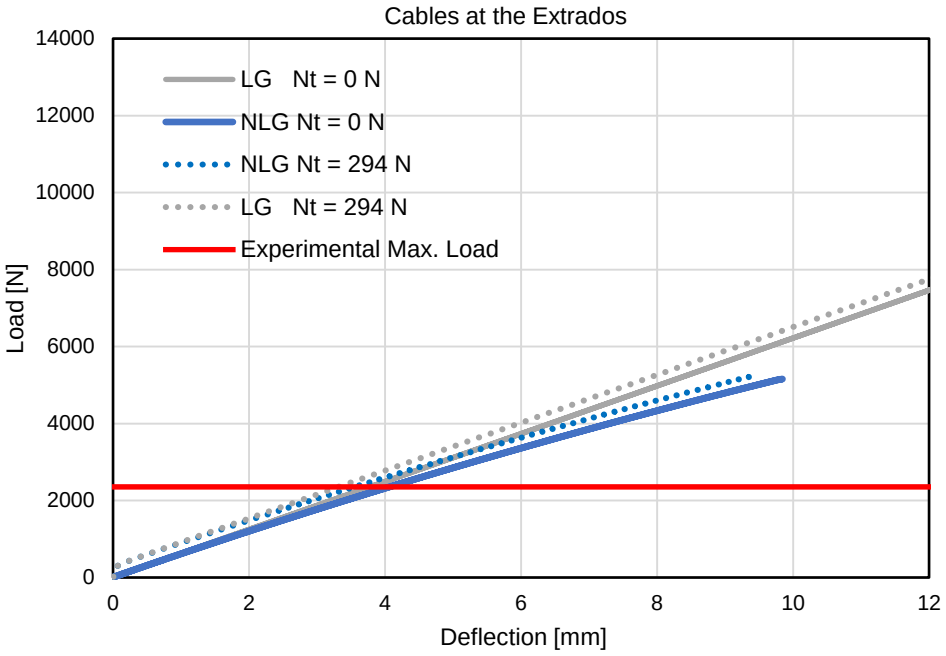

Figure 95 – Micro-models with anchored cables at the extrados results: force vs vertical displacement at the loading point. Linear and non-linear geometry analysis of no post tension and 294 N post-tension case.

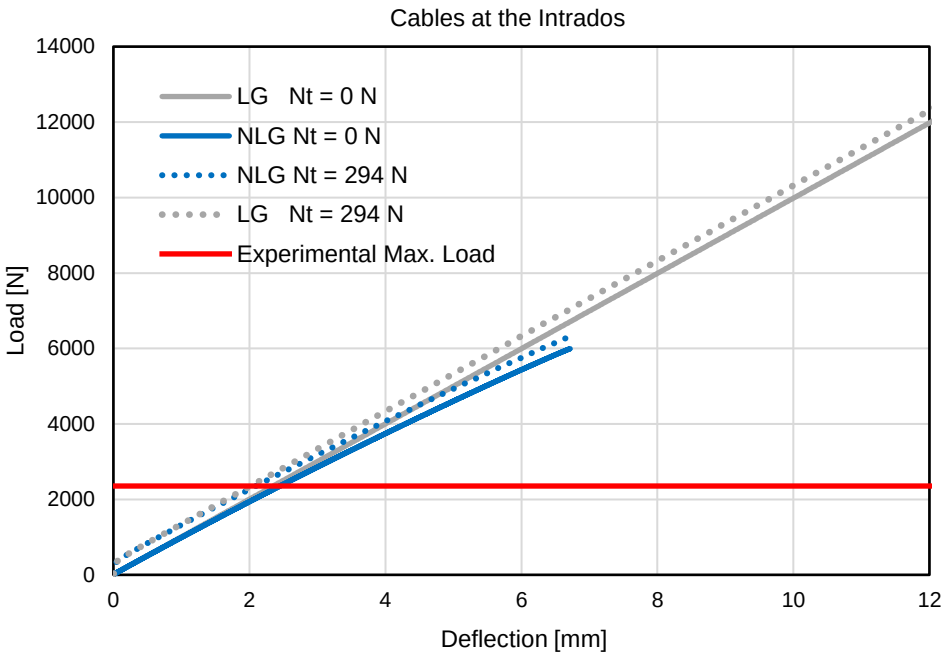

Figure 96 - Micro-models with anchored cables at the intrados results: force vs vertical displacement at the loading point. Linear and non-linear geometry analysis of no post tension and 294 N post-tension case.

It is evident also from the numerical results that the anchored cables are able to provide a much higher capacity, in terms of limit load and deformability. The capacity curve shows a linear behaviour in the case of linear geometry, and a quasi-linear one in the non-linear geometry analysis. In the first case, the analysis has been stopped without reaching the collapse, while in the second one a brittle collapse was reached, due to bucking phenomena. Nevertheless, as stated before, these results do not have a quantitative aim, since the numerical models do not take into account any material non-linearity. Even failures due to sliding between blocks is neglected. Therefore, these results only confirm the relevant amplification of the capacity of the arch, even largely overcoming the maximum load applied in the experimental tests of 2354 N, but they are not able to give a reliable indication of the new value of the collapse load. Moreover, it can be noticed that applying post-tension at the cables does not affect much the overall behaviour, since the improvement is rather negligible compared to the effect of the cable anchoring itself. In fact, in Figure 95 and Figure 96, it can be noticed that the post-tensioned case curve lays just slightly above the not-post-tensioned case one. Concerning the cable tension, in Figure 97 and Figure 98 is evident the difference between the cable tension trend in the anchored case and the sliding one, in a point chosen at ¼ of the semi-circumference. In the first one, the force is constantly increasing, while in the second one it remains substantially constant at the post-tension value.

In Figure 99 it can be noticed that, at an intermediate load step (300), the values of the tension of the cable is relevantly high, but rather uniform, likewise the one of radial interface stress. Nevertheless, shear stress is still relatively low, due to the extremely low friction angle chosen. This means that the great increase of overall strength is not due to friction increase, but to the increase of the confinement effect (one order of magnitude).

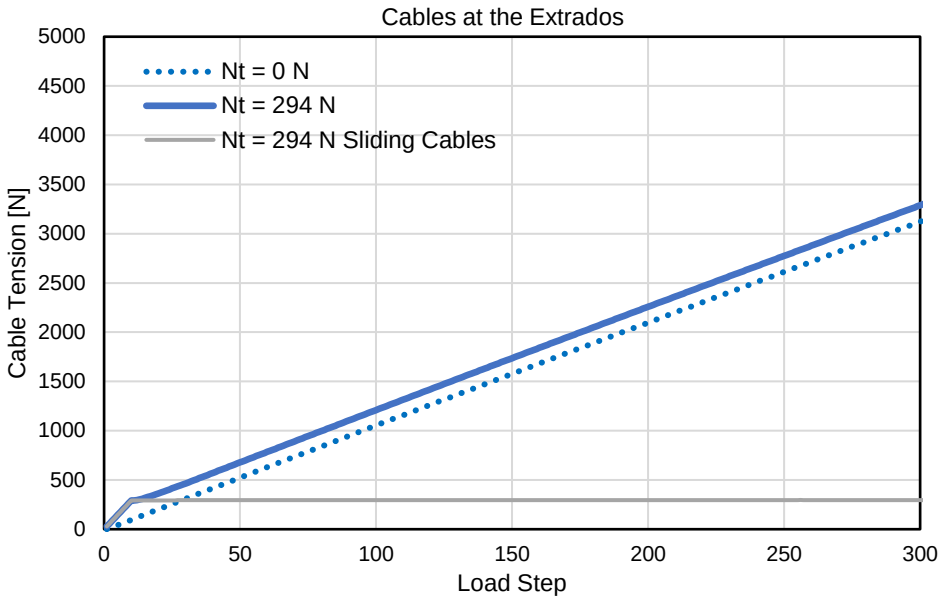

Figure 97 – Anchored cables at the extrados micro-model: cable tension trend at ¼ of the semi-circumference.

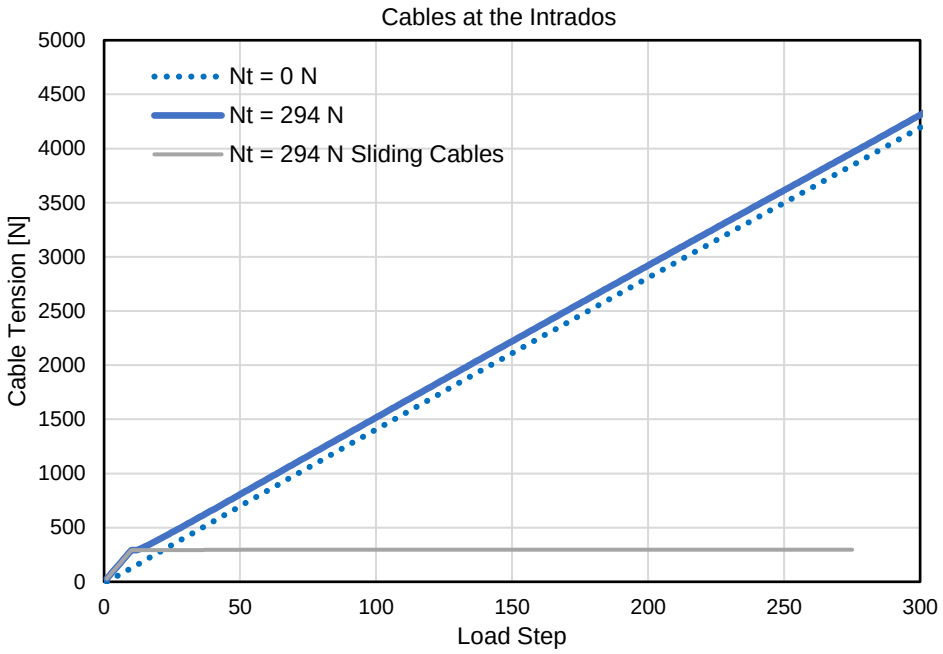

Figure 98 - Anchored cables at the intrados micro-model: cable tension trend at ¼ of the semi-circumference.

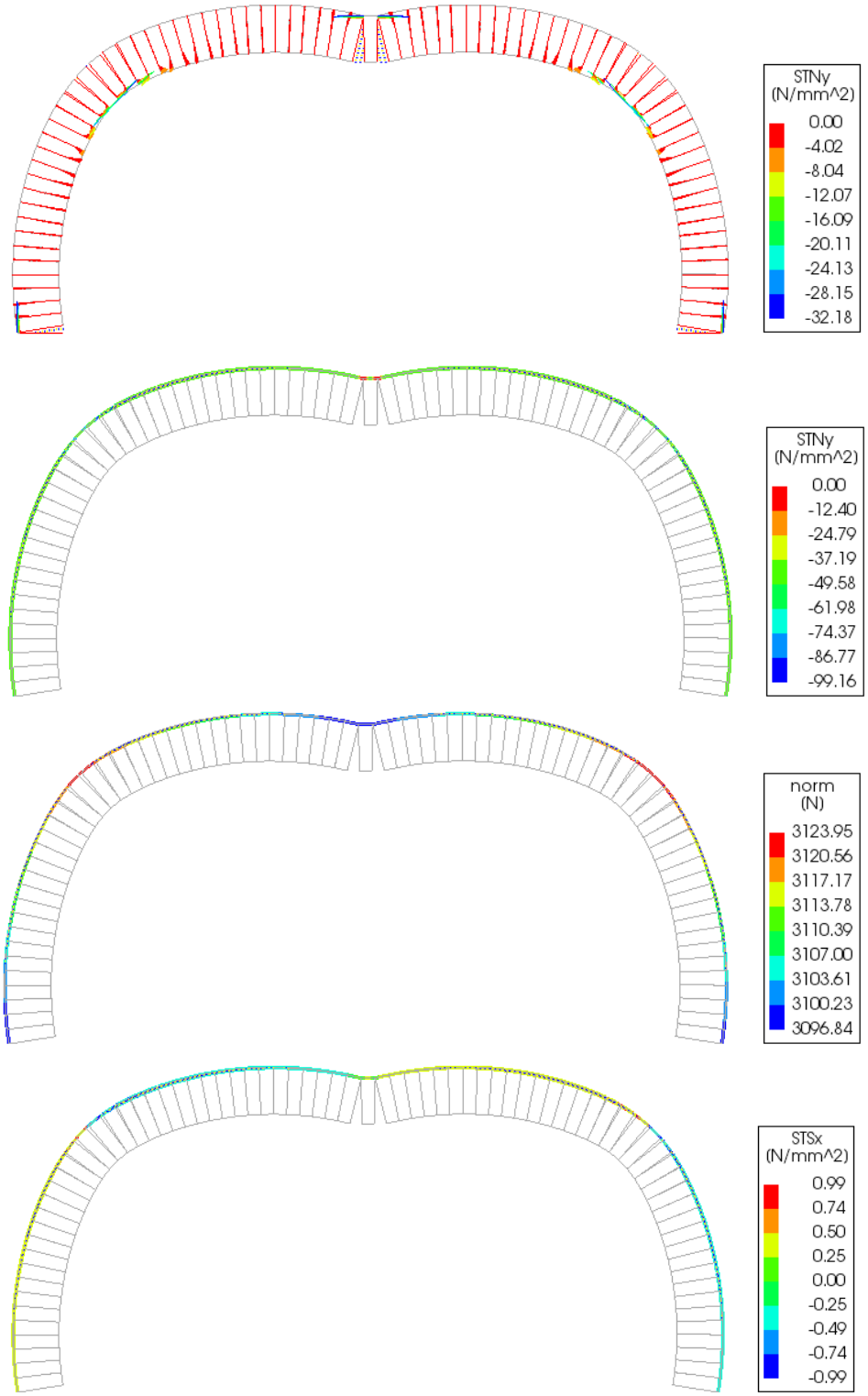

Figure 99 – Anchored cables at the extrados micro-model, no post-tension, step 300, deformation scale x10. From top downwards: compressive stress between blocks, normal stress at cable/arch interface, cable tension, shear stress at cable/arch interface.

7. NUMERICAL ANALYSIS: MACRO-MODELS

7.1 Hypothesis and Arch Body Material Parameters

The aim of this document is to investigate the behaviour of the RAM, also by means of macro-models. In fact, usually these kinds of models are more convenient for masonry structures, since they permit to produce a uniform material pattern, with averaged parameters of the elements composing masonry, including, in one only material, units and joints behaviour. This typically leads to a lower modelling effort and a lower computational time. The most diffused yield criteria used to simulate masonry non-linear behaviour are the ones based on the total-strain crack model, which includes smeared cracks patterns. In this case the subject of modelling is the experimental semi-circular arch, that entails no tension resistant joints and wooden-blocks. Therefore, the intrinsic behaviour of the elements and of the overall arch is rather different from the one of masonry structures. Nonetheless, it has been assumed that, once assessed coherent values of the parameters involved, macro-models can be a possible valuable alternative to micro-models. The parameters listed in Table 6, as in the previous case concerning micro-models' interface between cable and arch, have various levels of uncertainty. Some of them are known and some of them are unknown. What is important, when trying to define the unknown ones, is to understand their actual influence on the results desired. For instance, a reliable deformability analysis is not the scope of this study, but what is important is to obtain faithful results in terms of load capacity. To sum up, the macro-models' parameters have been calibrated to obtain equivalent models in terms of load capacity, while in micro-models the goal was to get the most faithful model compared with the experimental one. In Table 29 are reported the parameters involved in the smeared-crack model applied at the arch body, with their values and their level of uncertainty.

Parameter		Notation	Uncertainty Class	Value	Unit
Young Modulus*		E	Unknown	2000	MPa
Poisson Ratio		υ	Unknown	0.25	
Density	Unreinforced	ρ	Known	732	kg/m^3
	Extrados Reinf.	ρ	Known	667	kg/m^3
	Intrados Reinf.	ρ	Known	600	kg/m^3
Tensile Strength*		f_t	Unknown	0.001÷0.1	MPa
Tensile Fracture Energy*		G_f	Unknown	0.0001÷0.01	N/mm
Residual Tensile Strength		f_{t_res}	Unknown	0	MPa
Compressive Strength		f_c	Unknown	100	MPa
Compressive Fracture Energy		G_c	Unknown	160	N/mm
Residual Compressive Strength		f_{c_res}	Unknown	0	MPa

*Table 29 – Parameters of arch body in the macro-models. *These parameters are variable, and they have been object of a deeper analysis to determine better the valuable intervals.*

The most influencing parameters have been studied, in particular their effect on the resisting mechanism and the final value of load capacity. They are the Young modulus, the tensile strength and the fracture energy. Theoretically, the tensile strength should be set as null, but in this smeared crack model

problems due to incorrect failure arise, causing divergence. Therefore, a low but not null value of this parameter is needed. Compressive strength has been chosen extremely high to avoid any possibility of damage in compression. The value of fracture energy has been calculated with reasonable formulations concerning masonry, found in literature.

$$G_f \text{ [N/mm]} = 0.1\ f_t \text{ [N/mm}^2\text{]}$$
$$G_c \text{ [N/mm]} = 1.6\ f_c \text{ [N/mm}^2\text{]}$$

Once again, the density has been calculated depending on the depth of the arch concerned, to keep constant the overall weight.

7.2 Unreinforced Arch – Results

To understand the influence of the Young modulus and the tensile strength on the arch capacity, 4 macro-models have been produced, with different values of these parameters. As a sample, the unreinforced arch loaded at half span has been chosen, therefore the one with 82 mm of depth and 732 kg/m^3 of density. Concerning the Young modulus, two values have been considered: one reasonable for masonry (2000 MPa) and one as close as possible to the one of the wood used to shape the wedges of the experimental model (15000 MPa). As regards tensile strength, instead, three values have been considered: 0.0015 MPa, 0.01 MPa and 0.1 MPa (Table 30). Values of the tensile strength, lower than the ones chosen, induced unwanted severe cracking in the tangent direction, that led to early divergence, as will be shown more exhaustively in the next chapters. Analysis setup is reported in Table 31.

Model	f_t [MPa]	G_f [MPa]	E [MPa]
A	0.1	0.01	2000
B	0.01	0.001	2000
Γ	0.0015	0.00015	2000
Δ	0.01	0.00015	15000

Table 30 – Unreinforced macro-models loaded at half span: parameters setups for determining E and f_t influence on the vertical load capacity.

Element Type	4-noded
Element Size	7 mm
Steps increment of Displacement	0.002 mm
Iterative Method	Full Newton-Raphson
Convergence Control	Energy, Force, Displacements
Tolerance	0.01

Table 31 - Unreinforced macro-models' analysis setups for determining E and f_t influence on the vertical load capacity.

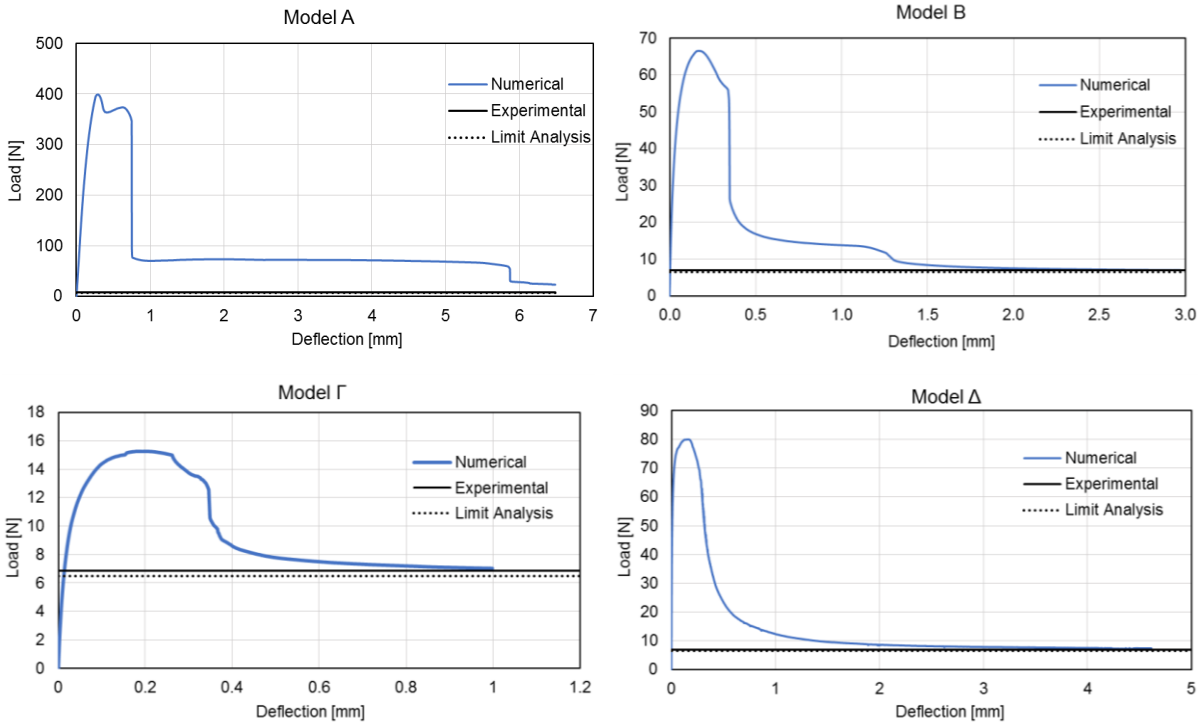

Figure 100 – Capacity curves obtained with macro-models, loaded at half span, with different values of E and f_t. Load vs loaded point deflection at half span.

Model	E [MPa]	f_t [MPa]	Collapse load [N]			Error to Numerical	
			Numerical	Limit Analysis	Experimental	Limit Analysis	Experimental
A	2000	0.1	18.1	6.5	6.9	179%	163%
B	2000	0.01	6.8	6.5	6.9	5%	-1%
Γ	2000	0.0015	7.0	6.5	6.9	9%	2%
Δ	15000	0.01	7.3	6.5	6.9	13%	7%

Table 32 – Macro-models of the unreinforced arch, loaded at half span. Comparison of capacity obtained with different values of tensile strength and Young modulus.

The first aspect that can be noticed is the presence of peaks, due to not null tensile strength. In fact, the models with higher tensile strength show higher peaks (Figure 100). These peaks are not representing the real behaviour of the experimental arch, since the absence of tensile strength does not allow such high value of the capacity. In these curves, the load capacity has to be interpreted as the residual value of resistance, obtained at high deformation values, when the collapse mechanism is fully developed. Nevertheless, it can be also noticed that even the residual resistance is affected from the tensile strength value. The results coming from model A, with higher value of tensile strength and lower Young modulus, show a much higher value of the capacity compared to the experimental results, while models B (Figure 101) and Γ, with tensile strength of one and two orders of magnitude lower, show much higher accordance with the experimental and limit analysis results (Table 32). Therefore, the value of tensile strength to be applied in the further analysis, even though is not exactly defined, should be of the order of magnitude of $10^{-2} \div 10^{-3}$ MPa, and consequently the tensile crack energy of $10^{-3} \div 10^{-4}$ N/mm.

Concerning the analysis performed with a higher Young modulus (model Δ), the final capacity obtained is slightly higher than the experimental value. Nevertheless, these results can still be rated as valuable. This means that the Young modulus is not a much affecting the final capacity of the structure, despite a lower value gives better results. Therefore, in further analysis a value of 2000 MPa has been kept.

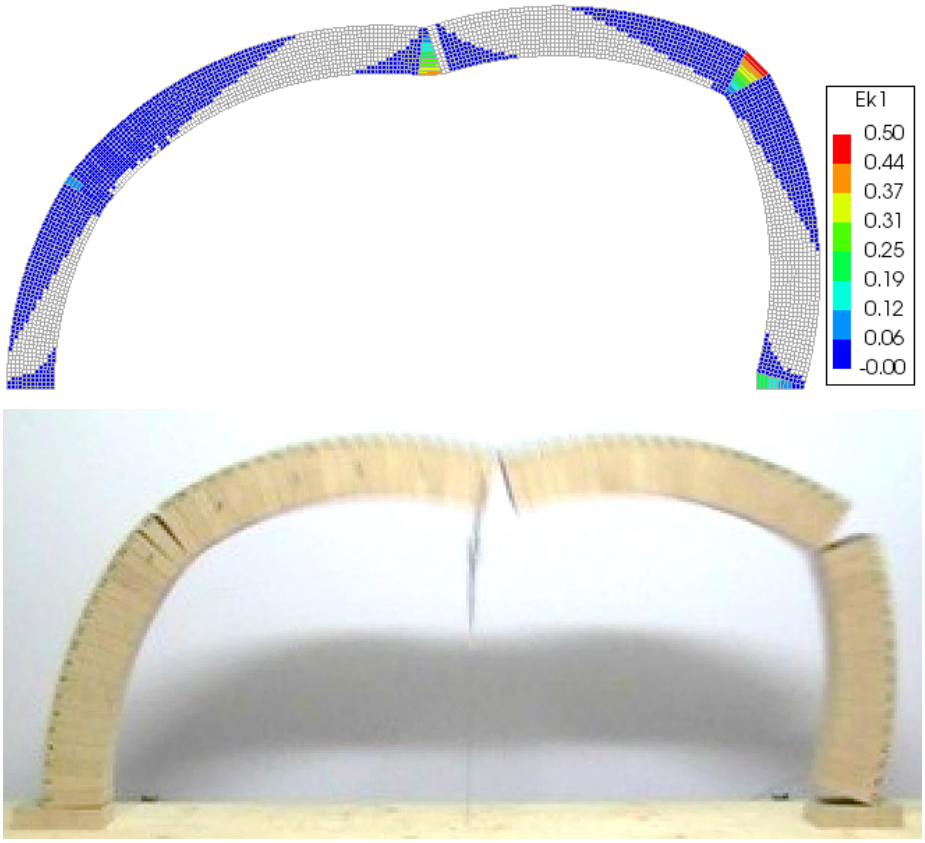

Figure 101 - Unreinforced arch, load at 1/2 of the span. Top: macro-model (82 mm depth, f_t = 0.01 MPa, E = 2000 MPa), collapse hinged mechanism, x15 deformation scale, principal crack strains. Bottom: experimental arch collapse configuration.

Even the case loaded at 1/6 of the span has been considered. Two different values of tensile strength have been applied, while Young modulus has been kept constant at 2000 MPa, reported in Table 33.

Model	f_t [MPa]	G_f [MPa]	E [MPa]
K	0.01	0.001	2000
Λ	0.0015	0.00015	2000

Table 33 - Unreinforced macro-models loaded at 1/6 of the span: parameters setups.

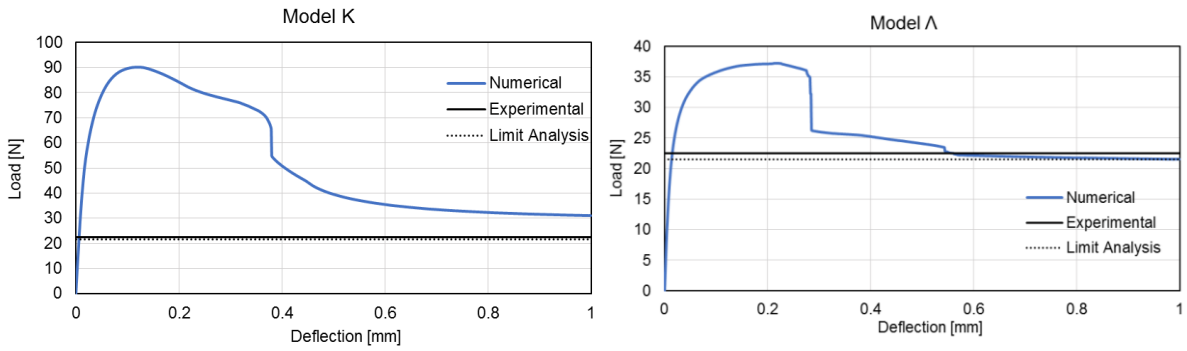

Figure 102 - Capacity curves obtained with macro-models loaded at 1/6 of the span. Left: model K (f_t=0.01 MPa). Right: model Λ (f_t = 0.0015). Load vs loaded point deflection at 1/6 of the span.

Model	E [MPa]	f_t [MPa]	Collapse load [N]			Error to Numerical	
			Numerical	Limit Analysis	Experimental	Limit Analysis	Experimental
K	2000	0.1	31.1	21.5	22.6	45%	38%
Λ	2000	0.015	21.5	21.5	22.6	0%	-5%

Figure 103 - Macro-models of the unreinforced arch, loaded at 1/6 of the span. Comparison of capacity obtained with different values of tensile strength.

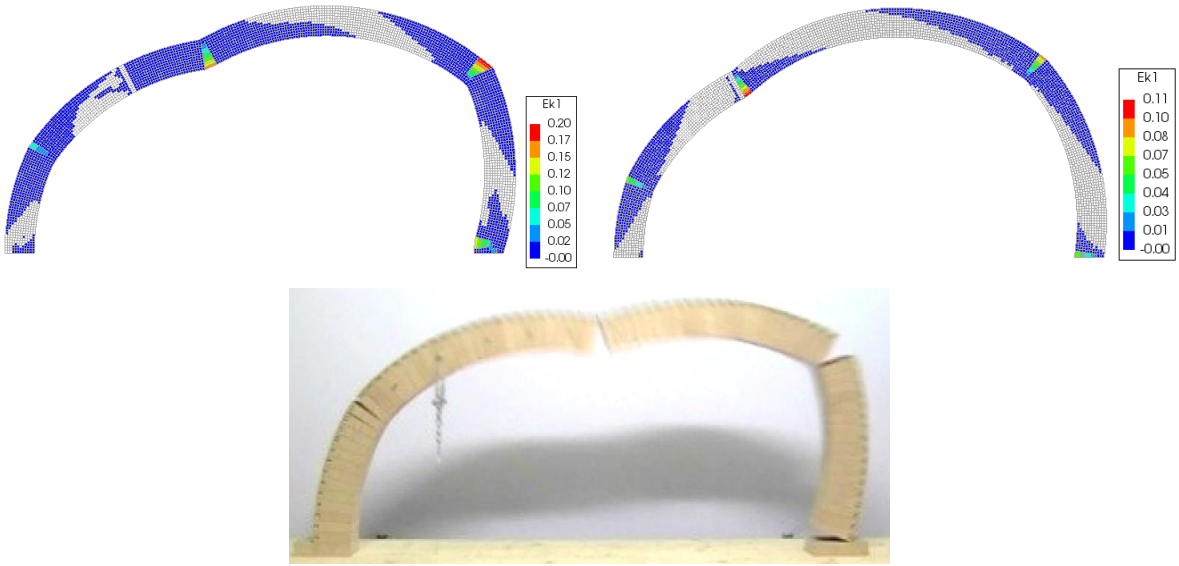

Figure 104 – Unreinforced arch, load at 1/6 of the span. Top: macro-model results (82 mm depth), collapse hinged mechanism, x30 deformation scale, principal crack strain: f_t = 0.0015 MPa (left), f_t = 0.01 MPa (right). Bottom: experimental arch collapse configuration.

In this second case, concerning the arch loaded at 1/6 of the span, the model with higher tensile strength (0.01 MPa), despite being a low value compared to the normal masonry ranges, showed a final value not negligibly higher than the one of the experimental results (Figure 102 and Figure 103). Moreover, the hinges distribution is much different than the experimental one (Figure 104). By reducing the value of the tensile strength to 0.0015 MPa, the value of the capacity converges to the one obtained with limit analysis, and the hinges distribution becomes more coherent with the experimental one. Therefore, the

correct value of the tensile strength is not unique, but can vary depending on the case analysed, in a limited range of values. This is a rather important drawback of macro-models, since the load capacity has shown to be affected from the tensile strength entity, even when its values are relatively low.

7.3 Reinforced Arch with Equivalent Radial Load - Results

The same cases analysed in 6.3 have been modelled also with macro-models, with the same geometry for the two reinforcement layouts. For these analysis, in general, a tensile resistance of 0.01 MPa has been used, with tensile crack energy of 0.001 N/mm. Lower values, in these cases, led again to problems of unwanted tangential cracking phenomena.

First, the case of radial load at the extrados is presented. Again, the only case of 294 N of post-tension has been studied. Analysis setup is reported in Table 34.

Element Type	4-noded
Element Size	8 mm
Steps increment of Displacement	0.001 mm
Iterative Method	Full Newton-Raphson
Convergence Control	Energy, Force, Displacements
Tolerance	0.01

Table 34 - Macro-models with equivalent radial load at the extrados, analysis setup.

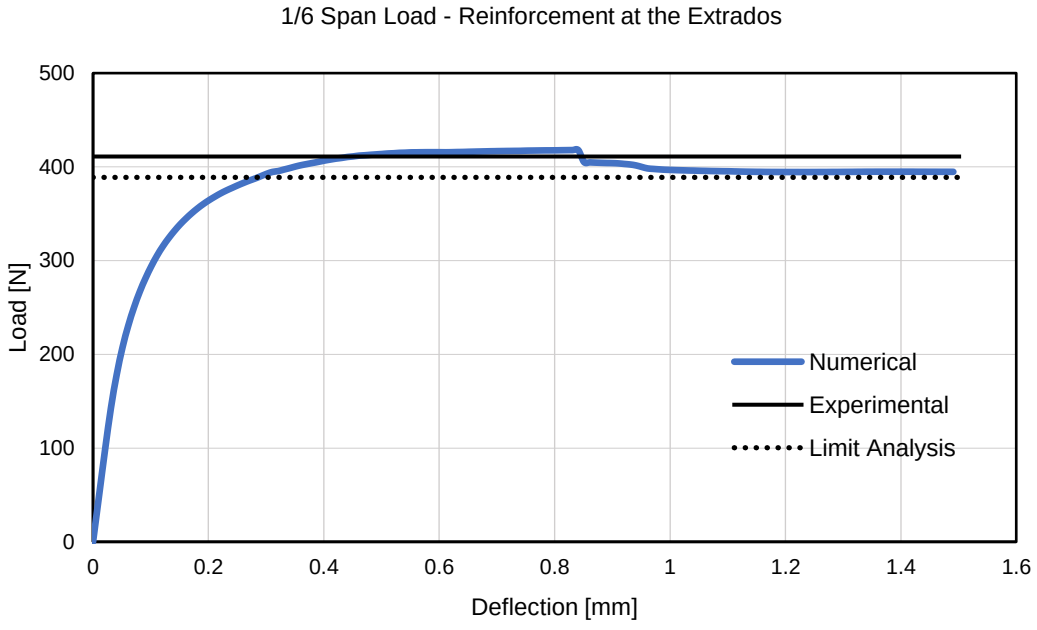

Figure 105 – Macro-model results: arch with equivalent radial reinforcement at the extrados (294 N post-tension), load at 1/6 of the span, deflection of loaded point vs load applied.

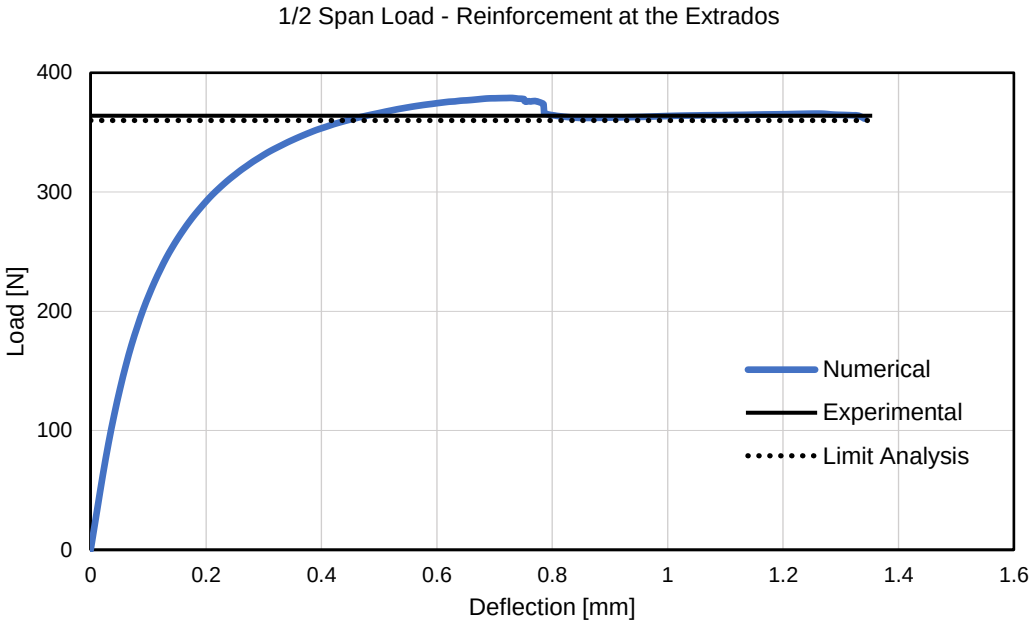

Figure 106 - Macro-model results: arch with equivalent radial reinforcement at the extrados (294 N post-tension), load at 1/2 of the span, deflection of loaded point vs load applied.

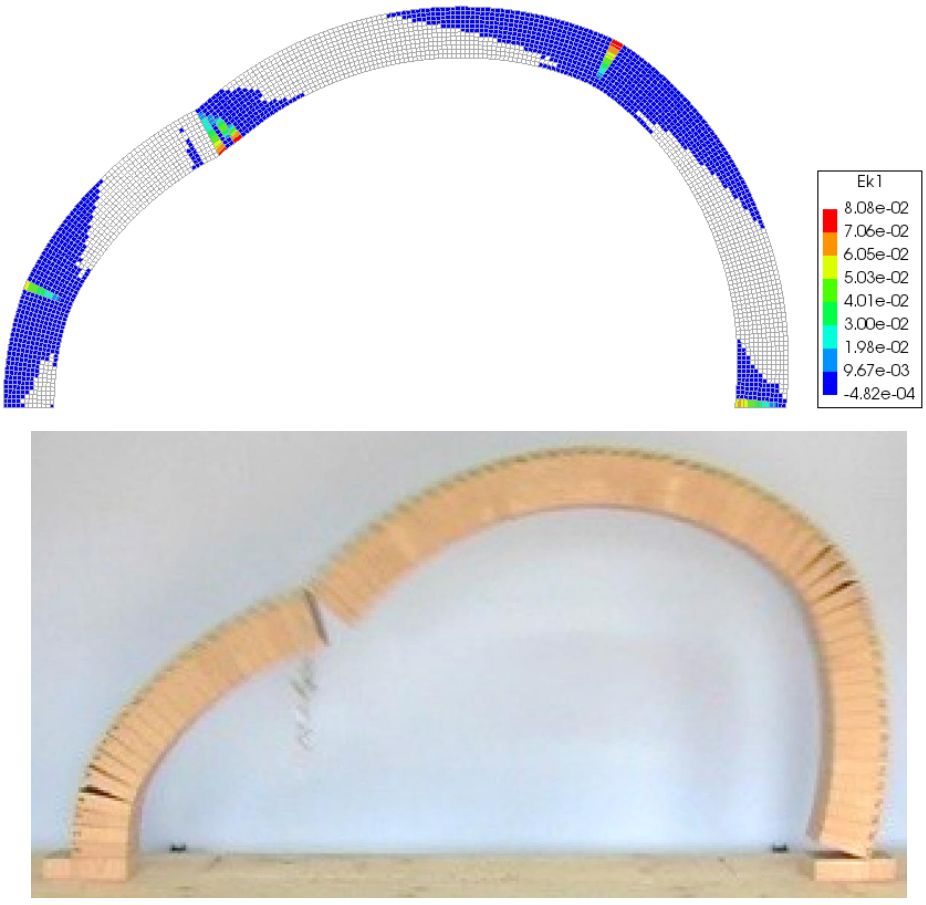

Figure 107 - Top: macro-model with equivalent radial reinforcement at the extrados, 90 mm depth, load at 1/6 of the span, principal crack strain at collapse deformed configuration (x20 amplification). Bottom: experimental collapse configuration.

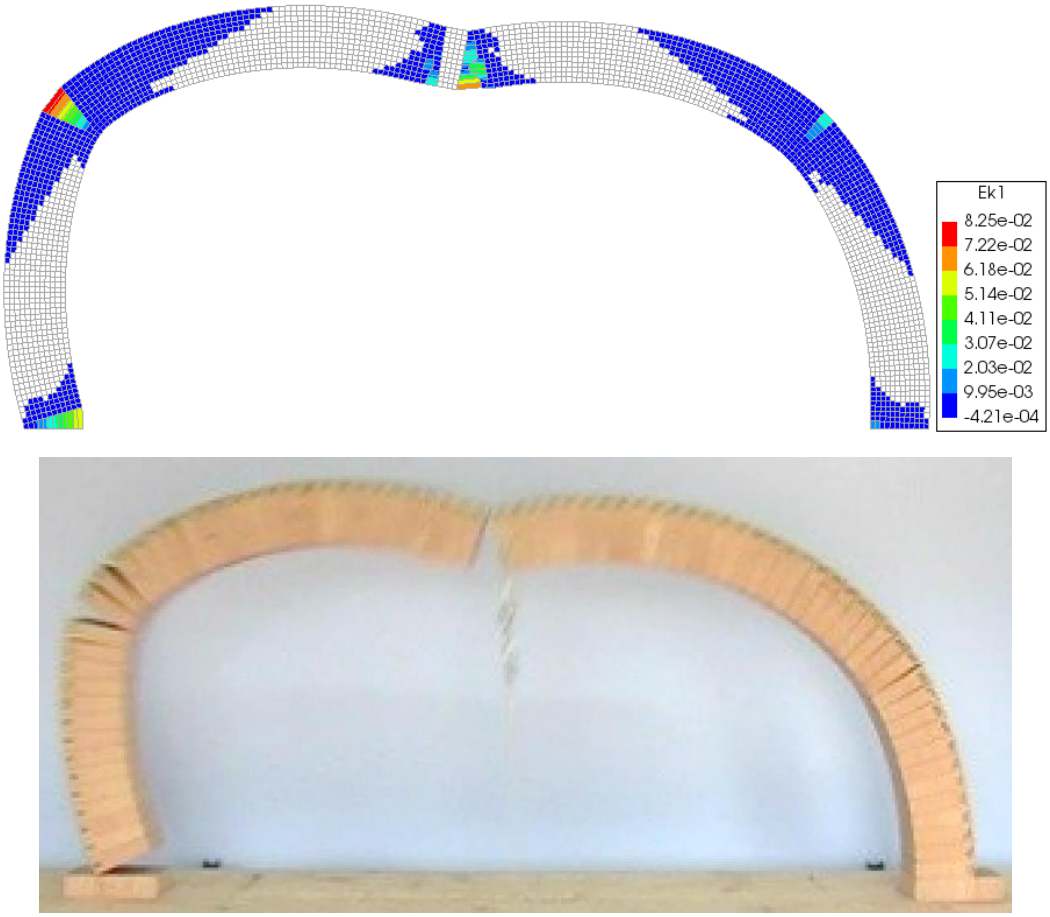

Figure 108 - Top: macro-model with equivalent radial reinforcement at the extrados, 90 mm depth, load at 1/2 of the span, principal crack strain at collapse deformed configuration (x60 amplification). Bottom: experimental collapse configuration.

Load position (span fraction)	Collapse load [N]			Error	
	Numerical	Experim.	Limit Analysis	to Experim.	to L. Analysis
1/6	395	411	389	-4%	2%
1/2	361	364	360	-1%	0%

Table 35 - Equivalent radial load reinforcement at the extrados: macro-models results and comparison with experimental and limit analysis ones.

The capacity curves obtained show final values in good accordance with the experimental ones (Figure 105, Figure 106 and Table 35). Also the collapse hinged configurations show a compatible layout (Figure 107 and Figure 108). This, as in the case of micro-models, confirms the consistency of the substitution of the cable with an equivalent radial load.

Even the cases with the cables at the intrados have been analysed, with the same geometry of the micro-models' cases (90 mm of depth). To avoid the problems of unwanted tangential cracking, the case loaded at ½ of the span, needed a higher value of the tensile strength (0.03 MPa). Analysis setup is reported in Table 36.

Element Type	4-noded
Element Size	8 mm
Steps increment of Displacement	0.001 mm
Iterative Method	Full Newton-Raphson
Convergence Control	Energy, Force, Displacements
Tolerance	0.01

Table 36 - Macro-models with equivalent radial load at the intrados, analysis setup.

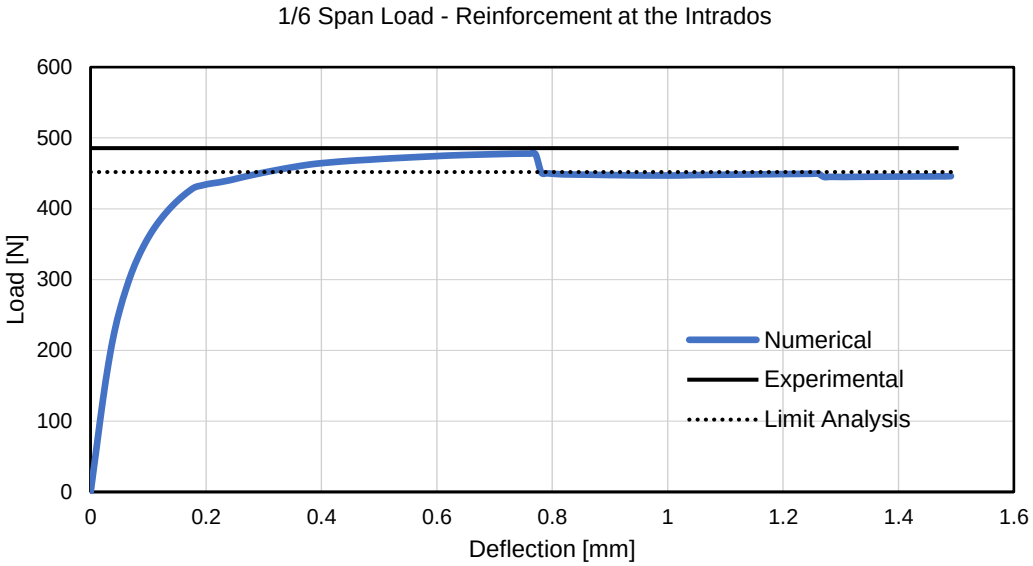

Figure 109 - Macro-model results: arch with equivalent radial reinforcement at the intrados (294 N post-tension), load at 1/6 of the span, deflection of loaded point vs load applied.

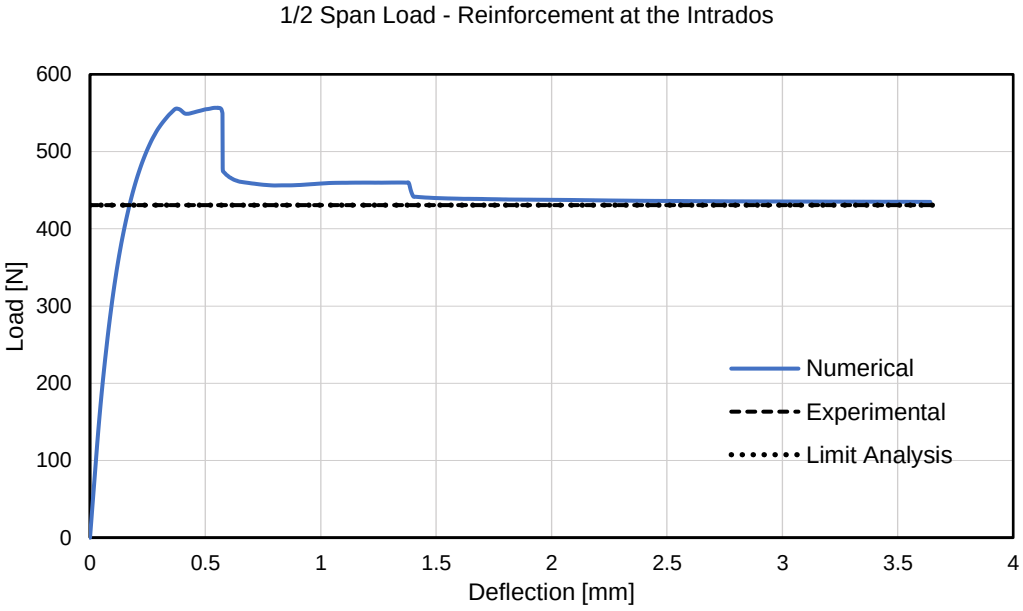

Figure 110 - Macro-model results: arch with equivalent radial reinforcement at the intrados (294 N post-tension), load at 1/2 of the span, deflection of loaded point vs load applied.

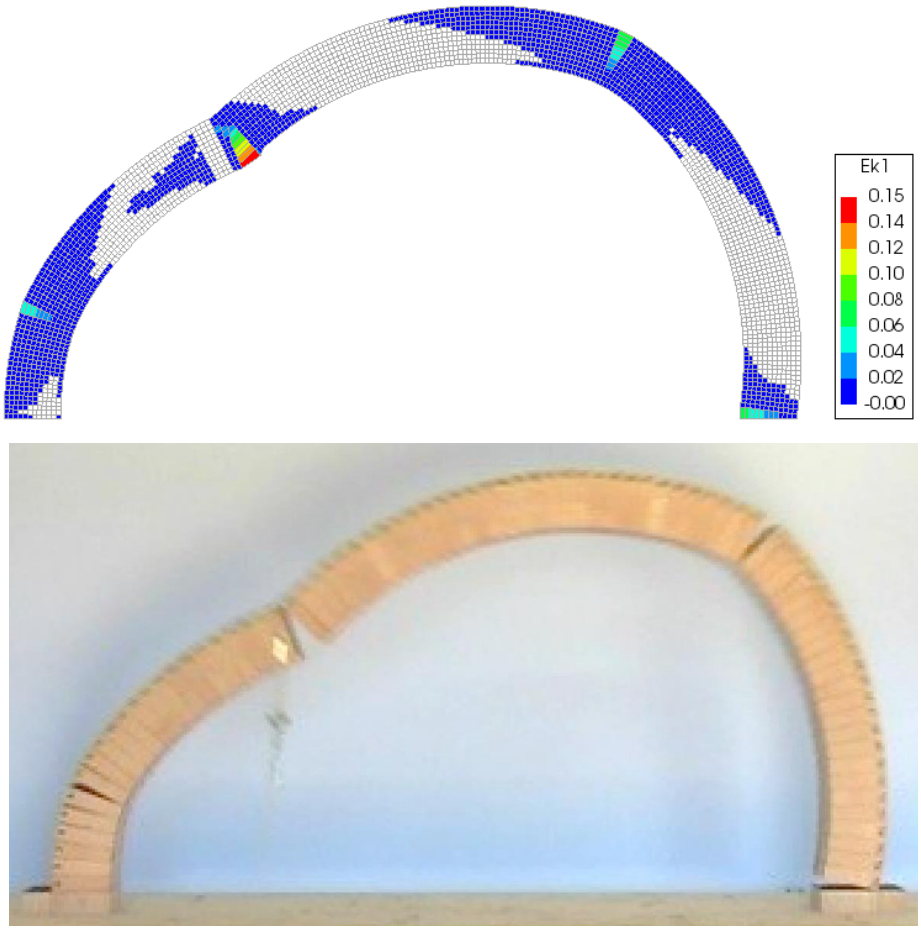

Figure 111 – Top: macro-model with equivalent radial reinforcement at the intrados, 100 mm depth, load at 1/6 of the span, principal crack strain at collapse deformed configuration (x20 amplification). Bottom: experimental collapse configuration.

A shown in Figure 109, Figure 110, Figure 111 and Figure 112, the results are in good accordance with the experimental and the limit analysis ones. The increase of tensile strength in the case loaded at ½ of the span causes a peak-like behaviour, clearly visible on the capacity curve trend. After the peak, the curve converges anyway from above to the experimental value of capacity.

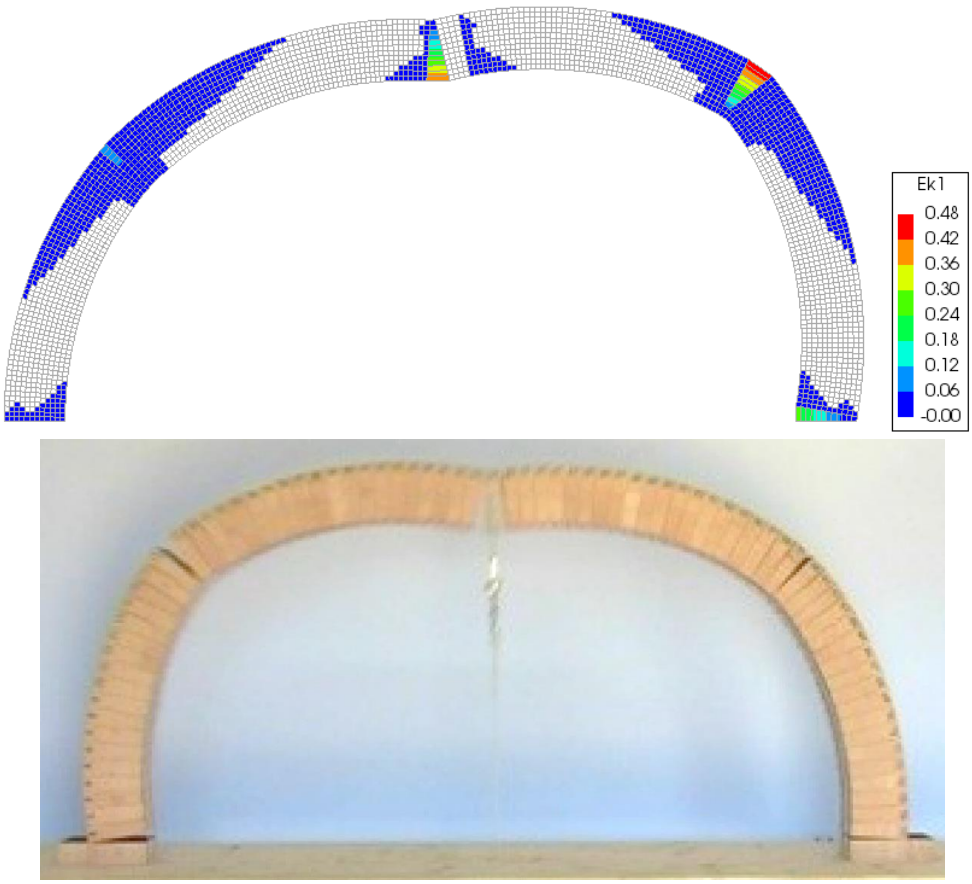

Figure 112 - Top: macro-model with equivalent radial reinforcement at the intrados, 100 mm depth, load at 1/2 of the span, principal crack strain at collapse deformed configuration (x10 amplification). Bottom: experimental collapse configuration.

Load position (span fraction)	Collapse load [N]			Error	
	Numerical	Experim.	Limit Analysis	to Experim.	to L. Analysis
1/6	446	486	452	-8%	-1%
1/2	435	431	431	1%	1%

Table 37 - Equivalent radial load reinforcement at the intrados: macro-models results and comparison with experimental and limit analysis ones.

The numerical results show, in general, an optimal accordance with the limit analysis ones (Table 37). Compared with the experimental ones they better fit in the case of load applied at half span, while for the load at 1/6 of the span they show a slightly lower value. This difference can be ascribed both at the uncertainty of the spreadsheet for graphic statics on the calculation of the depth (performed with the load at half span) and to the tensile strength value choice.

7.4 Modelling of Free Sliding Steel Cables Reinforcement - Results

Macro-models have been used also to simulate the cases with physical cable modelling. The value of the friction angle has been taken again as φ = 0.6°, so as to enable free sliding of the cables, as demonstrated with micro-models in 6.4.2. The other parameters involved, concerning the cable and the sliding interface behaviour, are the same as the ones used for micro-model analysis, reported in Table 25. As stated above, unlike the cases of micro-modelling, 4-noded plane stress elements have been used. Therefore, the elements used for the discretization of the steel cables are 2D linear enhanced-truss, and even interface ones are of the same order (linear). The same cases as before have been considered:

- Cable at the extrados (90 mm depth), 294 N of prestress, load at 1/6 and half of the span;
- Cable at the intrados (100 mm depth), 294 N of prestress, load at 1/6 and half of the span.

Even in this case, when the cables were applied at the extrados, debonding has been allowed (gap opening of the interface), while with cables at the intrados, the interfaces worked both in tension and in compression. In all the cases, linear geometry analysis has been performed. Concerning the arch body material, the same properties of the cases of the macro-models with the equivalent radial load reinforcements, explained in 7.3, have been applied. Analysis setup is reported in Table 38.

Element Type	4-noded
Element Size	6 mm
Steps increment of Displacement	0.001 mm
Iterative Method	Full Newton-Raphson
Convergence Control	Energy, Force, Displacements
Tolerance	0.01

Table 38 - Macro-models with cables modelling at the extrados, analysis setup.

Again, the normal stress at interface, if integrated along the width of the interface (0.1 mm), gives almost exactly the value of the equivalent confinement (Figure 113).

Equivalent Radial Load → p = T / R = 294 N / 695 mm = 0.423 N/mm

Confinement Effect from Cable Modelling → p' = σ_R x t = 4.23 MPa x 0.1 mm = 0.423 N/mm (maximum)

T: cable traction, R: external radius, σ_R: radial normal stress, t: interface width.

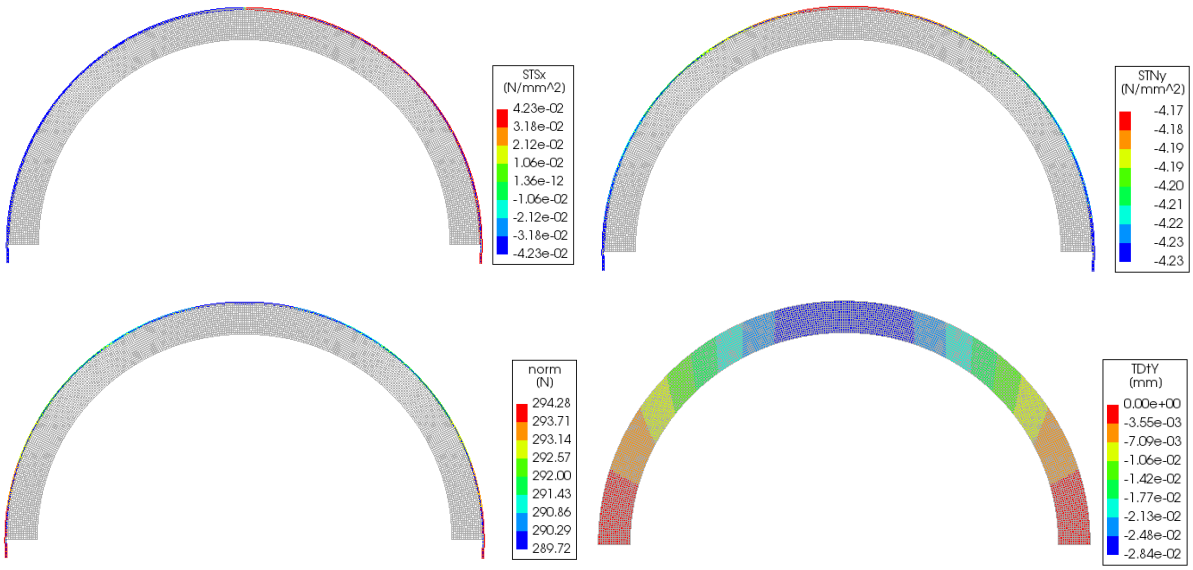

Figure 113 - Macro-model with physical reinforcement at the extrados (90 mm depth): end of the application of post-tension (294 N). Top: shear stress interface distribution (left) and normal stress interface distribution. Bottom: axial load in the reinforcement (left) and vertical displacements of the arch body (right). Deformation scale x200.

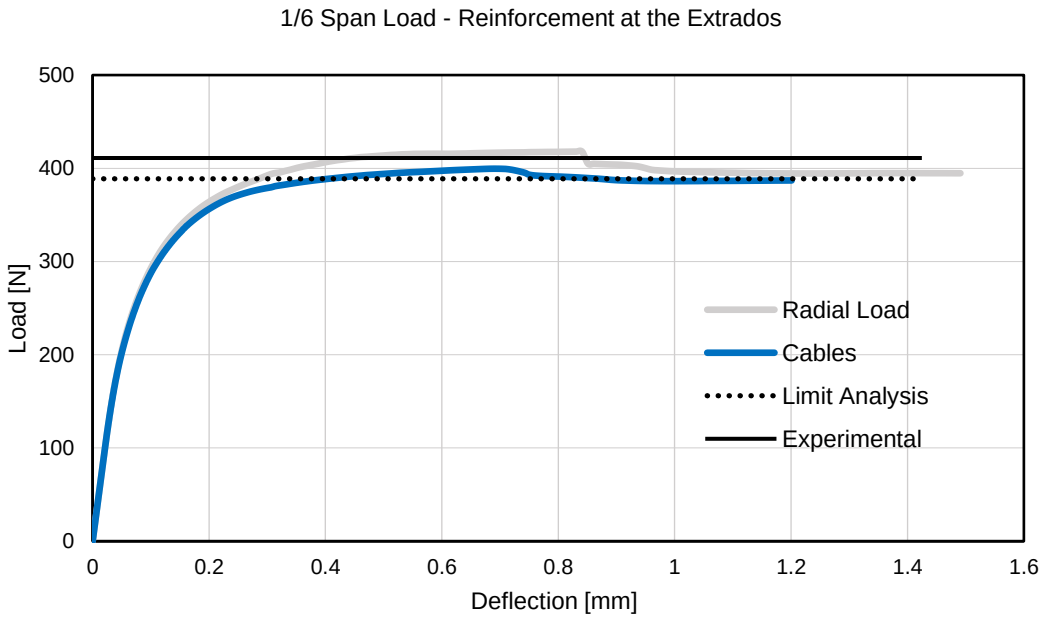

Figure 114 - Macro-model results: arch with physical cable at the extrados (294 N post-tension), load at 1/6 of the span, deflection of loaded point vs load applied, comparison with equivalent load case.

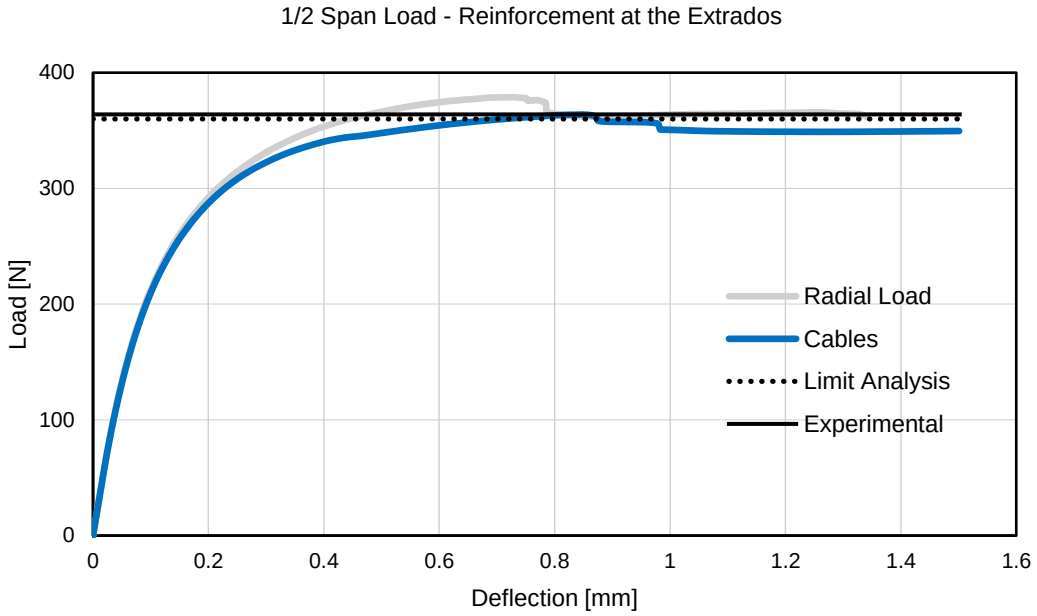

Figure 115 - Macro-model results: arch with physical cable at the extrados (294 N post-tension), load at 1/2 of the span, deflection of loaded point vs load applied, comparison with equivalent load case.

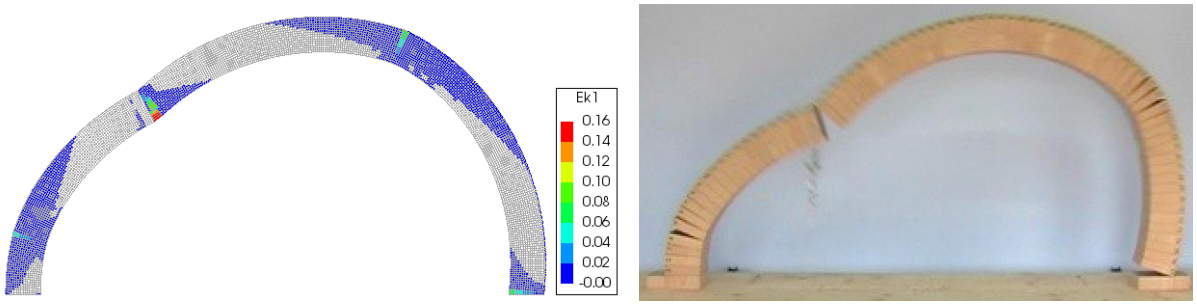

Figure 116 – Left: macro-model with physical reinforcement at the extrados, 90 mm depth, load at 1/6 of the span, crack strains at collapse deformed configuration (x40 amplification). Right: experimental collapse configuration.

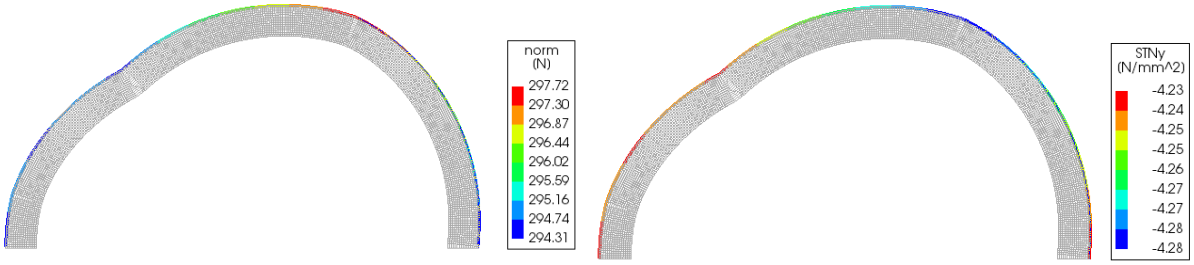

Figure 117 - Macro-model with physical reinforcement at the extrados, 90 mm depth, load at 1/6 of the span, collapse deformed configuration (x25 amplification). Left: axial force in the cable, right: interface normal stress.

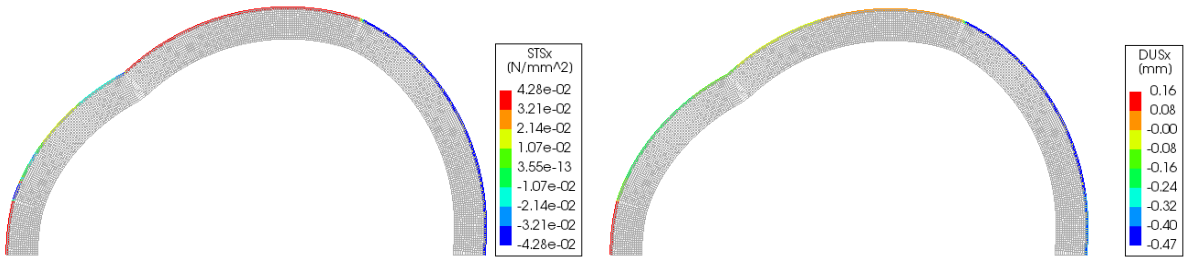

Figure 118 - Macro-model with physical reinforcement at the extrados, 90 mm depth, load at 1/6 of the span, collapse deformed configuration (x25 amplification). Left: shear stress in the interface, right: shear displacements.

The results show a good accordance with the previous ones (Figure 114, Figure 115, Figure 116 and Figure 119), despite a slightly lower value in the case loaded at half span (Table 39). Nevertheless, the validity of this kind of modelling is confirmed, but still the value of the tensile strength could be affecting the results. The contours of cable tension and radial load show, again, a rather constant distribution along the arch (Figure 117 and Figure 120). Shear stress remains low (Figure 118 and Figure 121)

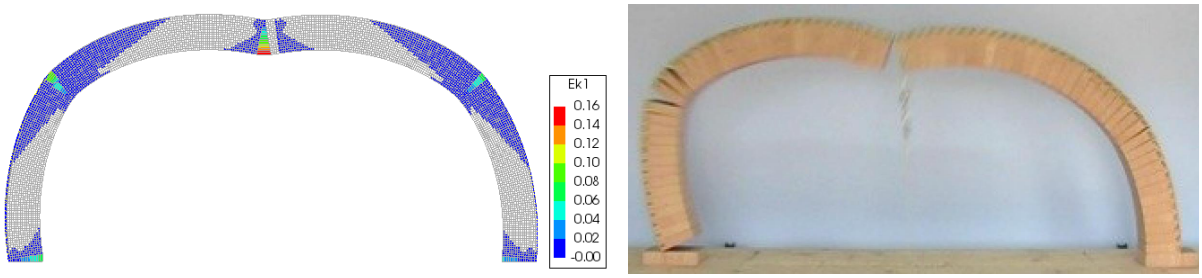

Figure 119 - Left: macro-model with physical reinforcement at the extrados, 90 mm depth, load at 1/2 of the span, crack strains at collapse deformed configuration (x40 amplification). Right: experimental collapse configuration.

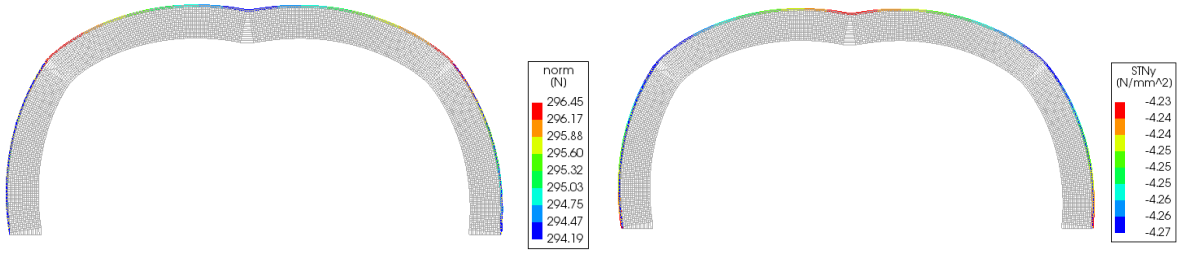

Figure 120 - Macro-model with physical reinforcement at the extrados, 90 mm depth, load at 1/2 of the span, collapse deformed configuration (x40 amplification). Left: axial force in the cable, right: interface normal stress.

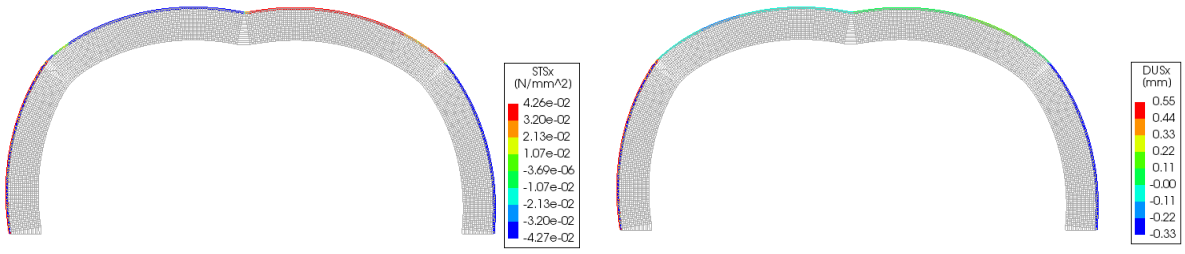

Figure 121 - Macro-model with physical reinforcement at the extrados, 90 mm depth, load at 1/2 of the span, collapse deformed configuration (x40 amplification). Left: shear stress in the interface, right: shear displacements.

Load position (span fraction)		Collapse load [N]				Error	
	Cables	Radial Confinement	Experim.	Limit Analysis	to Radial Confinement	to Experim.	to L. Analysis
1/6	387	395	411	389	-2%	-6%	0%
1/2	350	361	364	360	-3%	-4%	-3%

Table 39 – Cables at the extrados modelling: macro-models results and comparison with previous ones and experimental ones.

As in all the previous cases, even reinforcement at the intrados has been analysed. The model features are the same of the one used in the previous analysis, but with 100 mm depth and steel cable reinforcement at the intrados, with no possibility to debond at the interface with the arch (Figure 122). To avoid the problems of unwanted tangential cracking, again the case loaded at ½ of the span needed a higher value of the tensile strength (0.03 MPa). Analysis setup is reported in Table 40.

Element Type	4-noded
Element Size	7 mm
Steps increment of Displacement	0.001 mm
Iterative Method	Full Newton-Raphson
Convergence Control	Energy, Force, Displacements
Tolerance	0.01

Table 40 - Macro-models with physical cables at the intrados, analysis setup.

Equivalent Radial Load → p = T / R = 294 N / 600 mm = 0.49 N/mm

Confinement Effect from Cable Modelling → p' = σ_R x t = 4.84 MPa x 0.1 mm = 0.484 N/mm

T: cable traction, R: external radius, σ_R: radial normal stress, t: interface width.

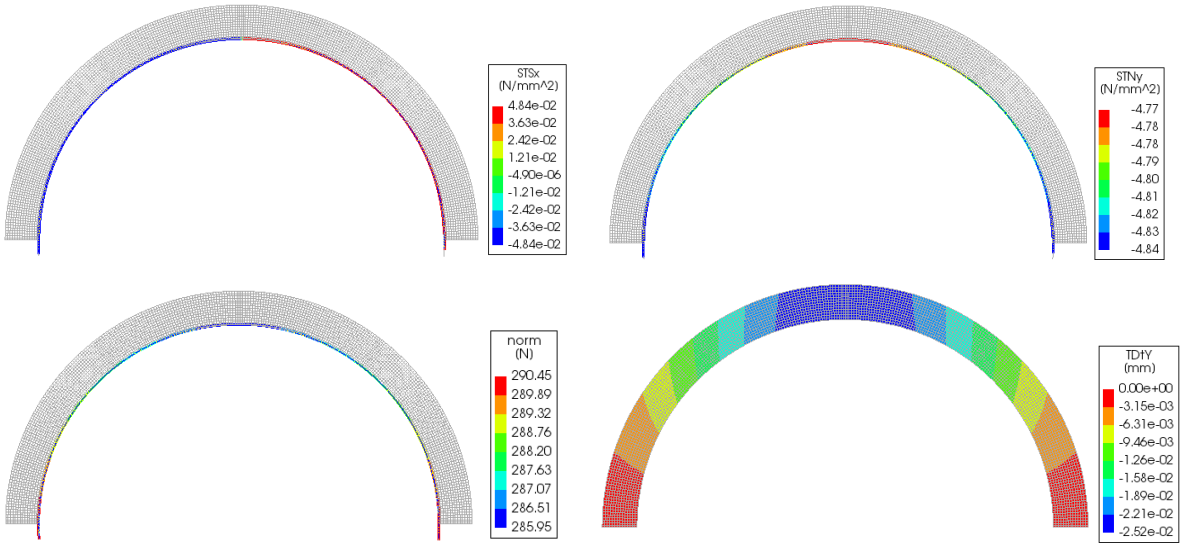

Figure 122 - Macro-model with physical reinforcement at the intrados (90 mm depth): end of the application of post-tension (294 N). Top: shear stress interface distribution (left) and normal stress interface distribution. Bottom: axial load in the reinforcement (left) and vertical displacements of the arch body (right). Deformation scale x200.

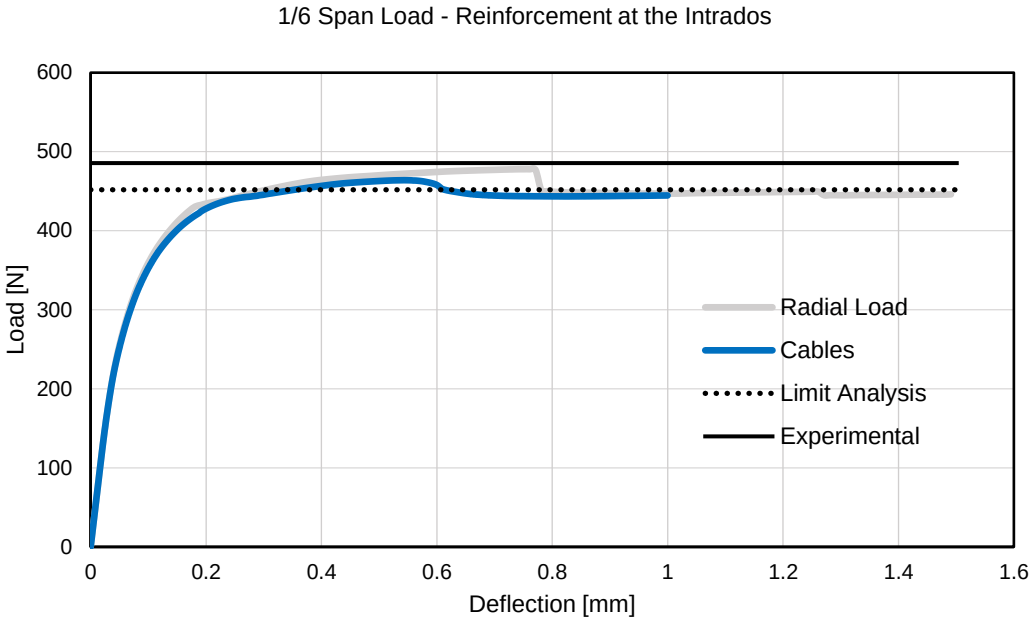

Figure 123 - Macro-model results: arch with physical cable at the intrados (294 N post-tension), load at 1/6 of the span, deflection of loaded point vs load applied, comparison with equivalent load case.

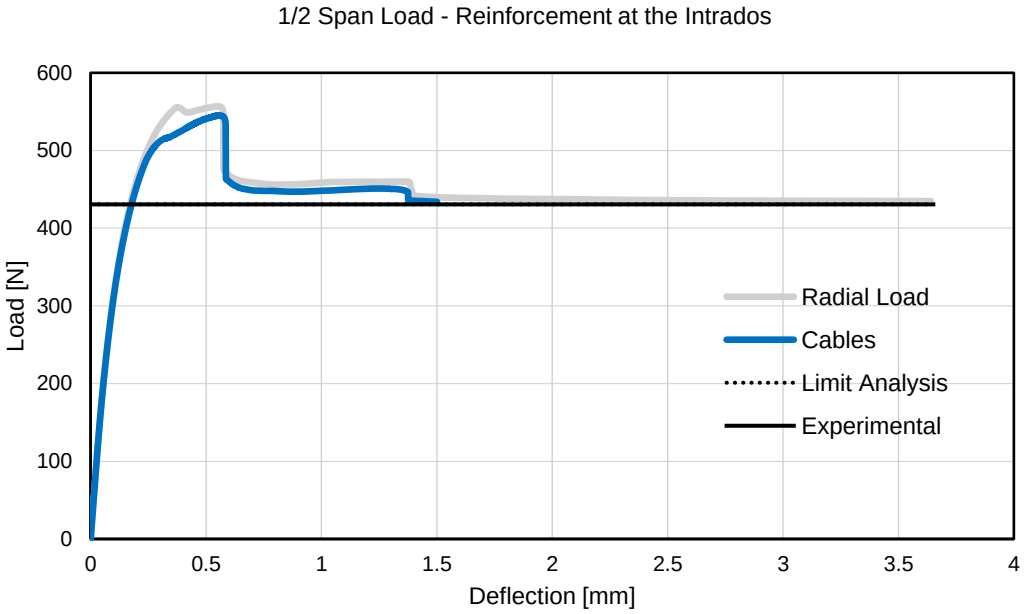

Figure 124 - Macro-model results: arch with physical cable at the intrados (294 N post-tension), load at 1/2 of the span, deflection of loaded point vs load applied, comparison with equivalent load case.

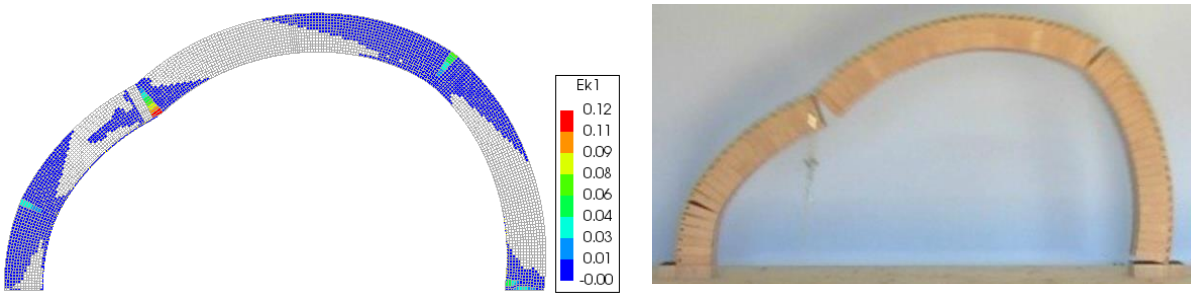

Figure 125 - Left: macro-model with physical reinforcement at the intrados, 100 mm depth, load at 1/6 of the span, crack strains at collapse deformed configuration (x amplification). Right: experimental collapse configuration.

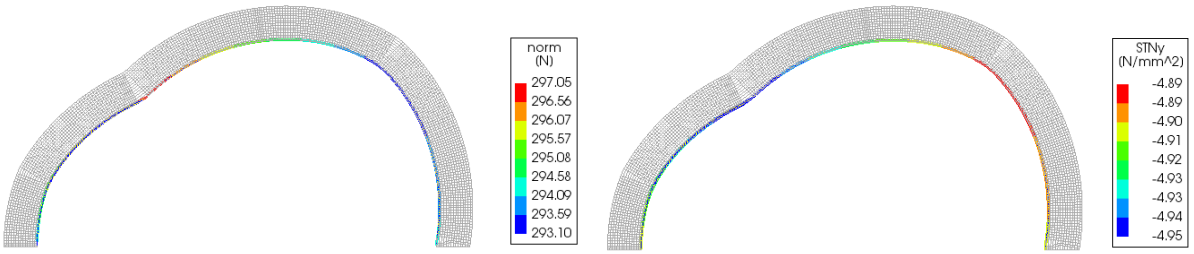

Figure 126 - Macro-model with physical reinforcement at the intrados, 100 mm depth, load at 1/6 of the span, collapse deformed configuration (x40 amplification). Left: axial force in the cable, right: interface normal stress.

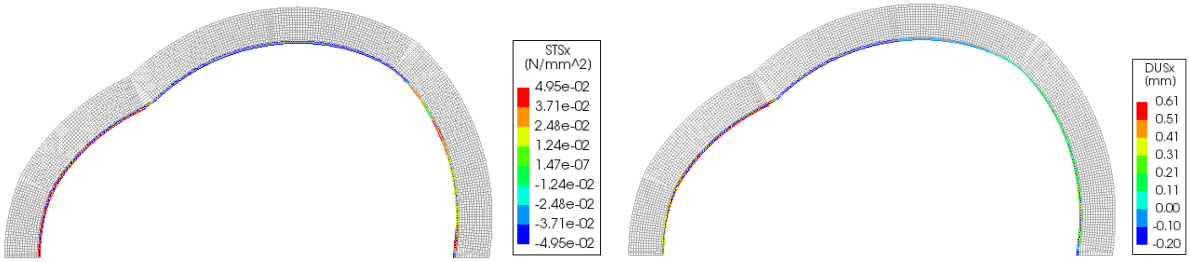

Figure 127 - Macro-model with physical reinforcement at the intrados, 100 mm depth, load at 1/6 of the span, collapse deformed configuration (x40 amplification). Left: shear stress in the interface, right: shear displacements.

Even in this last case, involving reinforcement at the intrados, the results show a good accordance with the previous ones, especially the ones coming from equivalent radial load reinforcement (Figure 123, Figure 124, Figure 125, Figure 128 and Table 41). This confirms the equivalence of these two procedures, and also the fact that the cables are not affected from significant friction phenomena. This is proved from the contours of the cable tension and of the radial interaction force (Figure 126, Figure 129), that both remain substantially constant all along the arch boundary. Even in this case, shear stress is low, confirming the sliding cables phenomenon (Figure 127 and Figure 130).

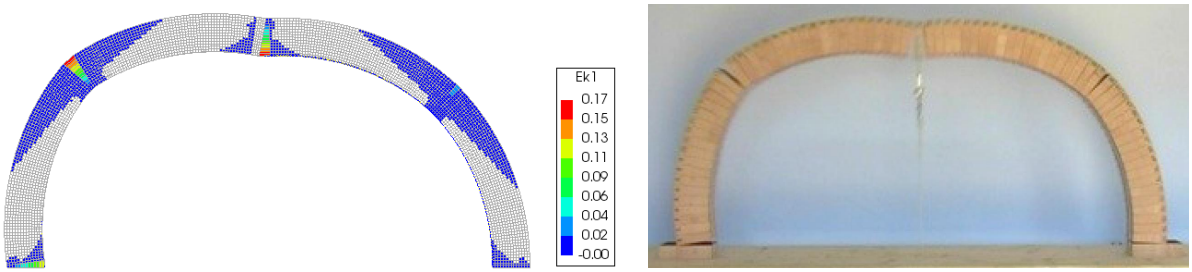

Figure 128 - Left: macro-model with physical reinforcement at the intrados, 100 mm depth, load at 1/2 of the span, crack strains at collapse deformed configuration (x amplification). Right: experimental collapse configuration.

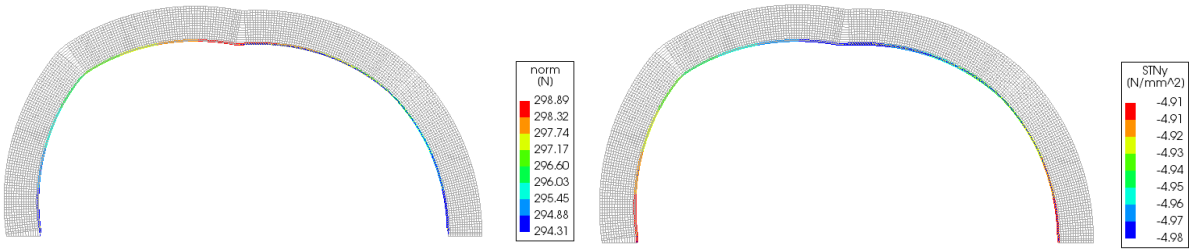

Figure 129 - Macro-model with physical reinforcement at the intrados, 100 mm depth, load at 1/2 of the span, collapse deformed configuration (x amplification). Left: axial force in the cable, right: interface normal stress.

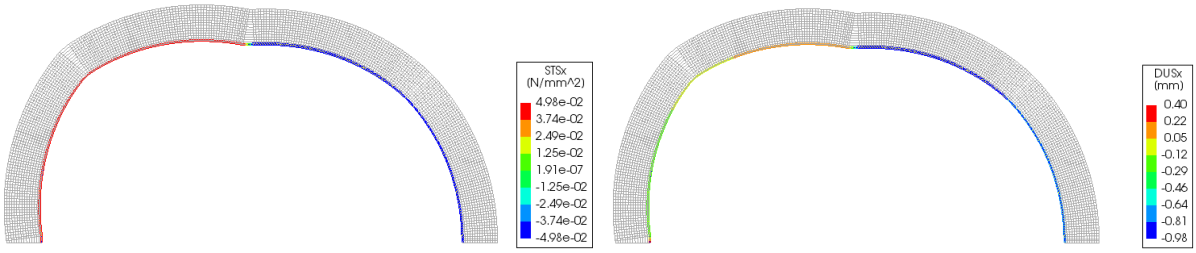

Figure 130 - Macro-model with physical reinforcement at the intrados, 100 mm depth, load at 1/2 of the span, collapse deformed configuration (x amplification). Left: shear stress in the interface, right: shear displacements.

Load position (span fraction)		Collapse load [N]				Error	
	Cables	Radial Confinement	Experim.	Limit Analysis	to Radial Confinement	to Experim.	to L. Analysis
1/6	445	446	486	452	0%	-8%	-2%
1/2	434	435	431	431	0%	1%	1%

Table 41 - Cable at the intrados: macro-models results and comparison with previous results and experimental ones.

8. COMPARISON OF RESULTS

In this last chapter, a brief comparison between micro and macro models' results is presented. The graphs shown concern only the case of sliding cables, therefore with friction angle φ = 0.6° and no constraint at the cable ends. First, the results concerning unreinforced arch are reported in Figure 131.

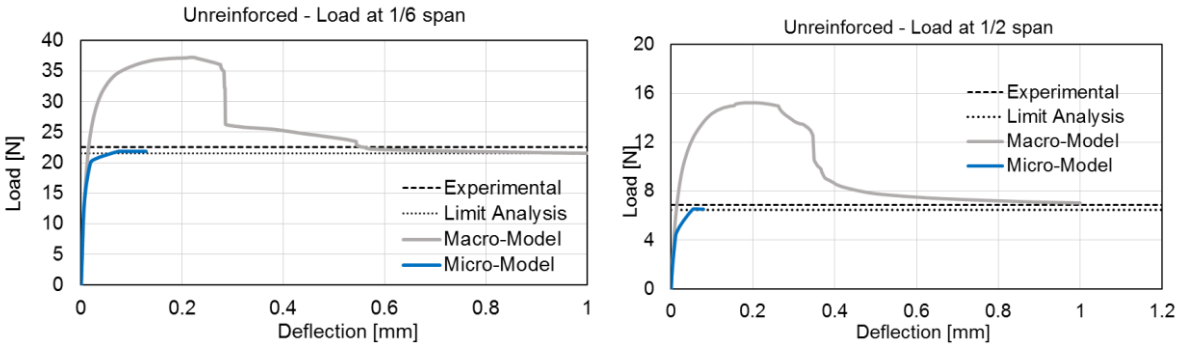

Figure 131 – Unreinforced arch: comparison between micro and macro-models results.

The graphs show a clear difference on the shape of the capacity curves obtained, for the unreinforced arch. The micro-models, in the both load positions cases, converge much faster, in terms of vertical displacement needed to reach the limit value, than the macro-models. This is due to the absence of tensile resistance between the arch voussoirs in the first ones, while in the second ones an extra resistance (not physically representative, but numerically necessary) is provided. This leads, in fact, to the presence of unwanted peaks, that do not represent the real behaviour of the structure. Despite this, in both types of model convergence to the expected values is reached. In macro-models, the convergence is reached from upper bound, in a sort of softening behaviour. Conversely, micro-models converge in a more physically consistent way, that is monotonically.

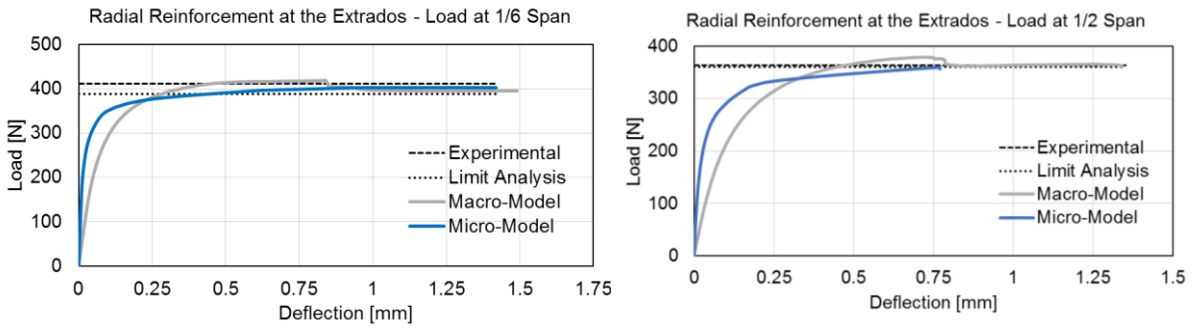

Figure 132 – Equivalent radial load at the extrados reinforced arch: comparison between micro and macro-models results.

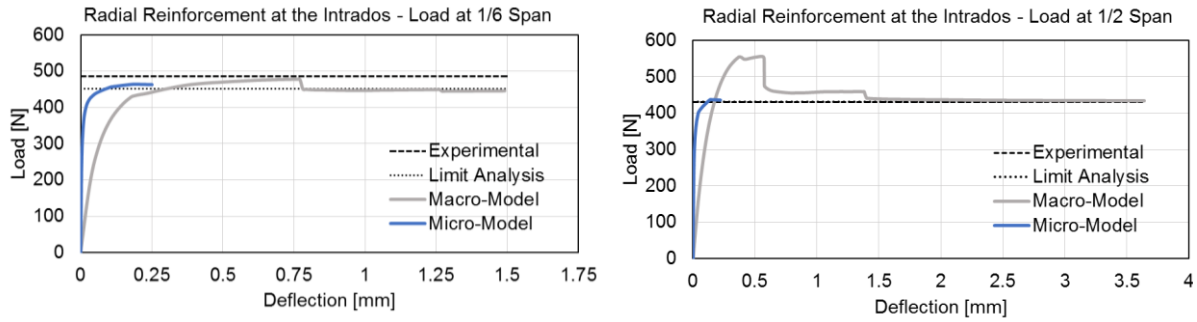

Figure 133 - Equivalent radial load at the intrados reinforced arch: comparison between micro and macro-models results.

Even the cases with the equivalent radial load reinforcement show the same tendencies of the unreinforced ones (Figure 132 and Figure 133). Nevertheless, the presence of the confinement effect tends to smooth the peaks and the discontinuities.

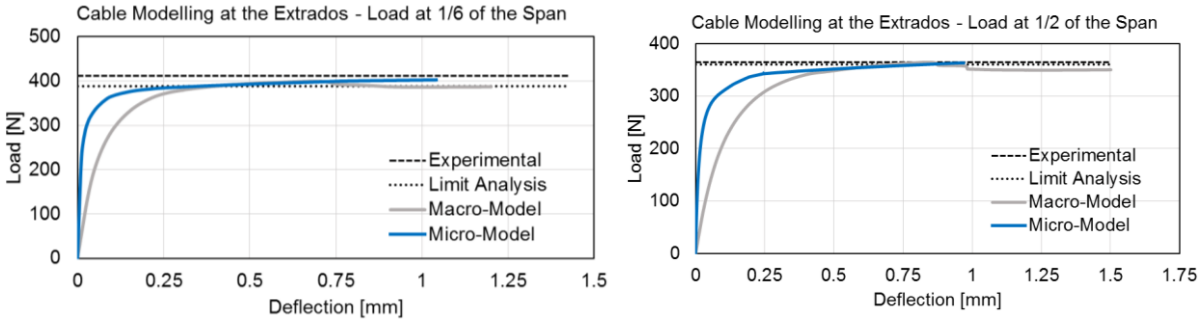

Figure 134 – Arch with modelling of reinforcement cable at the extrados: comparison between micro and macro-models results.

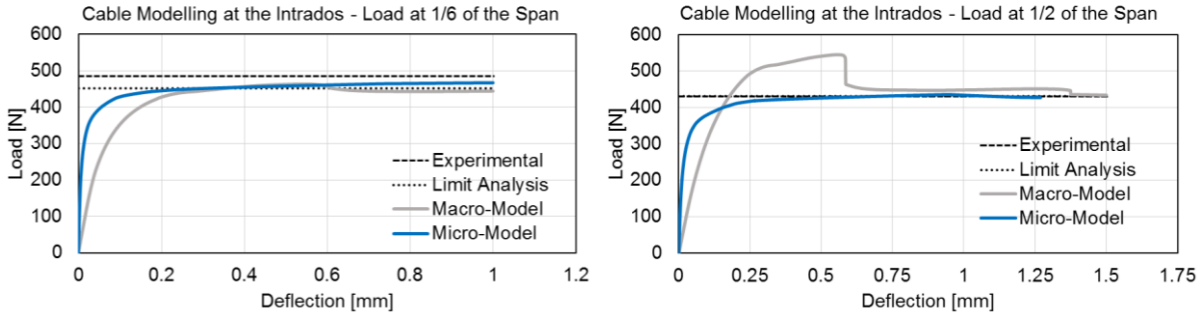

Figure 135 - Arch with modelling of reinforcement cable at the intrados: comparison between micro and macro-models results.

In the cases with physical cable modelling the two types of model show more comparable results, with a slight difference in the final values of the load capacity (Figure 134 and Figure 135).

In all the models, it can be noticed that the initial deformability is higher in the micro-models' cases. This is probably due to the cracking phenomena occurring in the macro-models from the early stages, due

to the low values of tensile strength. Moreover, the cracks distribution is more diffused than in the micro-models' cases. This fact causes a lowering of the stiffness from the beginning of the loading phase. The micro-models result, instead, due to the elastic behaviour of the blocks, show a stiffer response in the early stages, before hinges opening.

9. CONCLUSIONS

9.1 Summary

Arches, vaults and domes constitute a smart way to use masonry in constructions, because of their ability to work mainly in compression, given its poor tensile strength. This is why, still nowadays, many arched structures of the ancient times are still standing, even after centuries or millennia from their construction, and have become part of our architectural heritage. Nevertheless, arched structures have always been suffering from problems connected with non-uniform vertical loads, such as horizontal actions, differential settlements and pointed vertical loads. This led to the application of different types of strengthening devices throughout history. The Reinforced Arch method is a recent consolidation technique, that consists on the application of steel post-tensioned cables at the intrados or at the extrados of the structure. It is a rather novel procedure, but it can be classified also as a traditional one because of its basic working principles, its elevate compatibility, its simple materials and its easiness to apply. It has been largely tested by Professor Lorenzo Jurina at the Polytechnic University of Milan, with more than 500 experimental tests performed.

9.2 Conclusions

The present work aimed at confirming the effectiveness of this strengthening technique, through the use of finite element numerical models. Experiments on collapse of wooden blocks scaled roman arches were numerically reproduced and simulated. The validity of the results obtained have been confirmed by comparison both with the experimental data and limit analysis ones. After a calibration phase by means of limit analysis, to compensate geometrical problems connected with the reduction of the effective cross-section of the arch, numerical analyses have been performed. Two types of models have been considered and compared: micro-models, modelled with elastic blocks and hinge opening, and macro-models, that have been provided of a smeared crack yield criterion, suitable for masonry structures. All of the results obtained, in terms of vertical load capacity, have been compared, highlighting pros and cons of any modelling technique. Results showed good accordance with the experimental ones, and even more with the ones derived from limit analysis. Therefore, in general it can be stated that both micro and micro-models can be used to simulate the effect of this strengthening method. Nevertheless, micro-models showed a more reliable behaviour all along the loading path, while macro-models showed peaks with no physical significance, due to the presence of tensile strength. Reinforcement has been modelled in different ways: applying an equivalent radial confinement or actually modelling the post-tensioned cables, showing basically an equivalence in the results. Moreover, a more detailed analysis, based on micro-modelling, has been performed to investigate the influence of friction angle between cables and arch on the global behaviour and the capacity of the structure. This analysis underlined the transition from a sliding behaviour of cables to an adherence one, proportional

to the increase of this parameter. This was accompanied by an increase of the overall capacity. With the same models, also the cases of anchored cables have been studied, confirming the great increase of capacity highlighted in the experimental campaign, if compared with the cases of not anchored ones. Concerning macro-modelling, a sensitivity analysis on tensile strength of masonry has been performed, highlighting the influence of this parameter on the final capacity. This uncertainty on the value of tensile strength represents one of the main drawbacks of this type of models. Therefore, in general, it can be stated that micro-models are more reliable and better simulate the behaviour of such reinforced structures.

9.3 Future Development

The numerical tools can be further enhanced in terms of material definition of both the arch body and the reinforcement, especially for simulating the behaviour of real masonry arches. Possible future improvements can be carried out by assigning a non-linear material at the arch blocks in micro-models, to capture damage in compression. Also, non-zero tensile strength at the interfaces (mortar joints) can be added. Moreover, concerning the reinforcement modelling, a yield criterion for the cables' steel can be added, to capture possible post-elastic effects, in particular for obtaining a reliable capacity curve in the cases of anchored cables. Finally, non-fixed anchors can be introduced, to simulate potential displacements during the arch loading. All this treatise can be extended also to barrel vaults, by means of 3D models, to investigate the effect of diffusion of stresses in the third dimension, and perform a parametrical analysis for the optimization of the strengthening technique.

REFERENCES

Poleni, Giovanni. Memorie istoriche della gran cupola del tempio Vaticano e de'danni di essa e detristoramenti loro, divisi in libri 5. Nella Stamperia del seminario, 1748.

Ochsendorf, John. "Los Guastavino y la bóveda tabicada en Norteamérica." Informes de la Construcción 56.496 (2005): 57-65.

Gilbert, M. "Limit analysis applied to masonry arch bridges: state-of-the-art and recent developments." 5th International Arch Bridges Conference. 2007.

Heyman, Jacques. "The stone skeleton." International Journal of solids and structures 2.2 (1966): 249-279.

O'Dwyer, Dermot. "Funicular analysis of masonry vaults." Computers & Structures 73.1 (1999): 187-197.

Gilbert, Matthew, et al. "Application of large-scale layout optimization techniques in structural engineering practice." 6th World Congresses of Structural and Multidisciplinary Optimization (2005).

Lourenço, Paulo B. Computational strategies for masonry structures. Diss. TU Delft, Delft University of Technology, 1996.

Roca, Pere, Miguel Cervera, and Giuseppe Gariup. "Structural analysis of masonry historical constructions. Classical and advanced approaches." Archives of Computational Methods in Engineering 17.3 (2010): 299-325.

Clemente, R. "Structural analysis of historical buildings by localized cracking models" (in Spanish). PhD dissertation, Universitat Politècnica de Catalunya, Barcelona, Spain, 2006.

Lourenço, Paulo B. "Computations on historic masonry structures." Progress in Structural Engineering and Materials 4.3 (2002): 301-319.

Kumar, Pardeep, and N. M. Bhandari. "Non-linear finite element analysis of masonry arches for prediction of collapse load." Structural engineering international 15.3 (2005): 166-175.

Betti, Michele, Georgios A. Drosopoulos, and Georgios E. Stavroulakis. "Two non-linear finite element models developed for the assessment of failure of masonry arches." Comptes Rendus Mécanique 336.1-2 (2008): 42-53.

Milani, Gabriele, and Paulo B. Lourenço. "3D non-linear behavior of masonry arch bridges." Computers & Structures 110 (2012): 133-150.

Lemos, José V. "Discrete element modeling of masonry structures." International Journal of Architectural Heritage 1.2 (2007): 190-213.

Cundall, Peter A. "Formulation of a three-dimensional distinct element model—Part I. A scheme to detect and represent contacts in a system composed of many polyhedral blocks." International Journal of Rock Mechanics and Mining Sciences & Geomechanics Abstracts. Vol. 25. No. 3. Pergamon, 1988.

Hart, R., P. A. Cundall, and J. Lemos. "Formulation of a three-dimensional distinct element model—Part II. Mechanical calculations for motion and interaction of a system composed of many polyhedral blocks." International Journal of Rock Mechanics and Mining Sciences & Geomechanics Abstracts. Vol. 25. No. 3. Pergamon, 1988.

Hocking, Grant. "The discrete element method for analysis of fragmentation of discontinua". Engineering computations 9.2 (1992): 145-155.

Gilbert, M., and Melbourne, C. 1995. “Analysis of multi-ring brickwork arch bridges”. In Arch Bridges, ed. C. Melbourne. Thomas Telford, London, 225–238.

Bicanic, N., Ponniah, D., and Robinson, J. 2001. “Discontinuous deformation analysis of masonry bridges”. In Computational Modelling of Masonry, Brickwork and Blockwork Structures, ed., J.W. Bull. Stirling, UK: Saxe-Coburg Publications, 177–196.

Thavalingam, A., et al. "Computational framework for discontinuous modelling of masonry arch bridges." Computers & structures 79.19 (2001): 1821-1830.

Molins, Climent, and Pere Roca. "Capacity of masonry arches and spatial frames." Journal of structural engineering 124.6 (1998): 653-663.

Jurina, L. "Strengthening of masonry arch bridges with “RAM”–Reinforced Arch Method." Seminario IABMAS Stresa (VB), 2012.

Jurina, Lorenzo. "La possibilità dell'approccio reversibile negli intervento di consolidamento strutturale." Atti del XIX Convegno Scienza e Beni Culturali La reversibilità nel restauro. Riflessioni, Esperienze, percorsi di ricerche, Bressanone (2003): 1-4.

Jurina, Lorenzo. "Consolidamento strutturale e reversibilità." Atti del convegno nazionale su" Reversibilità, concezione e interpretazione nel restauro", Torino (2002).

Jurina, Lorenzo, et al. "L’intervento di restauro e consolidamento strutturale alla chiesa di Santa Caterina in Lucca." (2014).

Jurina, Lorenzo. "Il consolidamento delle strutture castellane." Atti del convegno" Sant'Angelo Lodigiano: un castello, un borgo un fiume…", Sant'Angelo Lodigiano 10 (2003).

Jurina, Lorenzo. "Le Necessità di Consolidamento Strutturale della “Ciribiciaccola”, La Torre Nolare dell’Abbazia Di Chiaravalle.", 2015.

Jurina, Lorenzo. "Una tecnica di consolidamento attivo per archi e volte in muratura." Proceedings of the conference on seismic performance of built heritage in small historic centers. 1999.

Manie, J and Schreppers, G.J.. “DIANA Finite Element Analysis User’s Manual Release 10.1”. DIANA FEA bv, Delftechpark 19a, 2628 XJ Delft, The Netherlands., 2016.

Vecchio, Frank J., and Michael P. Collins. "Compression response of cracked reinforced concrete." Journal of Structural Engineering 119.12 (1993): 3590-3610.

Bonfigliuoli, Sara. "Consolidamento strutturale e antisismico di archi e volte in muratura: una sperimentazione sulla tecnica dell'arco armato." (2011).

Giglio, S. M. “Consolidamento di archi e volte in muratura mediante la tecnica dell’arco armato. Approccio Sperimentale.” Diss. Tesi di Laurea, rel. Lorenzo Jurina, Politecnico di Milano A.A. 2007-2008, 2008.

Jurina, Lorenzo. "Il Consolidamento Strutturale Della Chiesa Di Santa Caterina In Lucca.", 2014.

Jurina, Lorenzo. "La possibilità dell'approccio reversibile negli intervento di consol-idamento strutturale." Atti del XIX Convegno Scienza e Beni Culturali La reversibilità nel restauro. Riflessioni, Esperienze, percorsi di ricerche, Bressanone (2003): 1-4.









ARCCHIP